

THE REDISPERSION OF SUPPORTED METAL CATALYSTS

by

PAWAN KUMAR HANDA

B.S., Indian Institute of Technology (Delhi), 1973

---

A MASTER'S THESIS

submitted in partial fulfillment of the

requirements for the degree

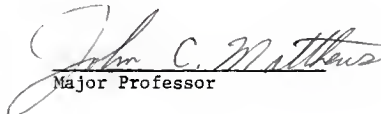
MASTER OF SCIENCE

Department of Chemical Engineering

KANSAS STATE UNIVERSITY  
Manhattan, Kansas

1978

Approved by:

  
Major Professor

## TABLE OF CONTENTS

	<u>Page</u>
CHAPTER 1. INTRODUCTION . . . . .	1
CHAPTER 2. SURFACE AREA OF SUPPORTS . . . . .	4
2.1 Introduction . . . . .	4
2.2 Specific Surface from the BET Plot. . . . .	4
2.3 Criticisms of the BET Model . . . . .	6
2.4 Adsorption Measurements by the Continuous Flow. . . . .	6
Technique	
2.4-1 Principle Steps Outlining the Technique . . . . .	6
2.4-2 Description of the Apparatus . . . . .	7
2.4-3 Preliminary Calibrations . . . . .	11
2.4-3a Calibration of the Soap Bubble . . . . .	12
Flowmeter	
2.4-3b Calibration of the Standard Cell . . . . .	12
2.4-3c Calibration of Attenuations. . . . .	12
2.4-3d Calibration of the Calibration . . . . .	17
Valve Loops	
2.4-3e Sample Preparation and Adsorption- . . . . .	22
Desorption Procedure	
2.5 Measurement of the Saturation Pressure of Nitrogen at . . . . .	23
the Temperature of Liquid Nitrogen	
2.5-1 Construction of the Manometer. . . . .	32
2.5-2 Use of the Manometer . . . . .	35
2.6 Results obtained from Surface Area Measurements . . . . .	35
2.7 Discussion of the Results . . . . .	35
2.8 Conclusions . . . . .	37
CHAPTER 3. CHEMISORPTION ON SUPPORTED METAL CATALYSTS . . . . .	38
REVIEW . . . . .	38
3.1 Introduction . . . . .	38

3.2	Methods used for Chemisorption Studies . . . . .	38
3.3	Characterization of Dispersion by Chemisorption. . . . .	39
	Methods	
3.4	Selection of Adsorbate . . . . .	40
3.4-1	Hydrogen Chemisorption . . . . .	41
3.4-2	Oxygen Adsorption and Hydrogen-Oxygen . . . . .	43
	Titration	
3.4-3	Carbon Monoxide Adsorption and Carbon . . . . .	46
	Monoxide-Oxygen Titration	
3.4-4	Comparison of Different Adsorbates . . . . .	50
3.5	Selection of Adsorption Parameters . . . . .	51
	EXPERIMENTAL . . . . .	53
3.6	Chemisorption Apparatus . . . . .	53
3.6-1	Sample Tube . . . . .	56
3.6-2	Burettes. . . . .	56
3.6-3	Burette-System Manometer . . . . .	56
3.6-4	Mercury Reservoirs . . . . .	59
3.6-5	Gas Purification Train . . . . .	59
3.6-6	Gas Storage Bulbs . . . . .	60
3.6-7	Vacuum System . . . . .	60
3.6-8	McLeod Gauge . . . . .	64
	3.6-8a Calibration of the McLeod Gauge . . . . .	67
3.6-9	Miscellaneous Items . . . . .	70
3.7	Calibration of Zero Bulb Volume. . . . .	70
3.8	Determination of Metal Dispersion from Hydrogen. . . . .	73
	Chemisorption	
3.8-1	Selecting the Sample Size . . . . .	73
3.8-2	Pretreatment of the Sample . . . . .	73

Page

3.8-3	Determination of the Dead Volume . . . . .	73
3.8-4	Measurement of the Isotherm . . . . .	77
3.8-5	Sample Calculations . . . . .	80
3.8-6	Platinum Dispersion, Surface Area and Crystal. . Size from Adsorption Isotherm	86
CHAPTER 4.	SURVEY OF REDISPERSION LITERATURE. . . . .	88
4.1	Introduction. . . . .	88
4.2	Review of Redisperison Work . . . . .	89
4.3	Redisperison and Sintering Models . . . . .	104
4.3-1	Crystallite Migration Model . . . . .	105
4.3-2	Atomic Migration Model . . . . .	107
4.3-3	Atom-Particle Migration Model. . . . .	110
4.3-4	Comparison of the Different Models . . . . .	111
4.4	Proposed Redisperison Procedure . . . . .	113
CHAPTER 5.	EXPERIMENTAL STUDIES OF PRETREATMENT AND REDISPERSION OF . .	116
	SUPPORTED METAL CATALYSTS	
	REVIEW . . . . .	116
5.1	Introduction. . . . .	116
5.2	Review of Catalyst Preparation. . . . .	116
5.2-1	Impregnation . . . . .	116
5.2-2	Precipitation . . . . .	117
5.2-3	Ion-Exchange . . . . .	117
5.3	Catalyst Preparation, Pretreatment and Redisperison . .	117
	Procedures of Other Investigators	
	EXPERIMENTAL . . . . .	121
5.4	Catalyst Preparation and Pretreatment . . . . .	121
5.5	Adsorption of Hydrogen on $Al_2O_3$ Support . . . . .	122
5.6	Adsorption of Hydrogen on Fresh Pt/ $Al_2O_3$ Catalyst . . .	124

Page

5.7	Effect of Reduction Conditions on the Dispersion . .	127
5.8	Effect of Treatment in Oxygen on the Dispersion . .	131
5.9	Discussion and Conclusion . . . . .	136
CHAPTER 6.	PROPOSED EXPERIMENTS . . . . .	140
	ACKNOWLEDGMENTS . . . . .	146
	REFERENCES . . . . .	147
	APPENDIX A CALIBRATION OF BURETTES . . . . .	151

## LIST OF FIGURES

<u>Figure</u>		<u>Page</u>
2.1	Flow Diagram of the Sorptometer . . . . .	8
2.2	Front View of the Sorptometer . . . . .	10
2.3	Calibration Arrangement for the Soap Bubble Flowmeter . . . . .	13
2.4	Standard Calibration Cell . . . . .	15
2.5	Peaks for Calibrating the Calibration Valve Loop . . . . .	20
2.6	Desorption and Calibration Peaks Used for Establishing a Point on the Adsorption Isotherm . . . . .	28
2.7	The BET Plot, $Al_2O_3$ Support . . . . .	29
2.8	Schematic Diagram of Manometer for the Measurement of the Saturation Pressure of Nitrogen at the Temperature of the Liquid Nitrogen Bath . . . . .	33
2.9	Arrangement for Preparation of Manometer. . . . .	34
3.1	Chemisorption Apparatus . . . . .	54
3.2	Sample Tube . . . . .	57
3.3	Mercury Cut-off . . . . .	61
3.4	Arrangement of Vacuum Pumps . . . . .	63
3.5	McLeod Gauge . . . . .	65
3.6	Calibration of Zero Bulb Volume . . . . .	75
3.7	Hydrogen Adsorption Isotherm for the Catalyst . . . . .	79
5.1	Hydrogen Adsorption Isotherm for the $Al_2O_3$ Support . . . . .	123
5.2	Hydrogen Adsorption Isotherm for the Fresh Catalyst . . . . .	125
5.3	Effect of Reduction Conditions on Hydrogen Uptake . . . . .	128
5.4	Effect of Treatment in Oxygen on Hydrogen Uptake . . . . .	133
6.1	Proposed Activity Measurement Experiments . . . . .	145

## LIST OF TABLES

<u>Table</u>		<u>Page</u>
1.1	Dispersion as a function of Metal Crystallite Size . . . . .	2
2.1	Legend for Fig. 2.1 . . . . .	9
2.2	Calibration of the Soap Bubble Flowmeter . . . . .	14
2.3	Calibration of the Standard Cell . . . . .	16
2.4	Calibration of Attenuations. . . . .	18
2.5	Calibration of Calibration Valve Loops . . . . .	21
2.6	Sample Calculations for the Specific Surface Area . . . . .	24
2.7	Summary of Terms used in Surface Area Measurements . . . . .	30
2.8	Surface Area of Catalyst Supports. . . . .	36
3.1	Legend for Fig. 3.1. . . . .	55
3.2	Calibrated Volume of the Burettes. . . . .	58
3.3	Calibration of the Capillary Portion of the McLeod Gauge . . .	58
3.4	Calibration of the Bulb Portion of the McLeod Gauge. . . . .	69
3.5	Calibration of the McLeod Gauge. . . . .	71
3.6	Calibration of Zero Bulb Volume. . . . .	74
3.7	Platinum Dispersion, Surface Area and Crystal Size . . . . .	87
5.1	Data on Pt Dispersion for the Pt/ $Al_2O_3$ Catalyst . . . . .	126
5.2	Results of Effect of Reduction Conditions on the Pt. . . . .	129
5.3	Results of Effect of Oxygen Treatment on the Pt. . . . .	134
A.1	Calibration of Linear Burette (B'') . . . . .	152
A.2	Calibration of Small Burette (B')	153
A.3	Calibration of Large Burette (B) . . . . .	154

CHAPTER 1  
INTRODUCTION

Supported metal catalysts consist of small crystals of the metal dispersed on a porous support. For noble metals the metal content of these catalysts generally varies from 0.1 to 2% and metal crystallites vary in size from 200 nm or more to smaller than 1 nm.

These catalysts find wide industrial application as hydrogenation, dehydrogenation and oxidation catalysts. They provide effective utilization of the metal since a large fraction of the metal atoms are at the surface of the small metal crystallites and an increased resistance to agglomeration of the metal because the metal crystallites are physically separated by the non-metallic support.

Sintering, the agglomeration process with accompanying decrease of metal surface area, decreases the number of surface metal atoms per unit mass of metal, and thereby decreases the utilization of the metal. Table 1 shows the rapid decrease in dispersion, the ratio of surface metal atoms to total metal atoms, as metal crystallite size increases (1). The causes of sintering are not completely understood, however, excessive temperatures and certain environments have been found to enhance the sintering rates.

Several processes, among them treatment with oxygen, steam, and halogens have been found to achieve redispersion of the metal on the support. Obviously in situ redispersion is of considerable industrial importance as it prolongs the life of the catalyst. The purpose of this work is to study the redispersion aspects of supported metal catalysts. The ultimate objective is to find optimum redispersion conditions. Emphasis is on measuring



Table 1  
Dispersion as a function of  
Metal Crystallite Size\*

No. of atoms in edge of crystallite	Length of crystal edge, nm	Total number of atoms in the crystal	Number of surface atoms in the crystal	Dispersion
2	0.55	6	6	1
3	0.825	19	18	0.95
4	1.1	44	38	0.86
5	1.375	85	66	0.78
6	1.65	146	102	0.70
7	1.925	231	146	0.63
8	2.2	344	198	0.58
9	2.475	489	258	0.53
10	2.75	670	326	0.49
11	3.025	891	402	0.45
12	3.3	1156	486	0.42
13	3.575	1469	578	0.39
14	3.85	1834	678	0.37
15	4.125	2255	786	0.35
16	4.4	2736	902	0.33
17	4.675	3281	1026	0.31
18	4.95	3894	1158	0.30

\*Assuming an fcc crystal of octahedral shape

increases in metal surface area or decrease in mean crystallite size rather than on changes in catalytic activity for a particular reaction.

Metal surface area and average crystallite size were determined by hydrogen chemisorption. The BET surface area of supports was determined by nitrogen adsorption in a flow apparatus. The catalyst chosen for study was Pt/Al<sub>2</sub>O<sub>3</sub>.

Chapter 2 of this thesis describes the calibration of the Perkin-Elmer Sorptometer and the measurement of the support surface area. Both sintering and redispersion are expected to vary with support area and pore size distribution. Chapter 3 presents a review of relevant chemisorption studies on supported metals as well as a description of the BET apparatus used for the chemisorption measurement in this work. A sample calculation of dispersion and average particle size is also given in Chapter 3. Chapter 4 is a comprehensive summary of the literature on redispersion. Chapter 5 provides a review of relevant catalyst preparation and pretreatment procedures and also the primary experimental results of this work which pertains to degassing of the metal for reproducible adsorption measurements, reduction of the catalyst and preliminary redispersion measurements. Chapter 6 is devoted to suggested improvements in the current effort and recommendations for future work.

## CHAPTER 2

## SURFACE AREA OF SUPPORTS

## 2.1 Introduction

The specific surface area of porous solids is usually measured by physical adsorption of a gas on the surface. The essence of the technique is the determination of the number of molecules of the gas comprising a monolayer. With this number known the surface area is determined as the product of the number of molecules and the area occupied per molecule.

Since physical adsorption is a multilayer phenomena, determination of the gas volume comprising the monolayer becomes a matter of interpretation of the adsorption isotherm. A number of theories have been proposed (2), the most useful of which is that of Brunauer, Emmett and Teller (3). It is based on a simplified model and is open to criticism on a number of grounds; but it leads to an equation - the "BET equation" - which has proved remarkably successful in the calculation of the specific surface.

## 2.2 Specific Surface from the BET Plot

The BET plot is the graphical representation of the BET equation:

$$\frac{p}{v_{\text{ads}}(p_0 - p)} = \frac{c-1}{v_m c} \frac{p}{p_0} + \frac{1}{v_m c} \quad (2.1)$$

where the measured variables are

$p$  = partial pressure of the adsorbed gas

$p_0$  = saturation pressure of the adsorption gas over the solid sample at the temperature of adsorption

$v_{\text{ads}}$  = total volume (STP) of adsorbed gas on the surface of adsorbent

and where:

$c$  = constant expressing the net adsorption energy

$v_m$  = volume (STP) of adsorbed gas when the entire adsorbent surface is covered with a monomolecular layer

With  $v_m$  and  $c$  constant for a given system, a plot of  $\frac{P}{v_{ads}(P_0 - P)}$  versus

$\frac{P}{P_0}$  is thus a straight line with slope

$$\alpha = \frac{c-1}{v_m c} \quad (2.2)$$

and intercept

$$\beta = \frac{1}{v_m c} \quad (2.3)$$

From the plot (Fig. 2.7), the slope and intercept can be evaluated graphically.

From Eq. 2-2 and 2-3, the following expression can be obtained for  $v_m$ :

$$v_m = \frac{1}{\alpha + \beta} \quad (2.4)$$

Once  $v_m$  is known, the total area of the sample can be calculated with the help of the value of the area covered by unit volume (STP) of adsorbate molecule:

$$s = v_m s_0 \quad (2.5)$$

where:

$s$  = the total area of sample

$s_0$  = area covered by unit volume (STP) monolayer of adsorption gas calculated from cross-sectional area of adsorbate molecule

The specific surface area of the sample,  $s_s$ , can be calculated using the following equation:

$$s_s = \frac{s}{w} = \frac{v_m s_0}{w} \quad (2.6)$$

where:

$w$  = the weight of the sample

For comparison of the results for different catalysts, it has become standard procedure to employ nitrogen at its normal boiling point (-195.8°C) as the adsorption gas.

### 2.3 Criticisms of the BET Model

A number of criticisms have been levelled at the BET model (4). The model assumes that the surface is energetically uniform, i.e. that all adsorption sites are exactly equivalent, but there is much evidence that the surface of most solids is heterogeneous in an energetic sense. A further criticism of the model is that it neglects horizontal interactions between the molecules within the adsorbed layer, and takes into account only vertical interactions. It has also been questioned whether the molecules in all layers after the first should be treated as equivalent. It is expected that the adsorption potential would diminish as the distance from the surface increases. Finally, the model assumes that the number of adsorbed molecular layers becomes infinite when the saturation pressure is reached. However in fairly numerous cases, the width of pores, cracks and capillaries of the adsorbents set a limit to the maximum number of layers that can be adsorbed even at saturation pressure.

Irrespective of all the assumptions involved in the BET model, it has proven remarkably successful in the calculation of surface area of solids and thus has been used for the present work.

### 2.4 Adsorption Measurements by the Continuous Flow Technique

In the present work, the adsorption measurements are made using the Perkin-Elmer Shell Model 212D Sorptometer which utilizes the continuous flow technique (5). Because the instrument was first used in this work, the calibrations are presented in detail for the convenience of future users.

#### 2.4-1 Principal Steps Outlining the Technique (6)

A known mixture of nitrogen and helium is passed over a sample and the effluent is monitored by a thermal conductivity detector. With the gas

mixture flowing, the sample is cooled to liquid nitrogen temperature. The cooling sample adsorbs a certain amount of nitrogen from the gas stream, and the resultant dilution of the effluent is indicated on the recorder chart as a peak, the area of which is proportional to the volume of nitrogen adsorbed. After adsorption equilibrium is established, the recorder pen returns to its original position. The liquid nitrogen bath is then removed from the sample tube. As the sample warms the adsorbed gas is evolved, enriching the effluent. A desorption peak, which is in the reverse direction of the adsorption peak, is produced on the recorder chart. When desorption is complete, a known volume of nitrogen is added to the nitrogen-helium stream, and the resulting calibration peak is recorded.

By comparing the areas of the desorption and calibration peaks, the volume of nitrogen adsorbed by the sample can be calculated. By repeating the measurement with different  $N_2/He$  ratios, an adsorption isotherm can be plotted. From the adsorption isotherm, the surface area of the sample can be found using the BET plot.

#### 2.4-2 Description of the Apparatus

Fig. 2.1 represents a schematic flow diagram of the apparatus, and a front view of the Sorptometer with all control knobs is shown in Fig. 2.2. The terminology used in Fig. 2.1 is explained in Table 2.1. The carrier (He) and adsorption ( $N_2$ ) gases are regulated as they enter. The gases are mixed in the mixing tank and are then passed through a cold trap which condenses any trace impurities. After leaving the trap, the gases enter the reference side of the detector. The detector consists of four tungsten filament thermal conductivity cells arranged as a Wheatstone bridge.

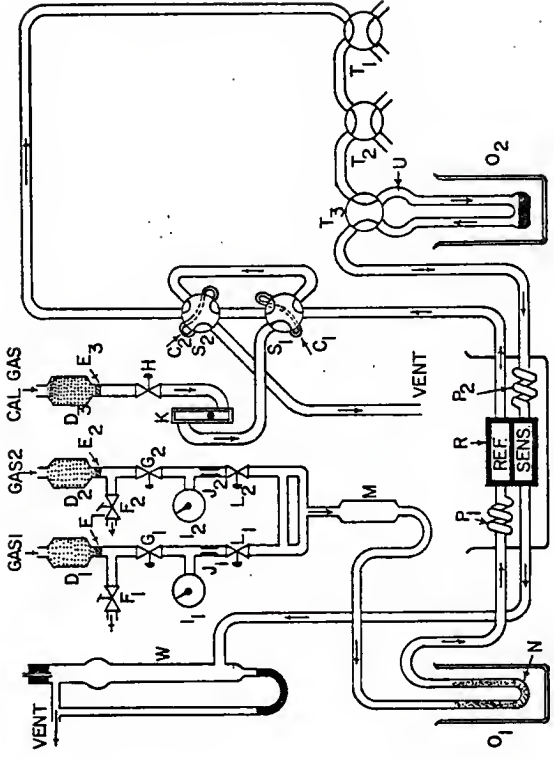


Fig. 2.1 Flow Diagram of the Sorptometer

Table 2.1  
Legend for Fig. 2.1

Gas 1	-	Adsorbate (nitrogen) inlet port
Gas 2	-	Carrier (helium) inlet port
Cal. Gas	-	Calibration gas inlet port
W	-	Soap bubble flowmeter
D1, D2, D3	-	Dryers
E1, E2, E3	-	Filter discs
F1, F2	-	Toggle valves
G1, G2	-	Pressure regulators
H	-	Needle valve
I1, I2	-	Pressure gauges
J1, J2	-	Restrictors
K	-	Flowmeter
L1, L2	-	Gas shut off valves
M	-	Mixing tank
S1, S2	-	Calibration valves (shown in "Charge" position)
C1, C2	-	Calibration valve loops
N	-	Cold trap
O1, O2	-	Dewar flasks
T1, T2, T3	-	Sample bypass valves
U	-	Sample tube
Q	-	Constant temperature bath
P1, P2	-	Heat exchangers
R	-	Detector



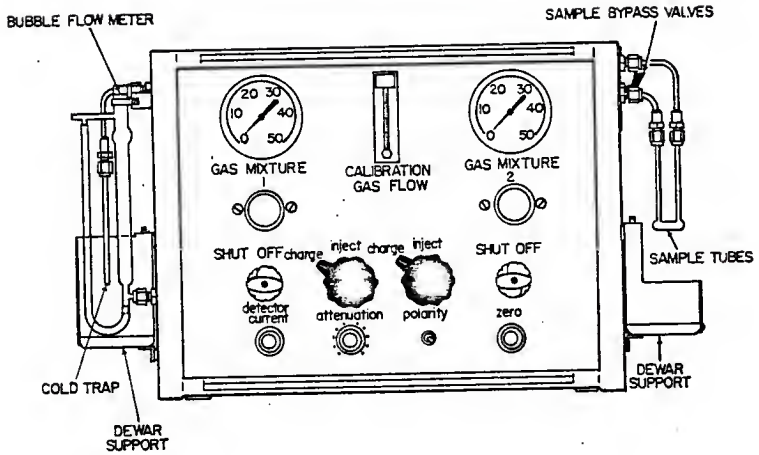


Fig. 2.2 Front View of the Sorptometer

Leaving the reference side of the detector, the gases flow through two calibration valves. With the valves in the CHARGE position, the gases flow through the sample manifold plumbing to the sensing side of the detector and out through the soap bubble flowmeter. The flowmeter is used for accurate measurement of gas flow rates. The series connection of the calibration valves permits the injection of the contents of both calibration loops into the system when the valves are in the INJECT position. The sample tube manifold permits the handling of multiple samples conveniently.

As long as the concentration of gas flowing through the reference and sensing thermal conductivity cells of the detector remains unchanged, the Wheatstone bridge is balanced, and the recorder output is zero. During sample adsorption or desorption, however, the concentration of the gas stream entering the sensing side of the detector changes. This causes a change in the resistance of the sensing elements of the conductivity cells, which unbalances the Wheatstone bridge, and produces an output signal. The signal is fed to a potentiometric recorder through an attenuator. The attenuator permits decreasing the amplitude of the signal from the detector bridge.

#### 2.4-3 Preliminary Calibrations

Before any surface area calculations are made, the volumes of the soap bubble flowmeter and the calibration valve loops must be known as well as the exact values of the attenuation factors. The calibration valve loops are calibrated against the standard cell, thus the exact volume of the standard cell must be known. These calibrations are performed as described below.

#### 2.4-3a Calibration of the Soap Bubble Flowmeter

Figure 2.3 shows the arrangement for calibration. The flowmeter was thoroughly cleaned and dried. It was filled with mercury then flamed and tapped to remove entrapped air and moisture. The weight of the mercury between the two reference marks was found and from the density of mercury at the temperature of measurement, the volume of the flowmeter was calculated. The results are listed in Table 2.2.

#### 2.4-3b Calibration of the Standard Cell

The standard cell is shown in Fig. 2.4. The lower part of the U-tube is the volume to be calibrated. The standard cell was thoroughly cleaned, dried and weighed. It was filled with mercury to a level slightly above the stopcocks, and flamed and tapped to remove entrapped air or moisture. The stopcocks were closed and the excess mercury above the stopcocks was drawn off. The cell was weighed again. From the net weight of mercury, and its density at the operating temperature, the volume of the standard cell was calculated. The results are listed in Table 2.3.

#### 2.4-3c Calibration of Attenuations

Seven attenuation positions, X1, X2, X4, X8, X16, X32 and X64 are incorporated in the Sorptometer. X1 and X64 provide the maximum and the minimum sensitivity of the output signal respectively. Since different attenuation positions may be used for desorption and calibration peaks, the successive factors by which different attenuation levels decrease the output signal must be known. These attenuation positions were calibrated as described below.

A fixed volume of nitrogen, either from the calibration valve loops or from a desorbing sample, was added to the helium-nitrogen stream flowing

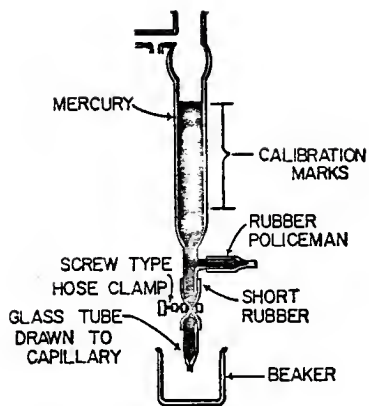


Fig. 2.3 Calibration Arrangement for the Soap Bubble Flowmeter.

Table 2.2  
Calibration of the Soap Bubble Flowmeter

S.No.	Mass of Hg, g	Temperature, °F	Density of Hg, g/cm <sup>3</sup> (7)	Volume, cm <sup>3</sup>	Average volume, cm <sup>3</sup>
1.	272.0	73	13.5385	20.0908	
2.	271.4	73	13.5385	20.0465	20.0699
3.	271.8	72	13.5409	20.0725	

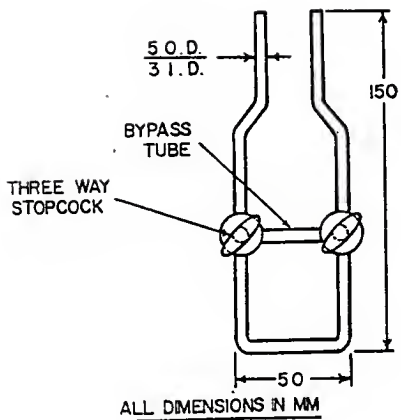


Fig. 2.4 Standard Calibration Cell

Table 2.3  
Calibration of the Standard Cell

S.No.	Mass of Hg, g	Temperature, °F	Density of Hg, g/cm <sup>3</sup> (7)	Volume, cm <sup>3</sup>	Average volume, cm <sup>3</sup>
1.	14.25160	75	13.5360	1.0529	1.0562
2.	14.34064	75	13.5360	1.0594	

through the sorptometer. The resulting output signal, in the form of a peak on the chart, was recorded at a particular attenuation position. The experiment was repeated with the same fixed volume of nitrogen introduced into the system, and the output peak was recorded at the next attenuation position. The ratio of the areas of the two peaks was noted. By introducing different fixed volumes of nitrogen, the ratios of the areas of the output peaks for successive attenuation positions were found. It was not possible to calibrate all attenuation positions with a single fixed volume because peaks having amplitude less than 30-40% of the recorder chart width were not considered because of loss of accuracy.

Since the ratios of the attenuation values rather than the absolute values were used in the calculations, attenuation level X2 was selected as reference and all other levels were calibrated against this. Allotting a value of 2 to X2 level and knowing the ratio of areas of the output peaks for successive attenuation levels, the values for other attenuation levels were found and are listed in Table 2.4. These values correspond to the average of six experimental runs for each calibration position.

#### 2.4-3d Calibration of the Calibration Valve Loops

The calibration valve loops provide known reproducible volumes of adsorbate gas for comparison with unknown volumes desorbed from samples. These loops were calibrated as follows.

The calibrated standard cell was filled with nitrogen by connecting it to one set of sample ports. With the nitrogen supply on, the sample bypass valve was turned to the SAMPLE position. After the cell was filled with nitrogen, both stopcocks of the cell were turned to the close position. The sample bypass valve was turned back to the BYPASS position and the



Table 2.4  
Calibration of Attenuations

Attenuation position	Factor by which Output Signal from Detector is decreased
X2	2.000
X4	4.054
X8	8.299
X16	17.319
X32	36.630
X64	76.886

helium supply was turned on. The CALIBRATION GAS FLOW needle valve was opened to fill the calibration valve loops with nitrogen. The sample bypass valve was turned to the SAMPLE position to purge air trapped above the charged volume in the standard cell. Thereafter both stopcocks of the standard cell were turned to open position, flushing the nitrogen from the standard cell into the system and the resultant peak was obtained on the recorder chart. The above procedure was repeated three times and the series of peaks recorded. Then one of the calibration valves was turned to the INJECT position, thereby flushing the nitrogen into the system and the peak was recorded. The procedure was repeated three times for both calibration valve loops. The standard cell peaks were recorded at attenuation position X16 and the calibration valve loop peaks at X4. The volume of the calibration valve loops was found from:

$$V_{\text{cal}} = V_{\text{cell}} \times \frac{A_{\text{cal}}}{A_{\text{cell}}} \times \frac{At_4}{At_{16}}$$

where:

$V_{\text{cal}}$  = the volume of nitrogen in the calibration valve loop

$V_{\text{cell}}$  = the volume of nitrogen in the standard cell (from Table 2.3)

$A_{\text{cal}}$  = the average peak area produced by nitrogen in the calibration valve loop

$A_{\text{cell}}$  = the average peak area produced by nitrogen in the standard cell

$\frac{At_4}{At_{16}}$  = the ratio of the attenuation levels 4 and 16 (from Table 2.4)

One set of peaks obtained from the standard cell (S.C.), calibration valve loop 1 (CL1) and calibration valve loop 2 (CL2) is shown in Fig. 2.5. The values of the volumes of calibration valve loops are listed in Table 2.5.

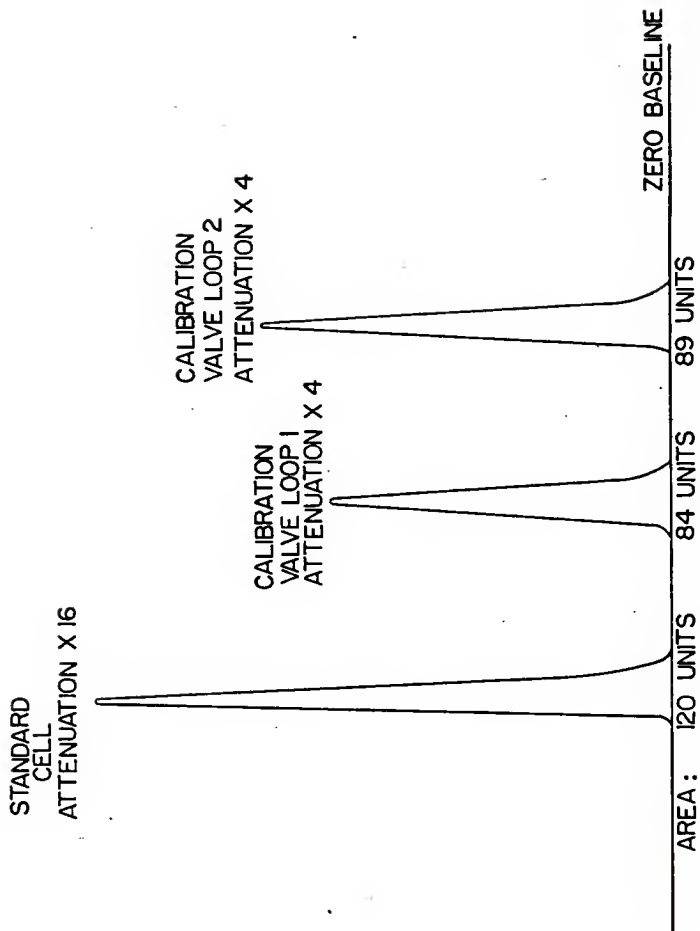


Fig. 2.5 Peaks for Calibrating the Calibration Valve Loops

Table 2.5  
Calibration of Calibration Valve Loops

	Peak Areas*			Average Peak Area	Attenuation	Volume, cm <sup>3</sup>
	1	2	3			
S.C.	120	116	124	120	16	1.0562
CL1	84	84	78	82	4	0.1689
CL2	89	95	93	92	4	0.1895

\* The peak areas are in arbitrary units

#### 2.4-3e Sample Preparation and Adsorption-Desorption Procedure

Before any sample was used for surface area measurements, it was degassed in flowing helium at temperature of 475-500°C for 2 hours to remove adsorbed gases. The weight of the degassed sample used for surface area measurements was noted.

A Dewar flask filled with liquid nitrogen was placed around the cold trap in the Sorptometer. The liquid nitrogen cold trap removed any moisture or contaminants from flowing gases. The helium supply was turned on and the GAS MIXTURE 2 pressure regulator was set to provide a flow rate of 25-28 ml/min. The flow rate of the helium was measured by noting the time required for one soap bubble to travel between two indices on the soap bubble flowmeter.

The sample ports were purged and the sample tube placed in position. The nitrogen supply was then turned on and the GAS MIXTURE 1 pressure regulator adjusted to provide a total gas flow rate of approximately 30-40 ml/min. The total flow rate was measured by the soap bubble flowmeter.

The sample bypass valve was switched to SAMPLE position and the recorder turned on. The Attenuation switch was turned to recorder input short (S) position and the ZERO switch on the recorder was adjusted to obtain a zero baseline. With the Attenuation switch in the bridge (B) position, the DETECTOR CURRENT control was reset to give a 40% deflection of the recorder pen. With the Attenuation switch in the position of least sensitivity (X64), the recorder zero baseline was checked, and if necessary, was adjusted with the ZERO control. The same procedure was repeated for lower attenuations until the recorder was zeroed at X1 attenuation.

With the Attenuation switch in some suitable position, a Dewar flask filled with liquid nitrogen was placed around the sample tube and the adsorption peak was recorded. The sample was allowed to reach equilibrium as indicated by the recorder pen returning to zero. The POLARITY setting was reversed and the zero readjusted. The Dewar was removed and a water bath applied to the sample tube. The desorption peak was recorded. The water bath around the sample tube helped in speeding up the desorption process and hence prevented excessive tailing of the desorption peak. A combination of calibration valve loops, which produced a peak area approximately equivalent to that of the sample, was selected. The calibration valves were set to the INJECT position and the resultant calibration peak recorded.

The data obtained by the above procedure provided one point on the adsorption isotherm i.e.  $p$  vs  $v_{ads}$ . A minimum of three points were used for the BET plot in this work. The other points were established by varying the adsorption gas ( $N_2$ ) flow rates and repeating the above steps.

The data taken and the surface area calculations performed for one of the samples are shown in Table 2.6 and Fig. 2.6 and 2.7. Table 2.7 lists the summary of terms used in surface area measurements.

#### 2.5 Measurement of the Saturation Pressure of Nitrogen at the Temperature of Liquid Nitrogen

In an ideal case, the temperature of liquid nitrogen is  $-195.8^\circ\text{C}$  and the corresponding saturation pressure is 760 mm Hg. However, this is never the case in actual practice for two reasons: (1) liquid nitrogen always contains trace impurities, e.g., oxygen dissolved from air, (2) the barometric pressure is usually different from 760 mm Hg. Thus, if accurate values of the saturation pressure of nitrogen are necessary, two possibilities exist:

Table 2.6

## Sample Calculations for the Specific Surface Area

SAMPLE: Amoco Active Carbon				
Degassing time: 2 hours		Degassing temperature: 500°C		
SYMBOL	MEASUREMENT OR CALCULATION	DIMENSION		RESULT
$w_2$	Mass of Sample	tube + sample: 12.35022		grams
$w_1$		tube: 12.34551		grams
$w$		sample: 0.00471		grams
$P_T$	Barometric pressure at $T^\circ\text{K}$ temperature	mmHg		730.377
$T_R$	Room temperature	$^\circ\text{K}$	273.16 + 23.0 =	296.16
$f$	Correction factor for STP conditions: $f = \frac{P_T \cdot 273}{760 \cdot T_R} = 0.3595 \frac{P_T}{T_R}$		0.3595 $\frac{730.377}{296.16}$ =	0.8866
	Inlet pressure of carrier gas (Helium)	in. Hg		25
$t_c$	Soap film transit time for He flow	sec.		43.0
$v_{\text{meter}}$	Volume of bubble flow meter between two calibration marks	ml.		20.0699
$F_c$	Flow rate of the carrier gas (helium): $F_c = \frac{60}{t_c} v_{\text{meter}}$	ml/min		28.0045

Table 2.6 continued

SYMBOL	MEASUREMENT OR CALCULATION	DIMENSION		RESULT	
$p_o$	Saturation pressure of $N_2$ at the temperature of the liquid $N_2$ used	mmHg	average <input type="checkbox"/> measured <input checked="" type="checkbox"/>	748	
$s_o$ (6)	Area covered by one cc (STP) monolayer nitrogen	$m^2/ml$		4.3700	
SYMBOL	MEASUREMENT OR CALCULATION	DIMENSION	FIRST RUN	SECOND RUN	THIRD RUN
	Inlet pressure of the adsorption gas ( $N_2$ )	in.	5	17	30
$t_t$	Soap film transit time for total gas flow	sec.	39.4	35.5	31.6
$F_t$	Total ( $He + N_2$ ) flow rate: $F_t = \frac{60}{t_t} v_{\text{meter}}$	ml/min	30.5633	33.9210	38.1074
$F_a$	Adsorption gas ( $N_2$ ) flow rate $F_a = F_t - F_c$	ml/min	2.5588	5.9165	10.1029
$A_{\text{des}}$	Area of the desorption peak	counts	221	249	236
$At_{\text{des}}$	Attenuation		32	32	32
$v_{\text{cal}}$	Volume of the injection tube used	ml.	0.3584	0.3584	0.3584
$A_{\text{cal}}$	Area of the calibration peak	counts	192	171	162
$At_{\text{cal}}$	Attenuation		4	4	4



Table 2.6 continued

SYMBOL	MEASUREMENT OR CALCULATION	DIMENSION	FIRST RUN	SECOND RUN	THIRD RUN
$v_{ads}$	Volume of adsorbed gas $v_{ads} = \frac{A_{des}}{A_{cal}} v_{cal} \frac{A_{des}}{A_{cal}} \frac{A_{des}}{A_{cal}}$	ml	3.7274	4.7154	4.7176
$v_{ads}$	Volume of adsorbed gas corrected to standard temperature pressure: $V_{ads} = v_{ads}^f$	ml	3.3048	4.1807	4.1826
$p$	Partial pressure of nitrogen $p = \frac{F_a}{F_t} P_T$	mmHg	61.1481	127.3923	193.6350
$p/p_o$	Relative pressure of nitrogen		0.0817	0.1703	0.2589
	$(p_o - p)$	mmHg	686.8519	620.6077	554.3650
	$V_{ads} (p_o - p)$	ml·mmHg	2269.9082	2594.5746	2318.6870
	$\frac{p}{V_{ads} (p_o - p)}$	ml <sup>-1</sup>	0.0269	0.0491	0.0835

THREE-POINT CALCULATION			
SYMBOL	MEASUREMENT OR CALCULATION	DIMENSION	RESULT
$\alpha$	The slope of the BET plot		0.2933
$\beta$	y-intercept of the BET plot		0.0025

Table 2.6 continued

SYMBOL	MEASUREMENT OR CALCULATION	DIMENSION	RESULT
$V_m$	Volume of adsorbed nitrogen for a monolayer: $V_m = \frac{1}{\alpha + \beta}$		3.3807
S	$V_{m,0}^s$	$m^2$	14.7737
$S_s$	Specific surface area of the sample $S_s = \frac{V_{m,0}^s}{w}$	$m^2/g$	3137

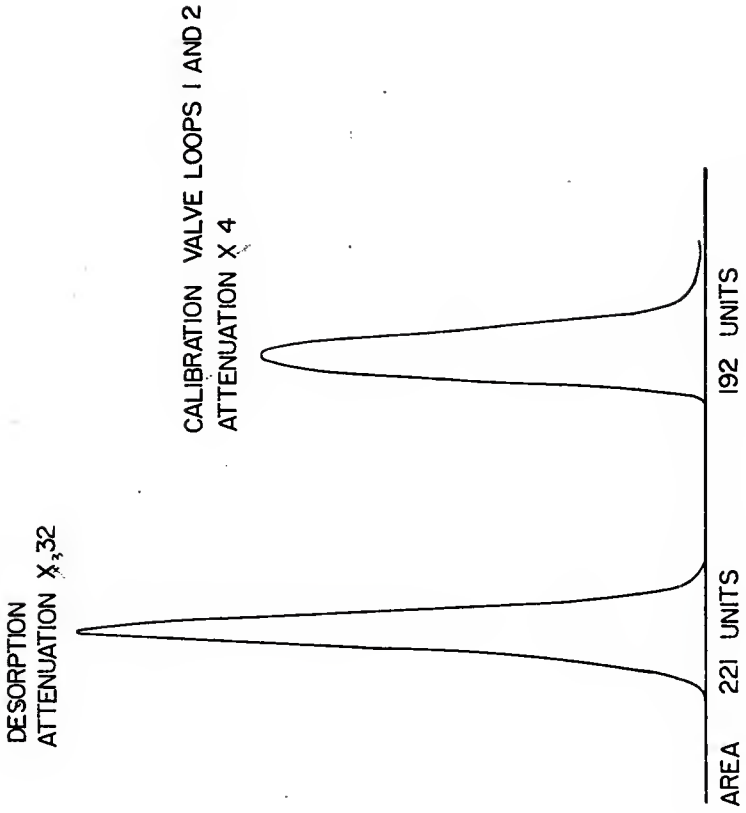


Fig. 2.6 Desorption and Calibration Peaks Used for Establishing a Point on the Adsorption Isotherm

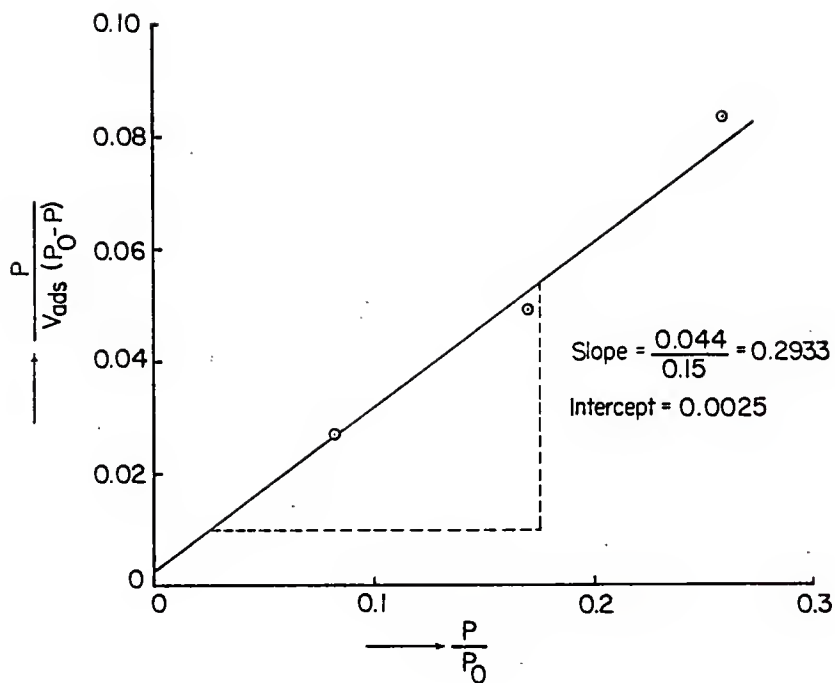


Fig. 2.7 The BET Plot,  $Al_2O_3$  Support

Table 2.7

Summary of Terms used in Surface Area Measurements

SYMBOL	DIMENSION	DEFINITION
$w_2$	g	Mass of the sample tube + sample
$w_1$	g	Mass of the sample tube
$w$	g	Mass of the sample
$t_R$	°C	Room temperature
$T_R$	°K	Room Temperature ( $T_R = 273 + t_R$ )
$P_T$	mmHg	Barometric pressure in °K at $T_R$ °K room temperature
$P_B$	mmHg	Barometric pressure reduced to 0° C
$t_c$	sec.	Soap film transit time for the carrier gas flow
$t_t$	sec.	Soap film transit time for the total (helium + nitrogen) gas flow
$v_{\text{meter}}$	ml	Volume of the bubble flow meter between two calibration marks
$F_c$	ml/min.	Carrier gas (helium) flow rate
$F_t$	ml/min.	Total (helium + nitrogen) flow rate
$F_a$	ml/min.	Adsorption gas (nitrogen) flow rate
$A_{\text{des}}$	Counts or $\text{cm}^2$	Area of the desorption peak
$v_{\text{ads}}$	ml	Volume of the adsorbed gas at $T_R$ and $P_T$
$V_{\text{ads}}$	ml	Volume of the adsorbed gas at STP conditions
$A_{\text{cal}}$	$\text{cm}^2$ or counts	Area of the calibration peak

Table 2.7 continued

SYMBOL	DIMENSION	DEFINITION
$v_{cal}$	ml	Volume of the calibration peak
$V_{cal}$	ml	Volume of the calibration peak at STP conditions
$p$	mmHg	Partial pressure of the adsorption gas
$p_o$	mmHg	Saturation pressure of the adsorption gas at the temperature of the coolant
$s_o$	$m^2/cc$	Area of one cc $N_2$ as a monolayer
$a$		Slope of the BET plot
$b$		y-intercept of the BET plot
$V_m$	ml	Volume of $N_2$ adsorbed as a monolayer (STP)
$S$	$m^2$	Area of $v_m$ as a monolayer
$S_s$	$m^2/g$	Specific surface area of the sample

- (1) To measure the temperature of liquid nitrogen bath and find the saturation pressure of nitrogen from proper tables.
- (2) To measure directly the saturation pressure of nitrogen at the temperature of the liquid nitrogen bath.

The saturation pressure of nitrogen varies from 760 mm to 900 mm Hg over the temperature range  $77.36^{\circ} - 78.83^{\circ}\text{K}$ . To have an accuracy of 1 mm Hg in the saturation pressure of nitrogen, a temperature measuring device with a precision of  $0.01^{\circ}\text{K}$  is required. Considering the practical difficulties involved in the first method, the second method was used for measuring saturation pressure of nitrogen.

A schematic diagram of the glass apparatus constructed for measuring the saturation pressure of nitrogen at the temperature of liquid nitrogen used is shown in Fig. 2.8.

#### 2.5-1 Construction of the Manometer

The Manometer was filled with mercury to approximately 50 cm in both legs. Then the arrangement shown in Fig. 2.9 was employed for the evacuation and nitrogen filling process. The three way stopcock was positioned to connect the manometer legs to the vacuum pump. While legs A and B of the manometer were being evacuated, the mercury column and the other glass tubes were heated to remove air and moisture from the walls. After evacuating for a sufficiently long time, leg A of the manometer was sealed off.

The position of the three way stopcock was switched to connect leg B of the manometer to the nitrogen system. Nitrogen was purified by passing it over copper turnings at  $350^{\circ}\text{C}$  to remove oxygen and then through a liquid nitrogen trap to remove moisture. The space above the mercury in leg B was filled with purified nitrogen to a pressure of approximately 900 mm Hg.

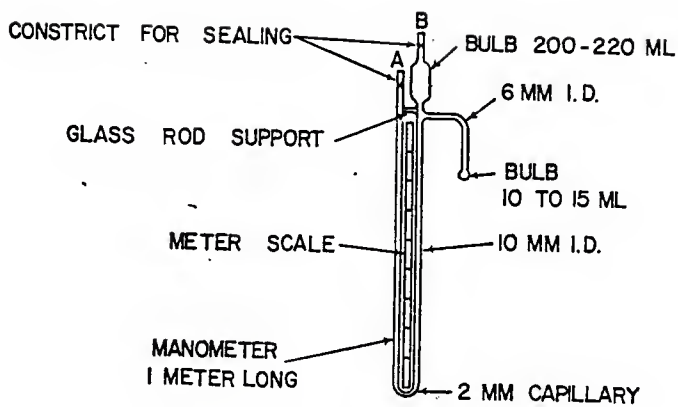


Fig. 2.8 Schematic Diagram of Manometer for the Measurement of the Saturation Pressure of Nitrogen at the Temperature of the Liquid Nitrogen Bath.



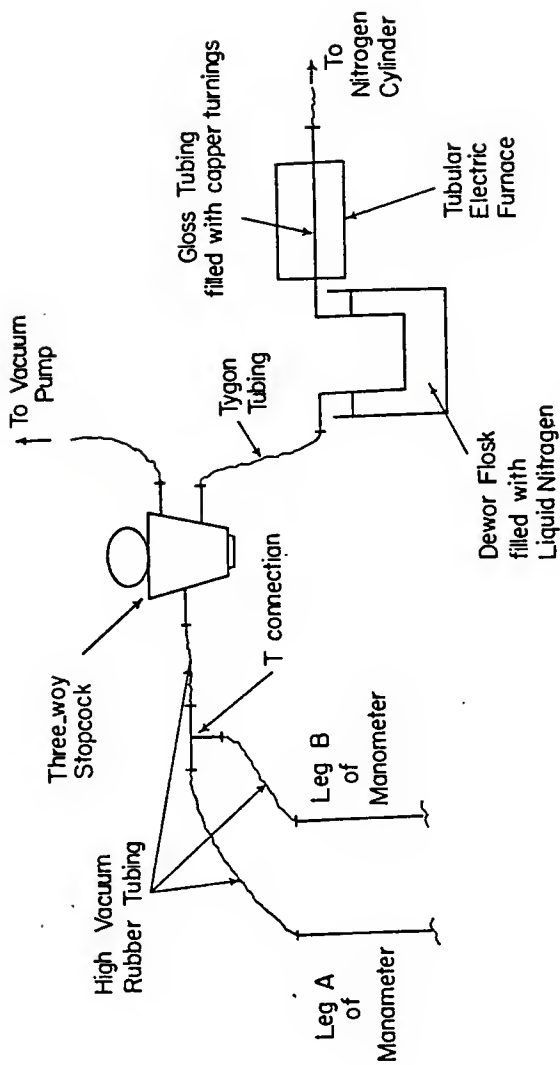


Fig. 2.9 Arrangement for Preparation of Manometer

By switching the position of the three way stopcock, leg B of the manometer was evacuated. The process of evacuation and filling with nitrogen was repeated twice to ensure that leg B was filled with pure nitrogen only and did not contain air. Leg B could not be sealed while above atmospheric pressure. The pressure in leg B was reduced to approximately atmospheric conditions by cooling the bulb on the manometer by immersing it in a liquid nitrogen bath and by cooling leg B of the manometer by passing liquid nitrogen through a tube wrapped around leg B.

#### 2.5-2 Use of the Manometer

The bulb on the manometer is immersed in the liquid nitrogen. Nitrogen condenses inside the bulb and thus its saturation pressure is established. The difference in height of the two legs of the manometer gives the saturation pressure directly.

#### 2.6 Results obtained from Surface Area Measurements

The sources of catalyst supports, the supplier's reported values of the surface areas, and the experimentally measured values are listed in Table 2.8.

#### 2.7 Discussion of the Results

Surface areas as low as  $1 \text{ m}^2/\text{g}$  and as high as  $3000 \text{ m}^2/\text{g}$  have been measured. It should be noted that with the exception of the Amoco active carbon the values supplied by the manufacturer are nominal values. The results are in excellent agreement with the reported values. In addition to experimental errors involved in adsorption measurements and personal error involved in measuring the peak areas by the planimeter (each peak area was measured 5 times and an average value was used in the calculations), a factor contributing to the discrepancy in the results might be the different methods used for surface area determinations, i.e. static method, flow method or gravimetric method, for reported values and in the present work.

Table 2.8  
Surface Areas of Catalyst Supports

Catalyst Support	Surface Area, $m^2/g$		% Deviation
	Reported Value	Measured Value	
Amoco Active Carbon	3070	3137	+2
Davison Grade 979 Alumina	400	427	+7
Davison Grade 980-25 Alumina	325	312	-4
Norton SA-5102 Alumina	0.7-1.3	0.86	—
Kaiser Alumina 20	—	322	—

## 2.8 Conclusions

Considering the excellent agreement between the experimental results and the reported values over a wide range of surface areas, it is concluded that surface areas can be found within a very reasonable accuracy using the Sorptometer.

## CHAPTER 3

## CHEMISORPTION ON SUPPORTED METAL CATALYSTS

REVIEW

## 3.1 Introduction

The adsorption selectivity that is required for the measurement of the metal surface area in a supported metal catalyst is achieved by measuring the uptake of a gas which is chemisorbed on the metal surface but which is absorbed on the support only to a relatively small extent. The method requires that the adsorbate forms a chemisorbed monolayer and that there exist a simple relation between the number of molecules adsorbed at saturation and the number of surface atoms. The chemisorption of hydrogen, oxygen and carbon monoxide have been used extensively for surface area measurements.

## 3.2 Methods Used for Chemisorption Studies

Three methods are available for determination of chemisorption capacities of supported metal catalysts:

- (1) static, volumetric adsorption system
- (2) flow adsorption system
- (3) gravimetric balance method.

The volumetric approach provides greater accuracy as compared to the dynamic method because it involves degassing of the samples at high vacuum levels and permits sufficient time for adsorption equilibrium to be established. The main disadvantage is the time consuming nature of the measurements due to the large time requirement to achieve high vacuum levels and because two uptake determinations, one of gas adsorbed on the metal and one to account for adsorption effects on the support are needed.

The flow adsorption method is less time consuming and simpler in operation because it does not require a high vacuum system and it is claimed (8, 9,10) that a blank correction for adsorption on the support is not needed. But this method is subject to experimental errors due to the possibility of incomplete displacement of the hydrogen used for reduction and the short time available for equilibration of the adsorbate with the metal surface (11).

The important advantage of a gravimetric apparatus is that continuous measurements of extremely small changes in the adsorption system can be made. In addition no dead space corrections are necessary (11). On the other hand, it involves high cost and severe operational problems (12). The accuracy of the method is in proportion to the molecular weight of the adsorbate used.

The volumetric adsorption method was selected for the chemisorption measurements in this work.

### 3.3 Characterization of Dispersion by Chemisorption Methods

The basic principle of measuring the specific adsorption on a supported metal surface is to select adsorbate and adsorption parameters that minimize adsorption on the support and facilitate full monolayer coverage on the metal. Corrections for the adsorption on the support can be made by measuring adsorption on the support only and by subtracting this value from the total adsorption on the catalyst. The net adsorption per unit weight of catalyst is a measure of metal dispersion for a given metal content. This net adsorption per unit weight of catalyst is converted to a ratio of number of atoms or molecules of gas adsorbed per metal atom present in the sample,  $(A/M)$ , so as to have a measure of dispersion which is independent of metal concentration. This ratio is the most significant measure of metal

dispersion since it can be obtained without specific knowledge of surface coverage or adsorption mechanism and without any assumptions regarding these two points. By assuming adsorption corresponding to a particular temperature and pressure as representative of a full monolayer and also assuming the adsorption stoichiometry, i.e., ratio of adsorbate atoms adsorbed to surface metal atoms, the ratio A/M is converted into the ratio of the number of surface metal atoms to the number of total metal atoms ( $M_s/M$ ) using

$$\frac{M_s}{M} = \frac{A}{M} \cdot \frac{M_s}{A} \quad (3.1)$$

where:

M total number of metal atoms

$M_s$  = number of surface metal atoms

A = number of atoms or molecules of gas adsorbed.

$\frac{M_s}{M}$  can vary from 0 to 1, corresponding to "zero dispersion" (bulk metal) and "complete dispersion" (monolayer or particles with no interior atoms) respectively. By assuming the nature of the exposed Pt planes and the geometry of the crystallites, surface area and average particle size of the metal may be calculated from the ratio  $\frac{M_s}{M}$  as shown in Table 3.7.

### 3.4 Selection of Adsorbate

The main considerations for adsorbate choice are (1) physical adsorption is minimal and (2) adsorption stoichiometry is nearly constant over a wide range of crystallite size.

The amount of physical adsorption on a given adsorbent decreases with decreasing boiling point of the adsorbate, with decreasing pressure and with increasing temperature (13). Therefore, to minimize physical adsorption, adsorption should be carried out at the highest possible temperature and the lowest possible pressure with a low boiling adsorbate which is chemisorbed

readily by the metal with very little or no chemisorption occurring on the support. Hydrogen, oxygen and carbon monoxide meet most of these requirements and have been used extensively for chemisorption work.

#### 3.4-1 Hydrogen Chemisorption

Several studies of Pt surface area and mean crystallite size using hydrogen as the adsorbate have been made. Spenadel and Boudart (14) measured hydrogen chemisorption at 250°C and 240 mm Hg pressure on Pt black and on Pt/Al<sub>2</sub>O<sub>3</sub> catalyst and also determined the mean crystallite size for Pt/Al<sub>2</sub>O<sub>3</sub> catalyst by X-ray line broadening. By comparing the BET and the hydrogen chemisorption results for Pt black, an H/Pt<sub>s</sub> ratio of 1 was established (H denotes the atoms of hydrogen adsorbed and Pt<sub>s</sub> represents the surface Pt atoms). It was assumed that the surface properties of small Pt crystallites were the same as that of bulk metal and hence using a ratio of H/Pt<sub>s</sub> of 1, surface area and average crystallite size for Pt/Al<sub>2</sub>O<sub>3</sub> catalyst were calculated from the chemisorption data. The values were in good agreement with those determined by X-ray line broadening.

Adams, Benesi, Curtis and Meisenheimer (15) measured hydrogen chemisorption at 0°C on a Pt/SiO<sub>2</sub> catalyst and determined the mean crystallite size both by X-ray line broadening and electron microscopy. Mean crystallite size was calculated from the adsorption data again assuming an H/Pt<sub>s</sub> ratio of 1. Fairly good agreement was found between the adsorption, X-ray line broadening, and the electron microscopy results.

Wilson and Hall (16) studied hydrogen chemisorption on Pt/Al<sub>2</sub>O<sub>3</sub> under different sintering conditions. Hydrogen chemisorption values found by extrapolating 25°C isotherms to zero pressure were in direct proportion with the Pt surface area. Areas estimated from electron micrograph particle



size distributions showed that hydrogen chemisorption properly reflected the changes in metal surface area. The particle size distributions from the micrographs were consistent with  $H/Pt_s$  ratio equal to 1 over the wide range of dispersions studied.

Dorling, Burlace and Moss (17) measured hydrogen chemisorption in the same way as Wilson and Hall but estimated the mean crystallite size from x-ray line broadening by a more complex method. They obtained a mean size  $> 50 \text{ \AA}$  from line broadening, estimated the weight of metal detected and hence included the contribution of crystallites  $< 50 \text{ \AA}$  in diameter. The latter was taken to have a mean of  $25 \text{ \AA}$  on the basis of electron micrographs. The number of exposed Pt atoms calculated from crystallite size measurements compared reasonably well with the number of hydrogen atoms adsorbed thus yielding an  $H/Pt_s$  ratio of approximately 1.

Freel (18,19) measured hydrogen uptakes at  $25^\circ\text{C}$  and also obtained mean crystallite size by electron microscopy and line broadening techniques. The particle sizes calculated were in acceptable agreement if it was assumed that each surface platinum atom adsorbed one hydrogen atom ( $H/Pt_s = 1$ ).

The above studies support the one to one correspondence between  $H/Pt$  and  $Pt_s/Pt$ , accordingly implying  $H/Pt_s$  equal to 1. Maximum deviations observed are of the order of  $\pm 20\%$  for  $0.1 < Pt_s/Pt < 0.9$  (19). These deviations can be explained by the uncertainties in independent measurement of size, and the calculation of  $Pt_s$  when the mean size is known.

Adler and Keavney (20), Poltorak and Boronin (21), Zaidman et al. (22) and Weller and Montagna (23) have reported  $H/Pt_s$  values greater than 1 and in limit equal to 2 for finely dispersed platinum. Several reasons have been suggested for this (24), (i) there may be sources of oxygen in the

system giving higher hydrogen uptakes (ii) there may be a hydrogen spillover from the metal to the support. Such effects are more pronounced at lower metal loading due to the low uptakes. However, different explanations have been given by others (25,26). Bond (25) explained the high values of  $H/Pt_s$ , exceeding unity, by the possibility of the chemisorption on the edges and apexes of the crystals of two and three times, respectively, the amount of hydrogen (calculated per Pt atom) that is chemisorbed on the faces. Karnaukhov (26) supposed that in the region of high dispersions, single atoms, two dimensional arrangements, and three dimensional crystallites may be present in unknown proportions. It is postulated that very small particles on the support have higher stoichiometries. Thus a  $H/Pt$  value of 2 is taken to indicate the presence of atomic Pt on the surface. Thus, according to this view, different stoichiometries should be used in different ranges of dispersion to calculate the metal area.

With a few possible exceptions, the available data show considerable accord despite the varied approaches. Invariably in the chemisorption studies,  $H/Pt_s$  is assumed equal to 1 and hence  $H/Pt$  is used as a measure of dispersion.

#### 3.4-2 Oxygen Adsorption and Hydrogen-Oxygen Titration

Gruber (13) studied oxygen chemisorption at 350°C and 150 mm Hg pressure on  $Pt/Al_2O_3$  catalyst. To establish oxygen adsorption stoichiometry, oxygen adsorption results were compared with hydrogen adsorption values for the same catalyst. A comparison between oxygen adsorption and hydrogen adsorption showed identical amounts of both gases being taken up by catalysts of high metal dispersion ( $\geq 0.8$ ). With catalysts of lower metal dispersion ( $\leq 0.5$ ) the amount of oxygen taken up substantially exceeded the amount of hydrogen adsorbed, the ratio of oxygen to hydrogen being close to 2. The

difference was attributed to the ability of oxygen at 350°C to penetrate the Pt lattice to some extent, forming surface films which are more than one layer thick and hence it was concluded that adsorption of oxygen at elevated temperatures cannot serve as a reliable measure of Pt dispersion. The catalysts were also subjected to complete reduction-oxidation cycles and a ratio of  $H:O:H_T$  equal to 1:1:2.9, for highly dispersed catalysts, was established.  $H$ ,  $O$  and  $H_T$  represent hydrogen adsorption on the fresh surface, oxygen adsorption on the fresh surface and hydrogen adsorption on the surface presorbed with oxygen.

Benson and Boudart (27) studied the titration of presorbed oxygen with hydrogen at 25°C as a measure of platinum dispersion. A single determination of oxygen adsorbed yielded an  $H_T/O$  ratio of 3.2 in accordance with a value of 3 obtained for platinum black. Two main advantages of this technique are (1) a threefold increase in sensitivity over direct hydrogen chemisorption, since three hydrogen atoms are consumed for each accessible platinum atom and (2) there is no need to exclude oxygen from the sample since the sample is deliberately exposed to oxygen.

Mears and Hansford (28) studied hydrogen titration of oxygen adsorbed on several  $Pt/Al_2O_3$  and  $Pt/SiO_2$  catalysts using static as well as flow methods. An  $H:O:H_T$  ratio equal to 2:1:4 was found. The value of 4 for the ratio of the net hydrogen titration to net oxygen adsorption was in conflict with a value of 3.2 found by Benson and Boudart (27). The discrepancy was attributed to the difference in the outgassing procedures used to prepare the surface for oxygen adsorption.

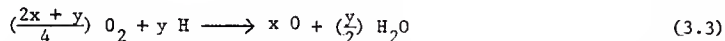
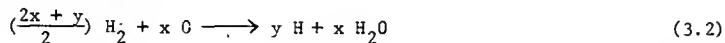
Wilson and Hall (16,24) studied hydrogen adsorption, oxygen adsorption and hydrogen-oxygen titration on several  $Pt/Al_2O_3$  catalysts under different

temperature conditions. At higher temperatures, hydrogen chemisorption fell but oxygen chemisorption remained fairly constant. By comparing chemisorption, electron microscopy and x-ray diffraction results, it was concluded that hydrogen chemisorption and not oxygen chemisorption reflected changing crystal dimensions. It was shown that the ratio  $H:O:H_T$  could vary from 2:1:4 to 1:1:3 depending on the heat treatment of the catalyst. It was concluded that these changing ratios were due to changes in the stoichiometry of oxygen chemisorption on platinum. Wilson and Hall suggested that approximately one oxygen atom was adsorbed per two surface platinum atoms on small crystallites, while a one-to-one relationship was approached on large crystallites. Due to changing oxygen chemisorption stoichiometry, it was concluded that neither oxygen chemisorption nor hydrogen-oxygen titration technique could be reliably used to determine Pt surface areas.

Weller and Montagna (23) studied oxygen chemisorption on  $Pt/Al_2O_3$  at 475°C and 525°C over a pressure range of 0 to 400 mm Hg.  $O/Pt_s$  ratio was found to vary with temperature as well as pressure from 1 to 3.7. The values greater than 1 were explained by additional oxygen uptake by alumina which was partially reduced during pretreatment with hydrogen at 550°C and the changing stoichiometry of oxygen adsorption with dispersion.

Kikuchi, Flynn and Wanke (29) studied hydrogen-oxygen titration for several  $Pt/Al_2O_3$  catalysts. The ratio of hydrogen uptake to oxygen uptake was found to depend upon the dispersion of the catalyst and hence the variable stoichiometry of chemisorption was supported. Hydrogen-oxygen titration stoichiometry,  $H_T/O$ , was found to vary from 4.48 to 1.30 over the temperature range 25°C to 500°C. This variation was attributed to a new type of surface oxygen sites formed at elevated temperatures which could only be partially reduced.

Freel (18,19) examined the reaction of adsorbed oxygen with hydrogen and its counterpart, the reaction of adsorbed hydrogen with oxygen on several Pt/Al<sub>2</sub>O<sub>3</sub> and Pt/SiO<sub>2</sub> catalysts. The reactions were represented by the generalized equations,



where H and O represent adsorbed atoms, while H<sub>2</sub>, O<sub>2</sub> and H<sub>2</sub>O, represent gas phase molecules.

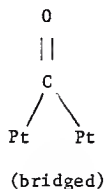
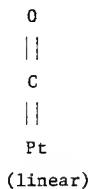
The chemisorption results showed that the relationship between x and y was not constant. The O/H ratio was found to vary from 0.4 for samples reduced for 1 hour at 500°C to 1.0 for samples reduced for 15 hours at 500°C. The ratio was largely independent of crystallite size. It was concluded that the variation in O/H ratio was due to changes in the stoichiometry of oxygen chemisorption on platinum as a result of the thermal history of the sample. This phenomena was attributed to changes of the platinum surface from a defective form to an equilibrated structure of minimum surface energy. Why such changes did not cause any significant difference in hydrogen chemisorption was not discussed.

The above studies indicate that O/H ratio varies from 0.5 to 1.0, which in turn implies the variation of H:O:H<sub>T</sub> ratios from 2:1:4 to 1:1:3 if titrations are reversible. No reasonable correlation of the ratio O/H with dispersion has been established (19).

### 3.4-3 Carbon Monoxide Adsorption and Carbon Monoxide-Oxygen Titration

Gruber (13) measured CO chemisorption on several catalysts of different metal dispersion and compared the results with H<sub>2</sub> adsorption on the same

catalyst samples.  $H_2$  chemisorption was measured by the static method and carbon monoxide chemisorption by a pulse method. CO/H ratio was found to vary from 1 to 0.7 for lowly dispersed to highly dispersed catalysts. This variation was explained based largely on the work of Eischens and Pliskin (30). They observed two infrared absorption bands for CO on supported alumina and ascribed these lower and higher energy bands to linear and bridge-bonded species, respectively, which are represented by the structures,



They found that the latter accounted for some 15% of the total adsorbed CO on a Pt/SiO<sub>2</sub> catalyst, but about 50% of the total uptake on Pt/Al<sub>2</sub>O<sub>3</sub>. It was suggested that the alumina carrier makes it easier for the platinum to donate electrons for bond formation, thereby favoring the bridged structure.

A CO/H ratio of 1 corresponds to all the CO in the linear form and a CO/H ratio of 0.67 corresponds to 50% in the linear and 50% in the bridge structure. Gruber (13) suggested that the variation in his values of the CO/H ratio from 1 to 0.7 were due to 100% linear bonding on poorly dispersed sample and 50% bridge bonding on well-dispersed samples.

Dorling and Moss (31) compared CO adsorption and X-ray line broadening measurements for several Pt/SiO<sub>2</sub> catalysts to determine adsorption stoichiometry. The ratio, (total Pt atoms exposed)/(CO molecules adsorbed) was found to vary from 1 to 2 with increasing platinum content of the sample.

This variation was explained based on the work of Eischens and Pliskin (30) and Brennan and Hayes (32).

Brennan and Hayes (32), based on their experimental and theoretical analysis of CO adsorption on evaporated metal film concluded that the permitted configurations of CO molecules on the (100), (110), and (111) planes of platinum yield limiting CO/Pts ratios of 0.8, 0.5 and 0.33, respectively. They argued that for denser configurations, the repulsive energy would be prohibitive, by reason of its absolute value relative to the surface bond and would necessitate an excessive activation energy of adsorption. To account for the experimentally observed value of the ratio of (CO adsorbed)/(Kr adsorbed), the authors proposed that the (111) face covered by bridge-bonded carbon monoxide must be present practically to the exclusion of the other two faces.

The work of Eischens and Pliskin (30) suggests that most of the CO molecules are linearly bonded on the small platinum crystallites in supported catalysts. From the analysis of Brennan and Hayes (32), the above does not necessarily imply a CO/Pts ratio of unity. To explain the near correspondence between the number of platinum atoms exposed and CO molecules adsorbed at low platinum contents, Dorling and Moss (31) suggested that where a large contribution to the total platinum area was from extremely small, irregular crystallites, the flat areas where the packing configurations of Brennan and Hayes apply was very small. The observed value of 2 for the ratio Pts/CO at higher platinum contents was attributed to the existence of linear, bridge or both type of bondings.

Based on their data on fine nickel-Aerosil catalysts, Hardeveld and Hartog (33) supported an alternative model proposed by Blyholder (34)

for CO chemisorption. This model ascribes the higher energy infrared band to linearly adsorbed carbon monoxide on surface atoms of low coordination (mainly 6 and 7).

Renouprez, Hoang-nan and Compagnon (35) determined the Pt surface area of several Pt/Al<sub>2</sub>O<sub>3</sub> catalysts by hydrogen chemisorption using a pulse technique, carbon monoxide adsorption using a gravimetric technique, electron microscopy and small angle X-ray scattering. The chemisorption data were converted to metal surface area assuming an adsorption stoichiometry (H/Pts or CO/Pts) of 1. The results showed good agreement in the values of metal areas obtained by X-rays and chemisorption and thus confirmed the value of 1 for the chemisorption stoichiometry of H<sub>2</sub> and CO on Pt catalysts. This stoichiometry was found to be independent of Pt crystallite size. For all the catalysts studied, metal area measured by hydrogen chemisorption was approximately 10% higher than that found from CO chemisorption or small angle X-ray scattering. The authors proposed that this difference could be because of the difference in experimental techniques employed for H<sub>2</sub> and CO chemisorption or that total area (accessible area + area of contact between metal and support) could be measured by hydrogen chemisorption, while only the accessible area could be measured by CO chemisorption and small angle X-ray scattering. Excellent agreement between CO chemisorption and small angle X-ray scattering results ruled out bridge-bonding of a few percent of CO molecules as the possible explanation for the above observed difference.

From most of the studies on CO adsorption of Pt catalysts, it is observed that for dispersions greater than about 0.25, the ratio CO/Pts varies from 0.8 to 1 and for lower dispersions, CO/Pts decreases dramatically (19). Because of the uncertainty with respect to existence or non-existence of bridged carbon monoxide species, the experimentally observed values of



CO/Pts ( $<1$ ) can be best explained in terms of spatial restrictions which govern carbon monoxide chemisorption (19).

Wentreck, Kimoto and Wise (36) measured metal surface area of bulk and supported platinum by means of CO titration of preadsorbed oxygen. The reaction was proposed to proceed rapidly at room temperature in accordance with the stoichiometry



where O and CO represent adsorbed species and CO(g) and CO<sub>2</sub>(g), gas phase molecules. The surface area value derived from the CO titration were compared with the BET and CO chemisorption results and an excellent agreement was found. For the metal surface area calculations, O/Pts and CO/Pts ratios were assumed to be 0.5 and 0.8, respectively.

For Pt/Al<sub>2</sub>O<sub>3</sub> catalyst, the measured values of CO/CO<sub>2</sub> and CO/O were found to be 2.03 and 1.56, respectively. According to the proposed reaction and adsorption stoichiometrics, CO/O = 2.0 should have been obtained. The authors explained the low value of CO/O ratio by oxygen adsorption on the support and its inactivity towards the CO added in the subsequent step.

#### 3.4-4 Comparison of different Adsorbates

Most of the studies which contain detailed measurements of crystallite size indicate that, within reasonable limits, each surface platinum atom adsorbs one hydrogen atom. Small variations may be due to different criteria used to define the hydrogen monolayer. It can be concluded that hydrogen chemisorption on small platinum crystallites is not very different from that on bulk platinum.

The volume of oxygen taken up by supported platinum catalysts does not bear a constant relationship to the corresponding volume of hydrogen. This

is ascribed largely to changes in the stoichiometry of oxygen chemisorption on the platinum surface.

The stoichiometry of carbon monoxide chemisorption is reasonably constant on small platinum crystallites and could conceivably correspond to CO/Pts equal to one with H/Pts some 15-20% higher. The independent measurements of size are not precise enough to distinguish between this and the preferred explanation in which H/Pts equal to one. Large platinum crystals adsorb much less carbon monoxide than hydrogen, which appears to be due to a decrease in CO/Pts.

Uncertainties in the stoichiometry of carbon monoxide chemisorption on large crystals, and of the stoichiometry of oxygen adsorption over essentially the entire range of crystallite size make them less desirable for surface area measurements. It follows that stoichiometries for  $O_2-H_2$  and  $O_2-CO$  titrations would be far more complex and their interpretation would be difficult. The stoichiometry of hydrogen chemisorption is relatively constant over a wide range of crystallite size. Hydrogen chemisorption is therefore the best determinate of platinum surface area and thus has been used in the present work.

### 3.5 Selection of Adsorption Parameters

The optimum temperature for the adsorption measurements is the one at which the difference in uptake on the metal and the support is a maximum. Gruber (13) determined hydrogen adsorption isobars on alumina at several pressures. A minima was observed for every isobar in the temperature range of 250° to 300°C. Based on this finding, Gruber (13) selected 250°C as the temperature for hydrogen adsorption measurements on Pt/ $Al_2O_3$  catalysts. Spenadel and Boudart (14) also used this temperature for chemisorption measurements.

Gruber (13) and Spenadel and Boudart (14) measured hydrogen adsorption isotherms on  $\text{Pt}/\text{Al}_2\text{O}_3$  catalysts at  $250^\circ\text{C}$  up to a pressure of 250 mm Hg. From the shape of the isotherms, Gruber (13) and Spenadel and Boudart (14) concluded that at hydrogen pressures of 100 and 240 mm respectively, complete saturation of the surface was approached. They used hydrogen adsorption measurements at these pressures for surface area determinations.

Both Gruber (13) and Spenadel and Boudart (14) found that about 90% of the total hydrogen adsorption was instantaneous followed by a slow gas uptake. Gruber (13) concluded from his experimental work that an adsorption equilibration time of 2 hours was sufficient and any gas uptake beyond this time was due to adsorption on the support only. Spenadel and Boudart (14) allowed a time of 30 to 45 minutes for adsorption equilibration.

Benson and Boudart (27) measured hydrogen adsorption isotherms at room temperature and above approximately 50 mm Hg for several  $\text{Pt}/\text{Al}_2\text{O}_3$  catalysts and alumina supports. The hydrogen isotherms for the  $\text{Pt}/\text{Al}_2\text{O}_3$  catalysts were nearly straight and with a positive slope and were found to be closely parallel to those for alumina which extrapolated thru zero. Based on this, the authors concluded that it was sufficient to measure the hydrogen uptake on the  $\text{Pt}/\text{Al}_2\text{O}_3$  catalyst over a range of pressures and extrapolate to zero pressure to get the uptake on the metal. Adsorption equilibrium time of about 45 minutes was required for the first point and thereafter 5 to 10 minutes was found to be sufficient. This method has then been used by several workers.

Hausen and Gruber (37) measured hydrogen adsorption isotherms for a  $\text{Pt}/\text{Al}_2\text{O}_3$  catalyst over the pressure range of 1 to 80 mm and for temperatures varying from  $60^\circ$  to  $510^\circ\text{C}$ . They observed a strong pressure dependence below

about 10 mm, but only a small increase in adsorption between 10 and 80 mm for all the isotherms. No measureable adsorption of hydrogen on the alumina support was found. The authors concluded that the measured isotherms represented net adsorption on the metal and the pressure dependence could not be ascribed to the support. Thus the intercept method of extrapolating the straight portion of the isotherm to zero pressure, as used by Benson and Boudart (27), is not applicable in general.

Low temperature adsorption measurements have also been used to determine surface area of supported platinum catalysts. Hasan et al (38) used chemisorption of hydrogen at liquid nitrogen temperature to determine the surface area of Pt/Al<sub>2</sub>O<sub>3</sub> catalysts. A blank correction was required at this temperature. Adams et al (15) measured hydrogen adsorption isotherms on platinum - silica gel catalyst at -78° and 0°C. The surface saturation was achieved at pressures above 0.1 mm Hg for both temperatures and also the amount of hydrogen required to achieve saturation was found to decrease with increasing temperature. Based on these findings, Dautzenberg and Woltern (39) used hydrogen adsorption at -78°C and 0.1 mm Hg to determine surface areas of Pt/Al<sub>2</sub>O<sub>3</sub> catalysts. Corrections were made for adsorption on the support in their work.

For the present work, hydrogen chemisorption values at 250°C and 240 mm Hg were selected. It is believed that at these conditions physical adsorption is minimal and the difference in adsorption on the metal and the support is very large.

## EXPERIMENTAL

### 3.6 Chemisorption Apparatus

A schematic of the apparatus is shown in Fig. 3.1, and the

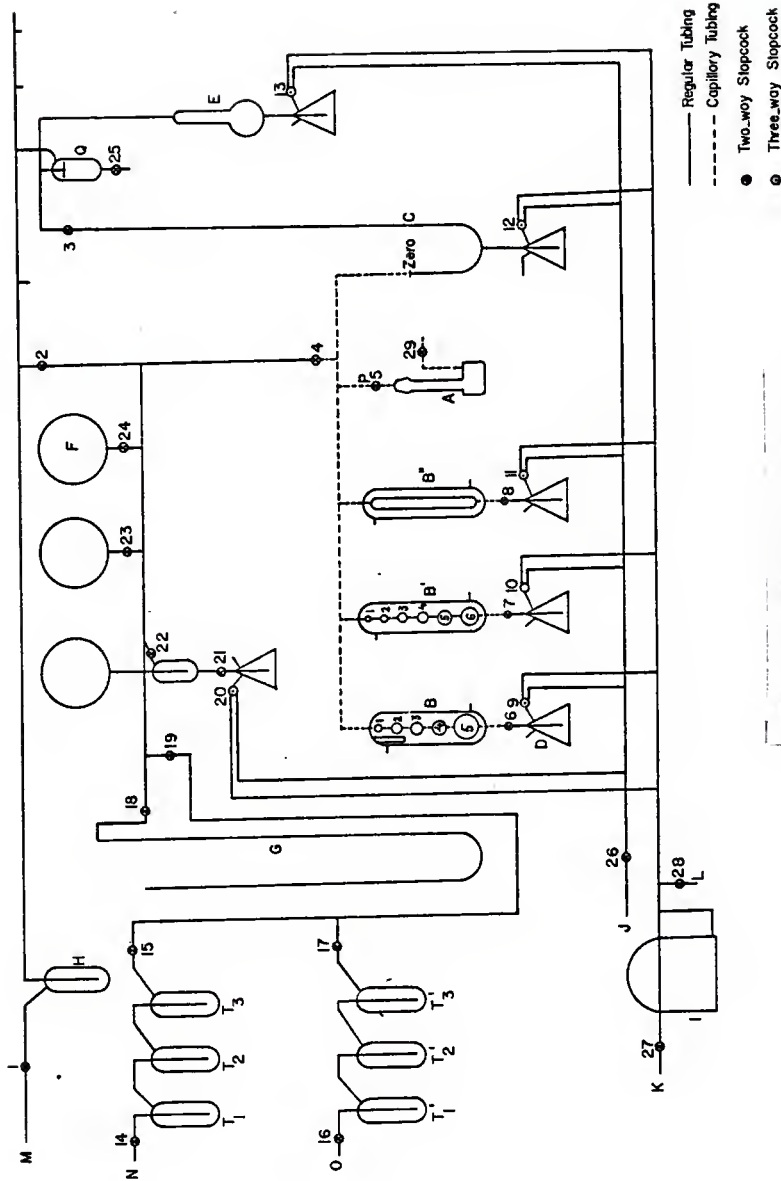


Fig. 3.1 Chemisorption Apparatus

Table 3.1

## Legend for Fig. 3.1

A	Sample tube
B, B', B''	Gas Burettes, calibrated, for measuring working volume of gas
C	Manometer to measure gas pressure over the sample and in the gas burettes
D	Mercury reservoirs for the manometer, Mcleod gauge and burettes
E	Mcleod gauge
F	Gas reservoirs for storage of purified gases
G	Manometer to measure gas pressure in reservoirs
H	Cold trap
I	Vacuum chamber
J	To source of air pressure
K	To mechanical pump
L	To atmosphere
M	To diffusion pump
N	To hydrogen cylinder
O	To helium cylinder
P	Gold foil to protect sample from mercury vapors
Q	Mercury trap
T1, T2, T3, T1', T2', T3'	Gas purification trains

terminology used is explained in Table 3.1. It consists of three integrated units: the sample tube, burettes, manometer, and mercury reservoirs; the gas purification trains and the gas storage bulbs; a high vacuum system that consists of an oil diffusion pump, a mechanical pump, a cold trap, and a McLeod gauge. The system was designed to be a multipurpose adsorption system. The entire system was made and assembled by Mr. Mitsugi Ohno.

### 3.6-1 Sample Tube

Various types of sample tubes may be used with an adsorption apparatus. The surface area and density of the catalyst and the proposed experiments dictate the size and shape respectively of the sample tube. The dimensions of the sample tube also depend on the size and shape of the available furnaces. The sample tube used is shown in Fig. 3.2. The flow through design facilitated in situ treatment of catalyst in different atmospheres. Close fitting glass rods were used to reduce the dead space in the sample tube.

### 3.6-2 Burettes

The measuring burettes B and B' consisted of a series of bulbs of various sized connected by short lengths of capillary tubing. Calibration lines were etched between bulbs and at the ends of each bulb train. Before the burettes were attached to the system, the volume of each bulb was determined by weighing the volume of mercury between appropriate reference marks. A calibrated linear burette, B'' was also used. The calibrated volumes of the burettes are listed in Table 3.2 and the calibration data are shown in Appendix A. The large variety of burette volumes are necessary when making readings at frequent pressure intervals. The burettes were thermostated by water jacketing.

### 3.6-3 Burette - System Manometer

Since it is necessary to know the exact volume of the system, the

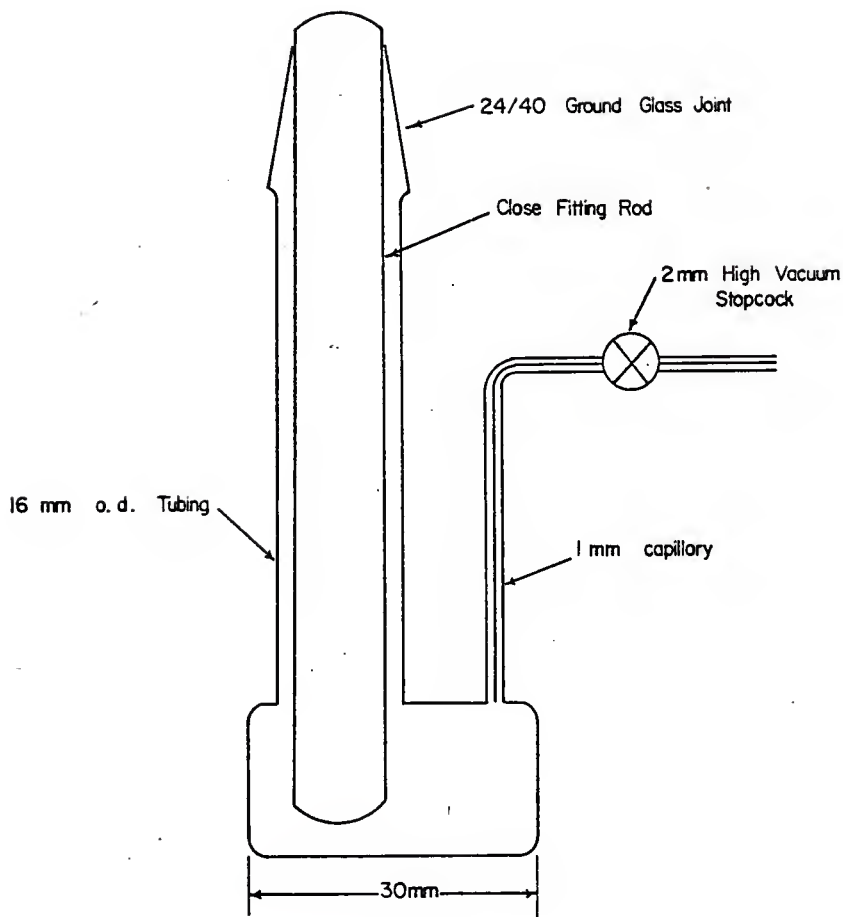


Fig. 3.2 Sample Tube



Table 3.2

## Calibrated Volume of the Burettes

Burette	Bulb No.	Volume, cm <sup>3</sup>
Linear (B'')	-	6.682
Small (B')	1	4.922
	2	9.833
	3	14.332
	4	21.942
	5	24.670
	6	31.724
Large (B)	1	4.628
	2	13.453
	3	24.372
	4	52.545
	5	131.741

mercury in the pressure leg of the manometer is always adjusted to a reference point corresponding to the zero point of the scale. To minimize meniscus effects of the mercury, the manometer was made of 10 mm tubing. To avoid capillary effects and to minimize the free space in the system, the junction of the 10 mm tubing and 2 mm capillary was chosen as the reference point. The manometer extended 250 mm below the reference point to avoid the danger of mercury being accidentally forced around the "U" bend during a rapid increase in pressure.

#### 3.6-4 Mercury Reservoirs

The Mercury reservoirs were constructed from 500 ml conical flasks. A ground glass joint was attached to the side of each reservoir to facilitate changing the mercury. The reservoirs were used to supply mercury to the burettes, McLeod gauge, and the manometer. This was done by applying air pressure or vacuum to the mercury surface in the reservoir through three-way stopcocks. The reservoirs were filled with more mercury than required to fill the burettes or the manometer or McLeod gauge to prevent mercury being forced into the high vacuum side or the sample side of the system.

#### 3.6-5 Gas Purification Train

The gases used in this work were hydrogen for catalyst reduction and adsorption, helium for dead space determinations and also as a carrier gas and oxygen for catalyst redispersion. Matheson ultra high purity grade hydrogen, 99.999% pure, was further purified by passing over an Engelhard Deoxo hydrogen purifier for removal of traces of  $O_2$ , through trap T1 containing 3A molecular sieves for  $H_2O$  removal, and through trap T2 cooled to liquid nitrogen temperature for removal of other condensable impurities. Helium, 99.995% pure, was further purified by passing over a Cu bed at  $350^\circ C$

for removal of traces of oxygen, through trap T1' containing 3A molecular sieves for H<sub>2</sub>O removal, and through trap T2' filled with activated coconut charcoal, 6 to 14 mesh, and cooled to liquid nitrogen temperature for removal of other gases and condensable impurities. Two additional traps, T3 and T3', were incorporated in the system to take care of future modifications in the purification scheme. Oxygen was purified by passing over a 3A molecular sieve column followed by a passage through a Dry Ice - acetone trap. The purified gases were stored in the storage bulbs.

### 3.6-6 Gas Storage Bulbs

Three gas storage bulbs were constructed from 3 liter round-bottom flasks. Two of these storage bulbs were used for helium and hydrogen, the third bulb was incorporated in the system for storing any other adsorbate to be used in future. The storage bulbs were evacuated before being filled with the gases. The gases were stored at pressure slightly above atmospheric to minimize contamination with air. An open end manometer was attached to the storage bulbs for determining the amount of gas in the bulbs. For safety, each storage bulb was wrapped with tape.

Some adsorbate gases dissolve readily in stopcock grease. To prevent this, a mercury cut-off was placed between one of the storage bulbs and the stopcock to the gas manifold of the system. The cut-off is shown in Fig. 3.3. When the cut-off is open the mercury is kept just below the end of the tube from the gas storage bulb. To close it, the mercury is raised in the cut-off up to the upper stopcock which is then closed. In this state the gas does not come into contact with the stopcock nor can air leak into the storage bulb and contaminate the gas.

### 3.6-7 Vacuum System

A "Speedivac" oil diffusion pump and mechanical pump were used for

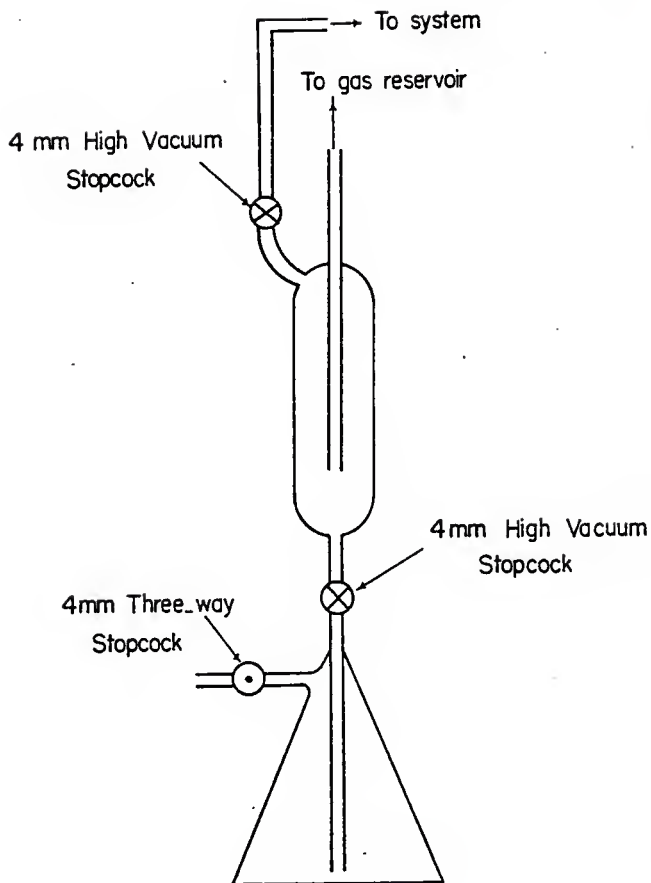


Fig. 3.3 Mercury Cut-off

achieving high vacuum in the system. The pumping system is shown in Fig. 3.4. For start-up, when the apparatus is at atmospheric pressure, the following procedure is adopted:

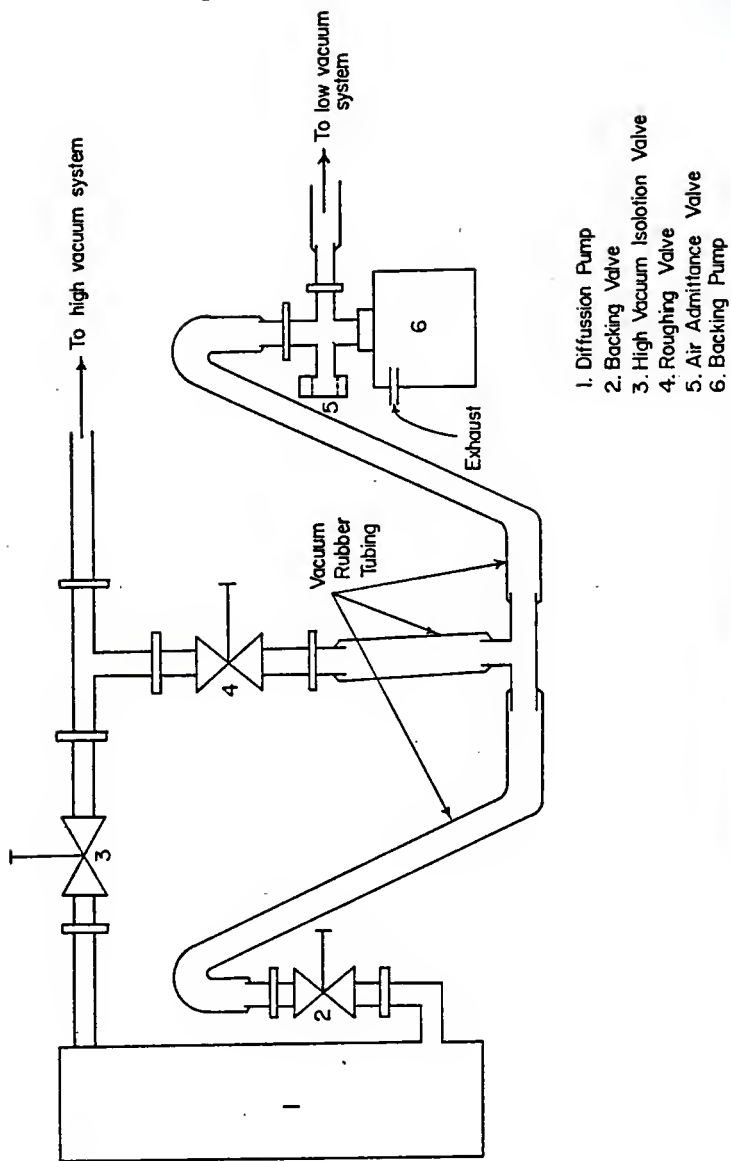
- (a) The high vacuum isolation valve and air admittance valve are closed and roughing valve and backing valve are opened.
- (b) Rotary pump is switched on.
- (c) When the backing pressure reaches 0.5 torr or better, cooling water to the diffusion pump is turned on and the diffusion pump heater is switched on.
- (d) After a warming up period of 10 to 15 minutes, the roughing valve is closed and the high vacuum isolation valve is opened.

For closing down the steps are:

- (a) The high isolation valve is closed, the roughing valve is opened and the diffusion pump heater is switched off. The pump is allowed to cool.
- (b) The backing valve is closed.
- (c) Air is admitted to the system and the rotary pump is switched off.

This method of closing down ensures that the diffusion pump is left evacuated, thus preventing the pump fluid from absorbing air. When subsequently starting up, the system is evacuated via the roughing valve to a pressure of about 0.5 torr and then the backing valve is opened.

Since the same mechanical pump was used as backing pump as well as for applying vacuum to the mercury reservoirs, a vacuum chamber of approximately 17 liters capacity was attached to the low vacuum side for convenience. The arrangement is shown in Fig. 3.1. When the system is first evacuated the stopcock on the low vacuum side is open and thus the pressure on both sides of the mercury is the same. After the vacuum chamber is



1. Diffusion Pump
2. Backing Valve
3. High Vacuum Isolation Valve
4. Roughing Valve
5. Air Admittance Valve
6. Backing Pump

Fig. 3.4 Arrangement of Vacuum Pumps

evacuated to a sufficiently high vacuum, the stopcock on the low vacuum side is closed and the chamber then supplies the vacuum capacity for the mercury reservoirs. This arrangement is advantageous because the mercury reservoirs can be evacuated without disturbing the high vacuum on the sample side of the system.

To protect the samples from oil resulting from backstreaming in the diffusion pump, and to keep mercury vapors from the pumps, a liquid nitrogen trap was used between the pumping system and the sample tube.

### 3.6-8 McLeod Gauge

Because of its simplicity of construction and operation, a McLeod gauge was used to measure the vacuum levels. The principle of the gauge consists in compressing a known volume of gas whose pressure is to be measured, to a much smaller volume and observing the resultant pressure. Assuming Boyle's law the original unknown pressure can then be calculated by the equation:

$$P_1 = \frac{P_2 V_2}{V_1} \quad (3.5)$$

where

$P_1$  = unknown pressure

$V_1$  = initial volume before compression

$P_2$  = final pressure

$V_2$  = final compressed volume

The McLeod gauge used is shown in Fig. 3.5A. The bulb B, to which was attached a capillary tube aa, was connected to a mercury reservoir. In order to avoid capillary effects, a capillary bb, of the same diameter as aa, was sealed on as a by-path to the larger tube E which was connected

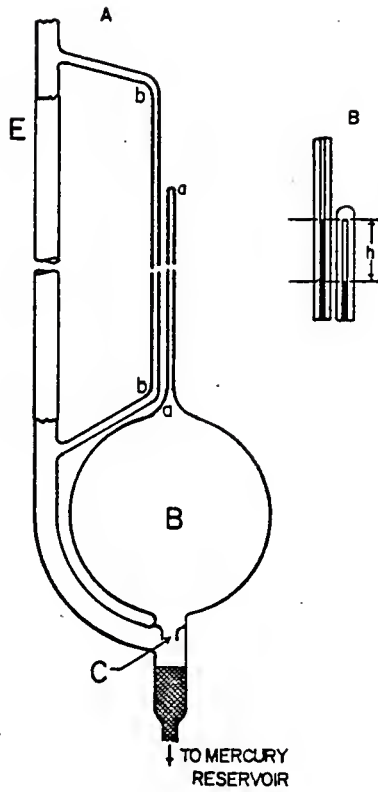


Fig. 3.5 McLeod Gauge



to the high vacuum system. To operate the gauge the mercury is forced to rise and enter the bulb B at C. The gas within the bulb and capillary aa is cut off from the rest of the system when the mercury passes through the ring at C. The gas in the bulb is compressed by the mercury until finally the mercury in the capillary bb is level with the top of the inside of the capillary aa, Fig. 3.5 B. The pressure on the gas in the capillary is then equal to sum of the pressure in the system and that of mercury column of length h, which is also the length of the capillary aa that contains the compressed gas.

Let V denote the volume of the capillary aa and of the bulb B down to the level C. Let  $P_s$  denote the pressure in the system. Also, let d denote the diameter of the capillary aa. Then

$$\text{volume of the gas trapped} = \frac{\bar{\Lambda}}{4} d^2 h$$

$$\text{pressure in the capillary} = P_s + h$$

Hence,

$$(P_s + h) \frac{\bar{\Lambda}}{4} d h = P_s V \quad (3.6)$$

or

$$\begin{aligned} P_s &= \frac{\bar{\Lambda}/4 d^2 h^2}{V - \frac{\bar{\Lambda}}{4} d^2 h} \\ &= \frac{0.7854 d^2 h^2}{V - 0.7854 d^2 h} \end{aligned} \quad (3.7)$$

It is evident that the sensitivity of the gauge can be made extremely high by increasing the ratio  $V/d^2$ . However practical considerations limit the magnitude of V (~200 ml) because of the weight of the mercury to be raised. Furthermore, in capillaries of very small bore (<1 mm), the

mercury tends to stick badly as the level is raised and the column breaks as the level is lowered, thus leaving a portion hanging in the capillary.

### 3.6-8a Calibration of the McLeod Gauge

A capillary of approximately 1 mm diameter was cleaned and dried. A short length of mercury was drawn up into the capillary tube and accurately measured using a cathetometer. The thread was then moved to the adjacent portion of the capillary and again the length was measured. This process was repeated until the entire length of the tube had been covered. The mercury was removed and weighed. Noting the temperature and density of mercury, the diameter of the capillary was calculated for each length measurement. The results are listed in Table 3.3. Since the variation in the diameter over the entire length of the capillary was found to be less than 0.6%, the average diameter was used for further calibrations.

The capillary was then fused at one end and the other end was sealed to the bulb B, and the ring seal C at the bottom of the bulb was made. The bulb was then filled exactly to the cut-off at C with mercury. The amount of mercury in the bulb was then determined by weighing the mercury and with temperature measurements the volume of the bulb was obtained. Correction in the volume obtained was made for the amount of mercury which entered the capillary portion. The results are listed in Table 3.4.

Having obtained the diameter of the capillary and volume of the bulb, V was calculated and Eq. 3.7 was simplified.

$$\begin{aligned}
 V &= \text{volume of bulb + capillary} \\
 &= 210.399 + \frac{\pi}{4} \times (0.10438)^2 \times 32.6 \\
 &= 210.678 \text{ cm}^3 \\
 P_s &= \frac{8.557 \times 10^{-3} h^2}{210.678 - 8.557 \times 10^{-3} h} \quad (3.8)
 \end{aligned}$$

Table 3.3

Calibration of the Capillary Portion of the McLeod Gauge

Capillary Level	Length of Hg thread, cm	Mass of Hg, g	Temperature, F	Density of Hg, g/cm <sup>3</sup> (7)	Diameter of the capillary, cm	Average diameter of the capillary, cm
1	2.578	0.29903	71	13.5417	0.10443	
2	2.575	0.29903	71	13.5417	0.10449	
3	2.592	0.29903	71	13.5417	0.10415	0.10438
4	2.593	0.29903	71	13.5417	0.10413	
5	2.563	0.29903	71	13.5417	0.10474	
6	2.583	0.29903	71	13.5417	0.10433	

Table 3.4  
Calibration of the Bulb Portion of the McLeod Gauge

S. No.	Mass of Hg, g	Temperature, F	Density of Hg, g/cm (7)	Volume of the bulb, cm <sup>3</sup>	Average volume, cm <sup>3</sup>
1	2849.8	72	13.5404	210.466-0.043* = 210.423	210.399
2	2848.5	76	13.5360	210.439-0.064* = 210.375	

\* Volume of the capillary portion filled with mercury

For  $h$  corresponding to the length of the capillary used in the system (=32.6 cm), the error resulting from the omission of the second term in the denominator was found to be less than 0.12% and hence this term was neglected. Thus Eq. 3.8 reduces to

$$P_s = 4.0616 \times 10^{-5} h^2 \quad (3.9)$$

where  $P_s$  and  $h$  are in cm. The equation was rewritten as

$$h = 496.1939 \sqrt{P_s} \quad (3.10)$$

where  $h$  and  $P_s$  are in mm.

A scale was prepared by calculating  $h$  for various  $P_s$  values. Zero of the scale coincided with the fused end of the capillary and pressure was directly read on this scale. A few selected values of  $P_s$  and corresponding  $h$  values are presented in Table 3.5.

### 3.6-9 Miscellaneous Items

A Hoskins tubular furnace and a Tecam fluidized bath were used for catalyst pretreatment and redispersion, and adsorption purposes respectively. A thermometer of 0° to 500°C range and an iron - constantan thermocouple were used for temperature measurements. Dewar flasks of 0.9 liter capacities were used to hold liquid nitrogen. A mercury trap was used between the burette system manometer, McLeod gauge and high vacuum line in the system so as to avoid the danger of mercury being accidentally forced into the high vacuum side of the apparatus.

### 3.7 Calibration of Zero Bulb Volume

Before any measurements were made with the apparatus, it was tested for

Table 3.5  
Calibration of the McLeod Gauge

$P_s$ , mm Hg	$h$ , mm
$1 \times 10^{-5}$	1.569
$5 \times 10^{-5}$	3.509
$1 \times 10^{-4}$	4.962
$5 \times 10^{-4}$	11.095
$1 \times 10^{-3}$	15.691
$5 \times 10^{-3}$	35.086
$1 \times 10^{-2}$	49.619
$5 \times 10^{-2}$	110.952
0.1	156.910
0.2	221.905
0.3	271.777

leaks. All ground glass joints were sealed with either Apiezon N or Apiezon H vacuum grease. The apparatus was evacuated and a vacuum tester was used to check the entire system for imperfections in the glassware. The system was then flamed several times to remove water and other condensable gases. After that, all stopcocks were closed and leaks caused by faulty greasing of ground glass joints were found by noticing changes in the vacuum level when the various units were connected. Faulty stopcocks were isolated and regreased. The above procedure was repeated until the desired vacuum level ( $>10^{-5}$  mm Hg) was achieved.

The section of tubing, Fig. 3.1, between stopcock 5, the top mark of the burettes, the zero reference of the manometer C and stopcock 4 is the zero bulb volume. To determine this volume,  $V_0$ , the system was evacuated and mercury in each burette was set at the top mark. The mercury was raised in the manometer C and with stopcock 5 closed, helium was introduced through stopcock 4 until the manometer C registered a pressure of about 600 mm. Stopcock 4 was then closed and manometer C was zeroed and the pressure recorded. The mercury was then lowered to some different reference point in the burettes and the pressure was redetermined. The procedure was repeated until five pressure readings were recorded. The total volume of the burettes which were not filled with mercury,  $V_e$ , for each pressure reading was already known. Since a fixed number of moles of helium were used and also the temperature remained constant during the calibration run, the following pressure - volume relationship was used to determine zero bulb volume:

$$PV = \text{constant} = A \quad (3.11)$$

but

$$V = V_0 + V_e \quad (3.12)$$

hence

$$P(V_0 + V_e) = A \quad (3.13)$$

or

$$PV_e = A - PV_0 \quad (3.14)$$

$$\frac{d(PV_e)}{dP} = -V_0 \quad (3.15)$$

The plot of  $PV_e$  vs  $P$  for each reading taken gave a straight line, the slope of which was the negative of the zero bulb volume. The results are listed in Table 3.6 and Fig. 3.5 shows the plot.

### 3.8 Determination of Metal Dispersion from Hydrogen Chemisorption

Before the metal dispersion can be determined from hydrogen adsorption isotherms, three preliminary operations must be performed. These include selecting the sample size, pretreatment of the sample, and determining the dead space.

#### 3.8-1 Selecting the Sample Size

The sample size depends on the metal concentration, dispersion and the dead space in the system. From an accuracy standpoint, the sample size was chosen such that moles of hydrogen adsorbed were comparable with moles of hydrogen present in the dead space and the burette system. 15 to 20 grams samples were found to be sufficient for the metal concentration and dispersion levels studied.

#### 3.8-2 Pretreatment of the Sample

This will be discussed in detail in Chapter 5.

#### 3.8-3 Determination of the Dead Volume

The volume of gas present in the free space of the sample tube and not adsorbed by the sample at equilibrium is called the dead volume and



Table 3.6  
Calibration of Zero Bulb Volume

Bulb	$V_e$ , ml	P, mm Hg	PVe
1B'	4.922	460.5	2266.581
1B' + 1B	9.550	367	3504.850
2B'	14.755	297	4382.235
2B' + 1B	19.383	256	4962.048
3B'	29.087	198	5759.226

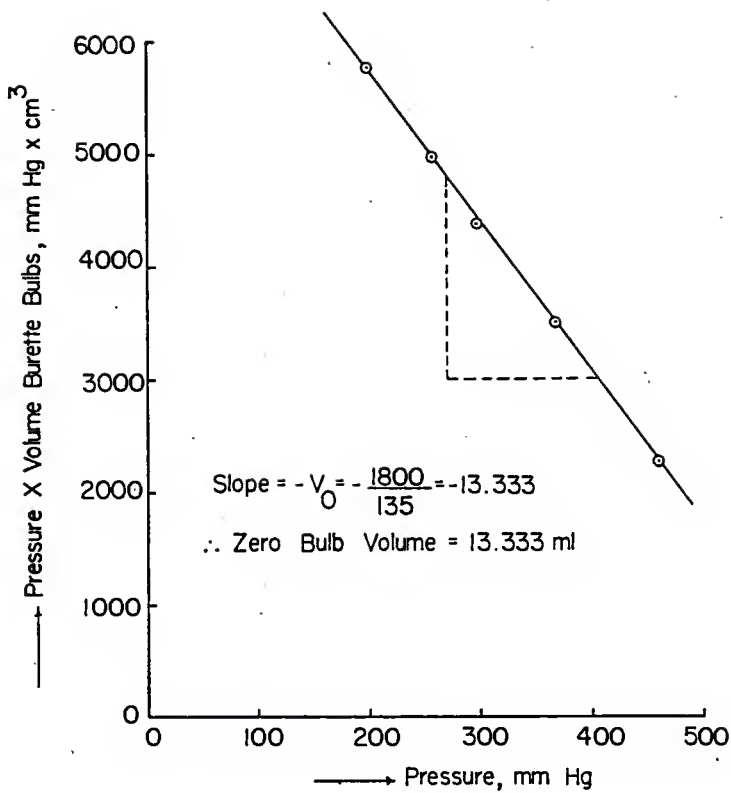


Fig. 3.6 Calibration of Zero Bulb Volume

is used in calculating the volume of gas adsorbed. This volume must be measured at the adsorption temperature. Helium is used to determine this volume because it does not adsorb.

With the sample attached to the apparatus, properly pretreated and under vacuum, the sample tube was isolated from the burette system by closing stopcock 5. Helium was admitted to the burette system through stopcock 4 until a pressure of 400 mm Hg was registered. The moles of gas taken were determined by using the relation

$$N = \frac{PV}{RT} \quad (3.16)$$

Three pressure readings were taken by adjusting the mercury in the burettes at different levels and an average value of the moles of gas taken was calculated.

An appropriate furnace was then placed around the sample tube and the temperature was brought to 250°C. Stopcock 5 was opened, and helium was allowed to expand into the sample tube. When thermal equilibrium was established, the pressure was read and the volume of helium in the sample tube was calculated using the following relation

$$N_{av} = \frac{PV_e}{RT_1} + \frac{PV_d}{RT_2} \quad (3.17)$$

where

P = equilibrium pressure

V<sub>e</sub> = volume of the burettes not filled with mercury + zero  
bulb volume

T<sub>1</sub> = room temperature

$V_d$  = unknown dead space volume

$T_2$  = adsorption temperature (=250°C)

$N_{av}$  = average value of the moles of helium taken

$R$  = gas constant

By adjusting mercury in the burettes, three pressure readings were taken and an average value of the dead volume was calculated.

Before proceeding with the surface area measurements, helium was removed from the adsorption system by evacuation.

#### 3.8-4 Measurement of the Isotherm

With the sample in position, the dead space factor determined, and the sample tube and burette system evacuated, stopcocks 2,4 and 5 were closed; hydrogen was admitted to the burette system through stopcock 4 until a pressure of 500 to 600 mm Hg was reached and then stopcock 4 was closed. The mercury was adjusted in manometer C, and the pressure read and recorded. The burette temperature was also recorded. By adjusting the mercury in the burettes to different levels, three pressure readings were recorded and an average value of the initial moles of hydrogen determined. With the furnace in place around the sample tube and heated to the adsorption temperature (=250°C), stopcock 6 was slowly opened. The pressure decreased as the hydrogen expanded into the evacuated sample tube and adsorption began. When equilibrium was reached, the pressure, the burette bulbs used, the burette temperature, and the adsorption temperature were recorded.

The volume in the burettes was then either increased or decreased by changing the mercury level so that a bulb combination occurred which caused the pressure in the system to either increase or decrease by approximately 50 mm Hg. When equilibrium was again established, another set of data, i.e.,

pressure, burette volume, burette temperature, and adsorption temperature, was recorded. The above procedure was repeated until the data in the desired range of pressure were obtained. From each set of data, the moles of hydrogen adsorbed at that particular pressure were calculated by using the relation,

$$N_{av} = \frac{PV_e}{RT_1} + \frac{PV_d}{RT_2} + N_{ads} \quad (3.18)$$

where

$N_{av}$  = average value of the initial moles of hydrogen

$N_{ads}$  = moles of hydrogen adsorbed at pressure P

A plot of the moles of hydrogen adsorbed, versus pressure was then prepared. From this plot, the moles of hydrogen adsorbed corresponding to a pressure of 240 mm Hg were determined (Fig. 3.7). This value represented the uncorrected monolayer adsorption capacity of the sample. A similar procedure was used to measure the hydrogen adsorption isotherm for the support. The moles of hydrogen adsorbed by the support at 240 mm Hg pressure were subtracted from the corresponding values for the catalyst to find the corrected monolayer adsorption capacity of the catalyst.

The following is an example of the recorded data and the calculations used in determining the moles of hydrogen adsorbed in a monolayer.

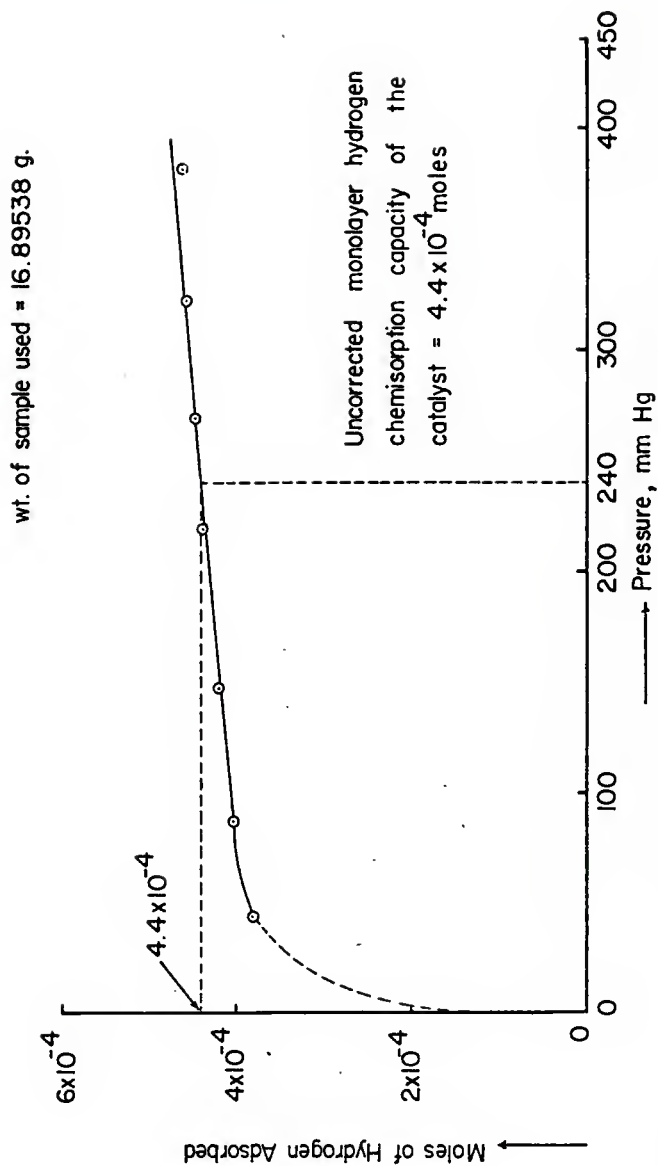


Fig. 3.7 Hydrogen Adsorption Isotherm for the Catalyst

## 3.8-5 Sample Calculations

Wt. of sample = 16.89538 g

Wt.% Platinum = 1.62002

Dead Space Measurement $T_1 = 300.778^\circ \text{K}$        $T_2 = 523^\circ \text{K}$ 

Line	Gas	Stopcock 5	Burette Bulb	P, mm Hg	$V_e, \text{cm}^3$
1	He	closed	Zero	402	13.333
2	He	closed	1B'	290.5	18.255
3	He	closed	2B'	190	28.088
4	He	open	2B'	103	28.088
5	He	open	1B'	128	18.255
6	He	open	Zero	144.5	13.333

Stopcock 5 closed

<u>Line</u>	<u>PV<sub>e</sub></u>
1	5359.866
2	5303.0775
3	5336.72

average = 5333.2211

$$\begin{aligned}
 N'_{av} &= \frac{PV_e}{RT_1} \\
 &= \frac{5333.2211}{760 \times 82.05 \times 300.778} \\
 &= 2.843488 \times 10^{-4}
 \end{aligned}$$

Stopcock 5 open

Line 4      P = 103 mm Hg

$$N'_{av} = \frac{PV_e}{RT_1} + \frac{PV_d}{RT_2} \quad (3.17)$$

$$\begin{aligned}
 2.843488 \times 10^{-4} &= \frac{103 \times 28.088}{760 \times 82.05 \times 300.778} + \frac{103 \times V_d}{760 \times 82.05 \times 523} \\
 &= 1.542481 \times 10^{-4} + 3.1582 \times 10^{-6} V_d \\
 V_d &= 41.19457 \text{ ml}
 \end{aligned}$$



Line 5            P = 128 mm Hg

$$2.843488 \times 10^{-4} = 1.245815 \times 10^{-4} + 3.9248 \times 10^{-6} V_d$$

$$V_d = 40.70712 \text{ ml}$$

Line 6            P = 144.5 mm Hg

$$2.843488 \times 10^{-4} = 1.027206 \times 10^{-4} + 4.4307 \times 10^{-6} V_d$$

$$V_d = 40.99312 \text{ ml}$$

$$\text{Average } V_d = 40.96494 \text{ ml}$$

Adsorption Measurement

$$T_1 = 297.444^\circ\text{K} \quad T_2 = 523^\circ\text{K}$$

Line	Gas	Stopcock 5	Burette Bulb	P, mm Hg	$V_e, \text{cm}^3$
1	H <sub>2</sub>	closed	2B + 2B'	506.5	46.169
2	H <sub>2</sub>	closed	2B + 3B'	386.5	60.501
3	H <sub>2</sub>	closed	2B + 4B'	283	82.443
4	H <sub>2</sub>	open	2B + 4B'	147.5	82.443
5	H <sub>2</sub>	open	2B + 2B'	219.5	46.169
6	H <sub>2</sub>	open	1B + 2B'	269.5	32.716
7	H <sub>2</sub>	open	1B + 1B'	322.5	22.883
8	H <sub>2</sub>	open	zero	404.5	13.333
9	H <sub>2</sub>	open	4B + 4B'	87	159.360
10	H <sub>2</sub>	open	5B + 6B'	44	347.495

Stopcock 5 closed

<u>Line</u>	<u>PV<sub>e</sub></u>
1	23384.5985
2	23383.6365
3	23331.369

---


$$\text{average} = 23366.5347$$

$$\begin{aligned}
 N_{av} &= \frac{PV_e}{RT_1} \\
 &= \frac{23366.5347}{760 \times 82.05 \times 297.444} \\
 &= 1.2597864 \times 10^{-3}
 \end{aligned}$$

Stopcock 5 open

$$\text{Line 4} \quad P = 147.5 \text{ mm Hg}$$

$$N_{av} = \frac{PV_e}{RT_1} + \frac{PV_d}{RT_2} + N_{ads} \quad (3.18)$$

$$\begin{aligned}
 1.2597864 \times 10^{-3} &= \frac{147.5 \times 82.443}{760 \times 82.05 \times 297.444} + \frac{147.5 \times 40.96494}{760 \times 82.05 \times 523} + N_{ads} \\
 &= 6.556143 \times 10^{-4} + 1.852723 \times 10^{-4} + N_{ads}
 \end{aligned}$$

$$N_{ads} = 4.188998 \times 10^{-4}$$

$$\text{Line 5} \quad P = 219.5 \text{ mm Hg}$$

$$1.2597864 \times 10^{-3} = 5.46371 \times 10^{-4} + 2.757103 \times 10^{-4} + N_{ads}$$

$$N_{\text{ads}} = 4.377051 \times 10^{-4}$$

Line 6            P = 269.5 mm Hg

$$1.2597864 \times 10^{-3} = 4.753588 \times 10^{-4} + 3.385145 \times 10^{-4} + N_{\text{ads}}$$

$$N_{\text{ads}} = 4.459131 \times 10^{-4}$$

Line 7            P = 322.5 mm Hg

$$1.2597864 \times 10^{-3} = 3.978738 \times 10^{-4} + 4.050869 \times 10^{-4} + N_{\text{ads}}$$

$$N_{\text{ads}} = 4.568257 \times 10^{-4}$$

Line 8            P = 404.5 mm Hg

$$1.2597864 \times 10^{-3} = 2.907696 \times 10^{-4} + 5.080857 \times 10^{-4} + N_{\text{ads}}$$

$$N_{\text{ads}} = 4.609307 \times 10^{-4}$$

Line 9            P = 87 mm Hg

$$1.2597864 \times 10^{-3} = 7.474828 \times 10^{-4} + 1.092793 \times 10^{-4} + N_{\text{ads}}$$

$$N_{\text{ads}} = 4.030243 \times 10^{-4}$$

Line 10           P = 44 mm Hg

$$1.2597864 \times 10^{-3} = 8.243352 \times 10^{-4} + 5.52677 \times 10^{-5} + N_{\text{ads}}$$

$$N_{\text{ads}} = 3.801835 \times 10^{-4}$$

### 3.8-6 Platinum Dispersion, Surface Area and Crystal Size from Adsorption Isotherm

The net adsorption of hydrogen on the metal was found by taking the difference between the total adsorption on the catalyst and the adsorption on the support at 250°C and 240 mm pressure. The values are reported in Table 3.7. The net adsorption per gram of catalyst was converted to a ratio of number of H atoms adsorbed per Pt atom in the sample. This ratio represented the metal dispersion based on the assumption that each platinum surface atom adsorbed one H atom. In order to translate the metal dispersion into platinum surface areas, the assumption was made that the low index planes (100 and 110) of platinum were equally exposed on the average on the surface. The site densities (number/cm<sup>2</sup>) of these planes are 1.31 x 10<sup>15</sup> and 0.93 x 10<sup>15</sup> respectively (14), giving an average of 1.12 x 10<sup>15</sup> sites/cm<sup>2</sup>. The metal dispersion was multiplied by the factor

$$\left(\frac{1}{195.09} \frac{\text{moles}}{\text{gPt}}\right) (6.023 \times 10^{23} \frac{\text{atoms}}{\text{moles}}) \left(\frac{1}{1.12 \times 10^{15}} \frac{\text{cm}^2}{\text{sites}}\right) \left(\frac{1}{10^4} \frac{\text{m}^2}{\text{cm}^2}\right)$$

in order to obtain specific surface area of Pt in m<sup>2</sup>/g.

In order to translate specific surface area into average crystal size, it was assumed that all particles were ideal cubes of uniform size with one face in contact with the support and the remaining 5 faces exposed. The length of one edge (d) of the cube was then related to surface area (s) and volume (V) or density (ρ) by

$$d = \frac{5V}{S} = \frac{5}{S\rho} \quad (3.19)$$

The density of Pt is equal to 21.45 g/cm<sup>3</sup> (7). All values are shown in Table 3.6.

Table 3.7

## Platinum Dispersion, Surface Area and Crystal Size

Catalyst	1.62002% Pt on Al <sub>2</sub> O <sub>3</sub>				
Adsorption at 250°C and 240 mm in moles H <sub>2</sub> /g	2.60426 x 10 <sup>-5</sup>				
<table style="border: none; margin-left: 20px;"> <tr> <td style="border: none;">}</td> <td style="border: none;">Sample</td> </tr> <tr> <td style="border: none;">}</td> <td style="border: none;">Support</td> </tr> </table>	}	Sample	}	Support	3.58067 x 10 <sup>-7</sup>
}	Sample				
}	Support				
Net Adsorption, moles H <sub>2</sub> /g sample	2.56845 x 10 <sup>-5</sup>				
H atoms adsorbed per Pt atom in sample	0.62				
Surface Area of Pt, m <sup>2</sup> /g Pt	171				
Pt crystal size, Å	14				

## CHAPTER 4

## SURVEY OF REDISPERSION LITERATURE

## 4.1 Introduction

The exposure of the supported metal catalyst to high temperature and to the impurities of the chemical atmosphere leads to a decrease in catalytic activity. Catalytic deactivation is a complicated phenomenon to which several distinct processes can contribute. A high area support material may undergo a reduction in porosity and surface area, and not only may this render some of the dispersed metal inaccessible, but there will be a more direct loss if the support itself has a catalytic activity.

With regard to the metal function in a dispersed catalyst, the extent of deactivation as indicated by reaction rate may or may not be necessarily paralleled by a decrease in the total metal surface area. If a reaction is site selective - for instance if the preferred site is a metal atom in a corner position rather than in a low index plane - it would be possible for catalytic activity to decrease as a result of a change in the surface topography of the dispersed metal, without a corresponding change in the metal dispersion. Or again, if deactivation was due to the adsorption of a poison at the metal surface, there would be no necessary correspondence between the decline in activity and any change in metal dispersion. However, the loss of exposed surface area of metal resulting from sintering of metal crystallite is one of the primary causes of deactivation in most of the industrial processes.

Of the above mentioned causes of deactivation, agglomeration of the metal crystallites is of particular interest in this work. The causes of sintering are not completely understood, however, excessive temperatures, local temperature excursions and certain environments have been found to enhance the sintering rates.

Since sintering of metal crystallites is one of the primary causes of deactivation, the redispersion of metal crystallites of aged supported metal catalyst is therefore an important area of study. The following regeneration procedures to achieve redispersion of metal crystallites have been suggested in the literature:

- (1) Heating the aged catalyst in an oxygen-containing atmosphere.
- (2) Heating the aged catalyst in an oxygen-containing atmosphere followed by reduction in a hydrogen atmosphere.
- (3) Heating the catalyst in a hydrogen atmosphere.
- (4) Heating the catalyst to high temperatures followed by rapid cooling.
- (5) Chemical dissolution and deposition of the metal.

#### 4.2 Review of Redispersion Work

In U.S. patent 3,134,732 (40), redispersion of platinum metal in a commercial platinum on activated alumina catalyst has been reported. The catalyst was used for hydroforming operation. It was stated that important factors contributing to deactivation of the catalyst were increased size of the platinum crystals, increased



rate of growth of platinum crystals and changes in the platinum crystal lattice. It was further stated that the deactivation resulting from the above mentioned factors should be distinguished from the simpler, more easily reversible, loss of activity of catalyst due to carbonization from the reaction or diminution in hydrocracking activity due to loss of halide which can be restored by halide addition. The reactivation process involved oxidation in air or an oxygen containing atmosphere at a temperature of 700° - 1100°F for 1 - 12 hours to remove carbonaceous material, and treatment with chlorine (1 - 8 weight percent of catalyst) at a temperature of 60° - 1250°F for several minutes followed by reduction with hydrogen at 400° - 1000°F with a hydrogenation pressure of from atmospheric to 1000 psig. Platinum crystallite sizes were measured by X-ray line broadening and found to be  $< 50 \text{ \AA}$  for the fresh catalyst,  $> 200 \text{ \AA}$  for the spent catalyst and again  $< 50 \text{ \AA}$  for the reactivated catalyst. The reported experimental data indicate that the reactivation was more than a restoration of halogen content. The chlorine content of the fresh catalyst was 0.23%, of the spent catalyst, 0.19%, and of the reactivated catalyst, 0.13%. It was mentioned that the time interval of treatment could be varied to obtain the desired degree of dispersion.

In U.S. patent 3,117,076 (41), a reactivation procedure for  $\text{Pt}/\text{Al}_2\text{O}_3$  catalyst has been proposed. The procedure comprised of contacting the deactivated catalyst with gaseous chlorine in a total atomic ratio of chlorine to platinum above about 2:1 at a temperature between 850° and

1000°F for a period of 0.25 to 24 hours. This procedure not only re-activated the catalyst, but also converted various impurities therein into volatile and soluble derivatives which were readily removed by steaming at a temperature of 700°- 1100°F for a period of 2 - 12 hours. The treatment with an aqueous medium also served to redistribute the platinum on the alumina support. It was indicated that increasing or restoring the chlorine content was not the cause of reactivation. No crystallite size measurements were made.

Koegler and Queck(42) reported a reactivation of Pt/Al<sub>2</sub>O<sub>3</sub> catalyst when treated with a 4% solution of NH<sub>4</sub>NO<sub>3</sub>-NH<sub>4</sub>Cl (pH 5-6), followed by heating at 170 °C under a stream of hot air and calcination at a maximum temperature of 450 °C. The activity of treated and new catalyst was found to be the same. Physical characterization of the catalyst was not attempted.

In U.S. patent 3,011,968 (43), a reactivation process for platinum and/or palladium containing catalysts involving subsection of the deactivated catalyst to oxidation-reduction cycle has been reported. It is claimed that the reactivation process not only restores the initial activity and selectivity, but also restores the initial stability. The decarbonized catalyst was rejuvenated by contacting it with air or any other gas containing oxygen at a partial pressure above 0.4 atmosphere and at a temperature of 1000°- 1200°F for a period of 1 - 24 hours followed by a hydrogen treatment at a temperature of 600°- 1000°F. It was noted that a catalyst which had become severely deactivated required a higher temperature, a higher oxygen partial pressure, and/or a longer exposure time. The author believes that loss of hydroforming activity

is due to annealing of the crystallites whereby they assume an unstrained state and the oxidation-reduction treatment regenerates the active centers. It was found that a catalyst subjected to accelerated deactivation in helium could also be reactivated by the above procedure. No mention of crystallite size was made.

U.S. patent 2,879,232 (44) is similar to the above. In it a method of reactivation in which the catalyst is subject to mild oxidation at a temperature of 750°F in an atmosphere containing 2 - 10% oxygen for a period of 0.2 - 5 hours to remove readily oxidizable carbon and then subjected to severe oxidation at a temperature of 1000°- 1200°F for a period of 0.1 - 4 hours, quickly quenched to ambient temperature (in about 10 seconds to about 10 minutes) and then reduced at a temperature of 600°- 1000°F is described. The process of reactivation is viewed very much as in U.S. patent 3,011,968 (43). No physical characterization of the catalyst was attempted.

In U.S. patent 3,278,419 (45) a method for restoring the activity and selectivity of spent halogenated Pt/Al<sub>2</sub>O<sub>3</sub> catalyst has been reported. The method comprises the combined steps of (1) chlorine pretreatment, (2) carbon burnoff and (3) reactivation. During the normal operation of the process when the catalyst is partially deactivated by the accumulation of carbonaceous deposits and by agglomeration of platinum metal crystallites, chlorine and water are introduced into the hydrocarbon feed, the rate of chlorine addition being between 20 ppm and 200 ppm by weight of hydrocarbon feed and the mole ratio of Cl<sub>2</sub> to H<sub>2</sub>O being between 0.0002 to 0.05. The catalyst is prechlorided to 0.3 -1.1% by weight. Carbonaceous deposits are removed from the catalyst by burning in the presence

of an inert gas containing oxygen (< 1%), the average temperature of the catalyst bed being maintained between 700° and 900°F. The reactivation step involves maintaining the catalyst bed at a temperature of 900°- 1000°F in the presence of an inert gas containing at least 20% oxygen and 300 to 750 ppm water for a period of at least 8 hours.

The author reports that this treatment restores the chlorine content of the catalyst and also effects a redispersion of the metal crystallites. It is noted that redispersion of the metal crystallites occurs during the reactivation step and is due to interactions between the chlorine, the air, the water content of air and the temperature. It is further noted that while the chlorine is the principal active reagent for redispersing the platinum, the presence of water in the reactivation step greatly increases the effectiveness of platinum redispersion. The effect of water in the reactivation step on platinum redispersion, measured in terms of hydrogen chemisorption capacity, was studied. It was concluded that an H<sub>2</sub>O content of greater than 100 ppm greatly enhanced the degree of platinum redispersion at all chloride levels, thereby increasing the available surface area of platinum.

Adler and Keavney(20) reported a redispersion of Pt/Al<sub>2</sub>O<sub>3</sub> catalysts when heated to 620 °C in a static 60 psig oxygen atmosphere for 2 hours. "Impregnated" as well as "Cogelled" catalysts were studied. The effects of different treatments were determined by physical measurements of H<sub>2</sub> chemisorption and X-ray line broadening.

The fresh catalysts were sintered by steaming at a temperature of 700°- 750°C and a partial pressure of water vapors between 0.35 and 1 atmosphere. The sintered catalysts were then reactivated in an oxygen

atmosphere. Hydrogen chemisorption capacity and particle size by X-ray line broadening were determined for the fresh, the sintered and the re-activated catalyst. The sintered catalysts showed significantly decreased  $H_2$  chemisorption capacity and after the oxygen treatment a part of the capacity was restored.

The adsorption data were related to particle size by assuming that the adsorption of hydrogen atoms occurred at the interstices of the platinum surface. It was further assumed that platinum atoms formed either a monolayer or a three-dimensional hexagonal pyramid aggregates on the alumina surface. In the monolayer approach,  $I$ , the number of surface interstices was determined from hydrogen chemisorption data and then by assuming the monolayer to consist of  $n$  rows of closed packed platinum atoms, the rows containing alternately  $n$  and  $n-1$  atoms, a relation was found between  $n$  and  $I$  and between  $n$  and  $T$ , the total number of platinum atoms in the monolayer. A similar approach was utilized with the hexagonal pyramid where the mean dimension of the aggregate was taken as the distance between opposite sides of the base. A plot of  $I/T$  vs mean particle dimension was prepared for both cases.

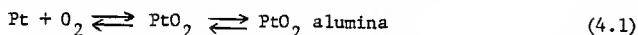
The average particle size as measured by means of X-ray line broadening and that calculated from adsorption measurements showed the same trend but the actual values were not in particularly good agreement. This was attributed to the low resolving power of the X-ray diffractometer ( $\sim 50\text{\AA}$ ). The results did show a decrease in particle size corresponding to increased hydrogen capacity as a result of the reactivation process. The authors viewed the results as follows:

"On the one hand, we do not believe that the results obtained on the reactivated catalysts should be taken to indicate a decrease in Pt particle size. Considerations of energetics would rule out the possibility of a platinum particle of over 200 Å dissociating into 20 Å particle as might be indicated for the cogelled catalyst containing 0.30% Pt. Instead, we interpret the apparent decrease in size after reactivation as due to disruption of the platinum lattice by oxygen atoms. These are removed by subsequent hydrogen dosing, leaving fissures in the sintered particle. These fissures are then responsible for an increase in Pt surface area which accounts for increased H<sub>2</sub> sorption. At the same time, the degree of ordering in the lattice is reduced and this accounts for the line broadening results."

Gruber(13) subjected several Pt/Al<sub>2</sub>O<sub>3</sub> fresh catalysts and a series of catalysts sintered at 500°C in hydrogen to complete cycles of reduction-oxidation, consisting of 2 hydrogen adsorptions at 250°C and 200 mm Hg followed by 2 oxygen adsorptions at 350°C and 150 mm Hg followed by 2 hydrogen adsorptions. Between each of the adsorptions the samples were evacuated for 16 hours at 500°C. The final hydrogen adsorption value served as a measure of the effect of the cycle on the metal dispersion. With catalysts of high dispersion no significant effect was found, however, all other catalysts, fresh and sintered, with low metal dispersion ( $\leq 0.5$ ) showed a significant increase in platinum dispersion. The author concluded that the increase in dispersion of the catalysts prepared with tetraminoplatinum hydroxide must be due to the reaction with oxygen since the catalysts do not contain halogen, on the other hand, the halogen may be partly responsible for the regeneration of the catalysts prepared with chloroplatinic acid.

Johnson and Keith(46) extended the idea proposed by McHenry et al(47), who postulated that the active component of Pt/Al<sub>2</sub>O<sub>3</sub> catalysts consisted of a platinum-alumina complex the extent of which can be measured by the amount of the platinum soluble with the alumina in aqueous hydrofluoric acid or acetylacetone. Johnson and Keith subjected 0.6% and 0.55% Pt/Al<sub>2</sub>O<sub>3</sub> commercial catalysts to different oxygen treatments. The variables considered were partial pressure of oxygen, temperature and time. After oxygen treatment, the catalysts were reduced in flowing hydrogen and the Pt dispersion as measured by CO chemisorption, the amount of soluble Pt and also the H<sub>2</sub>- D<sub>2</sub> exchange rate were measured. An excellent correlation was found between the three. It was suggested that the complex exists in the oxidized state and is desirable, not per se, but because it leads to a high dispersion of the platinum under subsequent reduction.

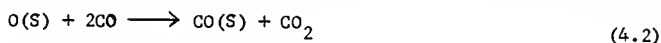
It was found that as the severity of oxidation treatments was increased a limit was reached such that a platinum dispersion decrease resulted from the treatment. To explain this the reaction



was suggested with the idea that as the catalyst is treated in a given oxygen partial pressure at successively higher temperatures, a limit is reached at which the oxygen pressure equals the decomposition pressure. Above this temperature the equilibrium shifts to the left forming platinum metal with the ultimate result of increased crystallite size. It was noted that the critical temperature increased as oxygen partial pressure increased and also the amount of platinum-alumina complex increased as

the oxygen partial pressure increased with temperature held constant. The critical temperatures for oxygen partial pressures of 0.21 atm and 1 atm were found to be 510°C and 580°C respectively.

Wentrock, Kimota and Wise(36), subjected a 0.6% Pt/Al<sub>2</sub>O<sub>3</sub> catalyst to a series of successive oxygen exposures (0.25 Torr). The surface area as determined by a CO titration technique based on the reaction



was found to increase after each oxygen exposure. The increase in surface area was of the order of 10% after five oxygen exposures.

It was proposed that the adsorption of oxygen appeared to cause surface reconstruction, which modified the number of binding sites available for subsequent H<sub>2</sub> or CO adsorption. It was further proposed that such surface reconstruction resulted in the formation of atomic steps and terraces that favor dissociation and chemisorption of hydrogen and also such rearrangements of lattice atoms on an atomic scale caused displacement and formation of surface structures favorable for CO adsorption, especially of bridge-bonded species.

Weller and Montagna(23) studied adsorption and desorption of oxygen on platinum-alumina and platinum-zeolite catalysts at 475° and 525°C and used H<sub>2</sub> chemisorption at 200°C as a measure of Pt dispersion. They observed sintering of Pt in Pt/Al<sub>2</sub>O<sub>3</sub> on exposure to oxygen and redispersion of Pt on exposure to hydrogen. The redispersed catalyst was found to be quite resistant to subsequent sintering in cyclic O<sub>2</sub> - H<sub>2</sub> treatment. Platinum-zeolite catalyst was more susceptible to sintering than platinum-alumina.



Wanke et al(48,49,50) studied the effects of treatment in oxygen and hydrogen at elevated temperatures on the dispersion of alumina supported Pt, Ir and Rh commercial as well as lab-prepared catalysts. Hydrogen adsorption uptake was used as a measure of metal dispersion. Five Pt/Al<sub>2</sub>O<sub>3</sub> catalysts (0.5 to 4.0 wt% Pt) were subjected to oxygen treatment at temperatures of 300° to 700°C and time periods of 1 to 128 hours. Significant increases in dispersion were observed at temperatures ≤600°C. At 500° and 550°C the increases in dispersion were relatively independent of treatment time. At higher temperatures, rapid, time dependent decreases in dispersions were observed. Significant redispersion for a heavily sintered catalyst was also observed.

The treatment in oxygen resulted in a small redispersion at lower temperatures and in a heavy sintering at higher temperatures for Ir and Rh catalysts. The hydrogen treatment resulted in sintering at temperatures higher than 550°C for all the three catalysts.

The authors attempted to determine whether redispersion is a transitory phenomenon. They treated 0.3% Pt/Al<sub>2</sub>O<sub>3</sub> catalyst in air at 575°C for short time periods and tried to monitor the rate of change of dispersion. However no evidence of redispersion was found but extensive sintering was noted. No explanation was offered for such behaviour. The authors concluded that rate of sintering or redispersion is very sensitive to both gas atmosphere and metal loading.

In most of the above references, the increase in surface area of metal caused by regeneration was detected indirectly by selective adsorption of H<sub>2</sub> or O<sub>2</sub>. Ruckenstein and Malhotra(51) observed the redispersion of platinum crystallites using transmission electron microscopy. The catalyst was prepared by depositing Pt crystallites on thin films of

nonporous alumina. It was found that heating the catalyst in air at 500° and 600°C for 24 hours followed by slow cooling to room temperature resulted in sintering. The average crystallites size increased from 31 Å (fresh catalyst) to 39 Å and 107 Å for 500°C and 600°C treatments respectively. However, reheating the catalyst, which had been treated in air at 600°C for 24 hours, to 500°C for 24 hours followed by slow cooling to room temperature resulted in redispersion of Pt crystallites and the average crystallite size decreased to 41 Å. A lower redispersion was observed when the second heating was at 400°C (83 Å). Rapid cooling to liquid nitrogen temperature after initial heating at 400°C caused the crystallites to disappear, i.e. either they fragmented into atomic particles which were beyond the resolving power of microscope ( $\sim 5$  Å) or completely evaporated.

The authors attributed splitting to the formation of a platinum-alumina complex in the presence of oxygen, the interfacial mismatch due to this complex causing a strain in the crystallites and relaxation of this strain energy resulting in splitting. Since redispersion is associated with the formation of the complex, it can only occur below the decomposition temperature of the complex. A contraction of the crystallites due to surface tension effects was also proposed by the authors.

Maat and Moscou(52) studied sintering of a 0.6% Pt/Al<sub>2</sub>O<sub>3</sub> catalyst by subjecting it to heat treatment in air at 780°C for 0 - 72 hours. The crystallite size measurements were made by H<sub>2</sub> chemisorption and electron-microscopy. It was mentioned that a special laboratory scale regeneration caused a part of the platinum to be redispersed into crystallites of 10 - 20 Å diameter as seen by the electron microscope.

Jaworska-Galas and Wrzyszczy(53) studied the effects of calcination temperature on support and metal surface area and also the effect of a regeneration procedure on metal dispersion for Pt/Al<sub>2</sub>O<sub>3</sub> catalysts. An O<sub>2</sub>-H<sub>2</sub> titration technique was used to determine metal surface area. It was found that the calcination of the support at high temperatures before impregnation resulted in a decrease in total(BET) surface area but an increase in platinum surface area. Heating the catalyst at elevated temperatures resulted in sintering. Regeneration of a used catalyst in a stream of air at 480°C followed by reduction in hydrogen for 1  $\frac{1}{2}$  hours resulted in redispersion of Pt crystallites. The metal surface area after regeneration was 197 m<sup>2</sup>/g. Pt as compared to 145 m<sup>2</sup>/g. Pt of fresh catalyst and 101 m<sup>2</sup>/g. Pt of used catalyst. The redispersion was attributed to oxidation of bulk platinum which leads to greater dispersion on reduction.

Spindler and Kraft(54) studied the effect of heat treatment in air and H<sub>2</sub> at 500°C and 600°C on several Pt/Al<sub>2</sub>O<sub>3</sub> catalysts. O<sub>2</sub>-H<sub>2</sub> titration, X-ray diffraction and "soluble Pt" measurements were used to characterize the catalysts. The results showed that highly dispersed platinum was converted completely to the soluble form by air treatment at 500°C increasing the platinum surface in this process. The mechanism of redispersion was explained via metal-support complex formation as proposed by Johnson and Keith(46). Heat treatment in air at 600°C resulted in redispersion for one catalyst and sintering for another. To explain this it was proposed that at temperatures above 500°C oxides of Pt start decomposing and in addition to an oxidation of small crystallites a growth of large crystallites takes place. The studies showed that "soluble Pt" may consist of various Pt forms including non-stoichiometric Pt-O compounds.

Furhman and Parravano (55) mentioned that an inversion point in the sintering of supported platinum in an oxidizing atmosphere exists: above about 550°C crystal growth takes place, below this temperature redispersion of Pt occurs.

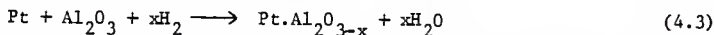
Hasan et al (56,38) studied the effect of vacuum, nitrogen, oxygen and hydrogen atmospheres on the sintering of Pt/Al<sub>2</sub>O<sub>3</sub> catalyst in the temperature range 300° - 800°C for a period of 2 hours. Surface area measurements by chemisorption of H<sub>2</sub> at liquid nitrogen temperature and activity measurements for hydrogenation of cyclohexene and decomposition of hydrogen peroxide were made.

At temperatures below 400°C, the treatment in these atmospheres resulted in sintering. The treatment at temperatures higher than 400°C in vacuum, N<sub>2</sub> and H<sub>2</sub> lead to redispersion. However, the treatment in O<sub>2</sub> showed a continuous sintering over the whole range of temperatures. The order of decreasing catalytic activity at temperatures < 400°C was O<sub>2</sub> > N<sub>2</sub> vac. > H<sub>2</sub> and at temperatures > 400°C the order of decreasing activity was H<sub>2</sub> > vac. > N<sub>2</sub> > O<sub>2</sub>. An excellent agreement was found between surface area and activity measurements. These results are contrary to those reported by Wanke et al (49,50).

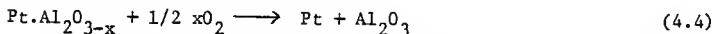
Dautzenberg and Wolters (39) studied the effect of heat treatments in air and hydrogen on Pt/Al<sub>2</sub>O<sub>3</sub> catalysts. H<sub>2</sub> chemisorption at -78°C and 0.1 Torr, X-ray diffraction and electron microscopy techniques were used to find average crystallite size. The results showed decreased hydrogen chemisorption capacity for both treatments.

During heat treatment in air above 500°C sintering of Pt was observed, which resulted in bimodal distribution of crystallite size (< 3nm and 10-15 nm). Oxygen treatment at temperatures below 500°C was found to be incapable of redispersing the sintered crystallites.

During heat treatment in hydrogen, increase in crystallite size did not occur but rather a certain amount of platinum became "inaccessible" for hydrogen chemisorption by, according to these authors, complexing with the support. The Pt-Al<sub>2</sub>O<sub>3</sub> complexing was represented by the reaction



Oxygen treatment at temperature about 500°C restored the lost Pt. The process was explained by the reaction

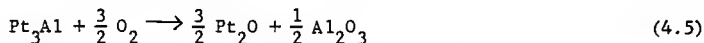


The increase in dispersion value obtained at a given oxidation temperature was found to be independent of the length of oxidation exposure and of the oxygen partial pressure.

Beyond about 600°C, the treatment in oxygen resulted in heavy sintering of the Pt crystallites. The dispersion ratio of these sintered catalysts could not be restored by air treatment at the preferred lower temperatures.

The authors concluded that the oxidation treatment could only recover the fraction of platinum lost by heat treatment in the hydrogen atmosphere, and that it was incapable of redispersing the sintered crystallites.

Den Otter and Dautzenberg(72) studied the hydrogen treated Pt/Al<sub>2</sub>O<sub>3</sub> catalysts to investigate the reasons for the apparent platinum loss upon treatment in hydrogen at high temperatures (> 500°C), as observed by Dautzenberg and Wolters(39). Hydrogen and oxygen chemisorption and H<sub>2</sub>-O<sub>2</sub> titration at 0°C and 0.1 mm Hg pressure were used to measure the dispersion of the catalysts. The chemisorption capacity was found to decrease for hydrogen but not for oxygen. The authors proposed that the apparent platinum loss was caused by the formation of a platinum-aluminum alloy. These alloy sites chemisorb oxygen but not hydrogen. On treatment in oxygen at high temperatures, the alloy decomposes and a part of the lost Pt is restored. The process was explained by the reaction



The conversion of n-hexane into cracking, isomerization and dehydrocyclization products was also studied for a hydrogen and an air treated catalyst. The product distribution was found to be quite different when quantities of both samples representing an equal hydrogen-detectable platinum surface area were used. It was concluded that the sintering in hydrogen and in air leads to completely different catalytic properties due to a change in the state of the platinum on the support. Nuclear magnetic resonance (NMR) studies indicated that after reduction at 400°C, the Pt was present as zero valent species while after reduction at 675°C a change in the Pt species was observed which was attributed to alloy formation.

Baker, Thomas and Thomas(57) used the technique of controlled atmosphere electron microscopy to follow the behaviour of platinum particles when heated to 920°C in oxygen and nitrogen. Platinum was introduced on an alumina film in three different ways (a) as the pure metal by vacuum evapor-

ation of platinum (b) from 0.5% solution of chloroplatinic acid and (c) from a 0.5% solution of tetrammine platinous hydroxide.

Heating in 2 Torr oxygen atmosphere resulted in sintering of Pt crystallites below 800°C and redispersion above 800°C. The particle growth from the chloroplatinic acid preparation was significantly lower than the other two. The catalyst prepared by vacuum evaporation of platinum metal on alumina, on exposure to HCl at room temperature after being heated in oxygen at 500°C, showed the same particle growth rate as was found for the catalyst prepared from chloroplatinic acid. This led the authors to believe that the chloride ion had a strong inhibition effect on the sintering of Pt supported on alumina in an oxygen atmosphere.

In 2 Torr nitrogen atmosphere, the particle growth was significantly faster than in oxygen and no redispersion was observed at temperatures > 800°C. It was proposed that the decrease in particle sizes at temperatures >800°C is influenced by the tendency of platinum to form a volatile oxide at elevated temperatures.

#### 4.3 Redispersion and Sintering Models

Three mathematical models based on postulated mechanisms for redispersion and sintering have been proposed. The model developed by Ruckenstein and Pulvermacher(58,59) envisages the sintering of supported metal catalysts to occur by migration of metal crystallites over the surface of the support, and the resulting collision and fusion of metal particles causes the loss in dispersion. This model will be referred to subsequently as the crystallite migration model. The second model proposed by Flynn and Wanke(60,61) considers the sintering to occur by dissociation of atomic or molecular species from the metal crystallites. These atomic or molecular species migrate over the support surface and become incorporated into the metal

crystallites upon collision with the stationary metal crystallites. This model will be referred as the atomic migration model. The third model, proposed by Ruckenstein and Dadyburjor(62) accounts for the behaviour of a population of small metal crystallites on a substrate by the splitting of single metal atoms and multiatom particles from larger particles, their diffusion along the substrate and the coalescence of particles (or of a particle and an atom) that collide. This model will be referred as the atom-particle migration model.

The transport of metal or metal compounds through the vapor phase is another possible mechanism for the sintering of supported metal catalysts. The transport of metal by this mechanism in non-oxidizing atmospheres is negligible for group VIII metals at temperatures below 1000 °C; in oxidizing atmospheres the transport via metal oxides may be appreciable at lower temperatures. Little loss of Pt has been observed under normal temperatures encountered in the sintering of supported metal catalysts(63).

The phenomenon of redispersion almost certainly involves interactions between the metal, the support, and the environment. These interactions are extremely complex. In ultrahigh vacuum on homogeneous surfaces, binding energies between the metal and the support are low enough to be attributed to Van der Waals interactions ( $\sim 20$  kcal/g atom). However, in the presence of some atmospheres, particularly oxygen, stronger interactions arise which are not necessarily removed by reduction or evacuation. Surface contamination and heterogeneity also increase the energy of interaction.

#### 4.3-1 Crystallite Migration Model

The crystallite migration model postulates that metal crystallites migrates as entities along the surface of the support. Rapid diffusion of



metal atoms on the surface of a metal crystallite causes metal atoms to accumulate on one side of the crystallite by random fluctuations. This rapid, random fluctuations causes the motion of the particle on the support(64). The crystallite migration is size dependent and is very small for particles larger than about  $50 \text{ \AA}$  (64).

Two limiting cases of the crystallite migration model were developed: (1) surface diffusion controlled (i.e., the rate of migration of crystallites is the rate determining process), and (2) sintering controlled (i.e., the merging of two metal crystallites coming into physical contact by collision is the rate determining process). For both of these cases, the solution of the kinetic equations led to a family of rate equations for the total exposed surface area,  $S$ , of metal of the form,

$$\frac{dS}{dt} = -KS^p \quad (4.6)$$

The index  $p$  was found to depend upon the relative magnitude of the diffusion coefficient and the coalescence constant as well as the particular size dependencies used for these parameters. For the sintering controlled case,  $p$  is equal to 2 or 3, and for the surface diffusion controlled case  $p \geq 4$ .

Wynblatt and Gjostein(64) obtained values of  $p \approx 13$  in their sintering experiment on supported Pt. They considered an additional, slow, nucleation step in the growth of the larger particles to explain the large values of  $p$ .

A number of criticisms have been levelled at the crystallite migration model(60). These include:

1. It cannot account for large values of  $p$ .

2. It cannot account for redispersion.

3. Platinum agglomeration has been observed to continue when the size of the metal crystallites exceeds the size of the alumina support particles(60). The occurrence of this growth by crystallite transport over long distances of the irregular support, by diffusion from one particle to the next, seems unlikely.

4. There is little evidence of motion of the crystallites over the appreciable distances needed to account for sintering of supported metal catalysts. Controlled atmosphere electron microscopy (CAEM) (57,65,66,67) has been used to obtain direct evidence of crystallite migration, but the results show very slight motion. Ruckenstein and Dadyburjor(62) noted that CAEM cannot observe particles smaller than  $25 \text{ \AA}$  and concluded that the fact that not much migration could be observed by CAEM experiments is perhaps due to this resolution limit.

Wynblatt and Gjostein(64) observed minimal migration, less than  $100 \text{ \AA}$  in 16 hours at  $1000^\circ\text{C}$  in a hydrogen atmosphere, for Pt particles of an average size of  $75 \text{ \AA}$  on an alumina support. They concluded that particle migration is too slow a process for particle size greater than  $50 \text{ \AA}$  to account for the observed sintering rates. Ruckenstein and Dadyburjor(62) explained that the size dependence of the diffusion coefficient in the crystallite migration model accounts for the fact that the larger particles have a negligible migration. However, the larger particles grow because the smaller particles, which migrate much faster, would coalesce with them.

#### 4.3-2 Atomic Migration Model

The model presented by Flynn and Wanke(60,61) considers sintering

to occur as a three step process: (1) escape of metal atoms (or molecules such as metal oxides in an oxygen atmosphere) from the metal crystallite to the support surface, (2) migration of these atoms along the support surface, and (3) either capture of these migrating atoms by metal crystallites upon collision or immobilization of the migrating atoms by a drop in temperature or by encountering an energy well on the support surface. This process results in the growth of the large metal crystallites and in a decrease in size of the small metal crystallites. The driving force for transfer of metal from smaller to larger crystallites is reduction in surface energy.

Two cases of this model were analyzed: (1) the rate of capture of migrating surface atoms is large, and (2) the rate of capture is small. For both cases rate of surface migration was assumed to be large, i.e., there are no concentration gradients of migrating atoms on the support surface. The rate of loss of atoms from the metal crystallites was taken to be independent of the crystallite size. The temperature dependence of the rate of loss of atoms from the crystallites was assumed to follow the Arrhenius law.

Both cases of the atomic migration model predict a strong dependence of the rate of sintering on the metal particle size distribution (PSD). Catalysts with broad or bimodal PSD are predicted to sinter more rapidly than catalyst with narrow PSD. Initially, unisized PSD on homogeneous supports would not sinter at all according to the model, and statistical fluctuations in particle sizes would be required to initiate sintering.

For the case of rapid capture, the metal dispersion decreases monotonically with time, while for low rates of capture the metal dispersion

can increase initially and then decrease. This increase in dispersion is due to the migrating surface atoms which have a dispersion of unity. Re-dispersion will occur if these migrating atoms are trapped at high energy sites on the support surface or the nucleation of small metal particles from these migrating species is brought about by rapid cooling. The rate of loss, which partly governs the concentration of migrating atoms, is greatly influenced by the atmosphere due to the influence of the atmosphere on metal-support interaction. Large metal-support interactions increase the ease with which atoms or molecules can escape from the crystallite to the support.

In order for appreciable rates of sintering to be predicted by this model at temperatures of 500° to 800°C, the activation energy for the escape of metal atoms (or molecules) from the crystallite has to be  $\leq 75$  kcal/g atom. The heat of sublimation of Pt is 135 kcal/g atom and hence metal-support interaction has to be of the order of 60 kcal/g atom or higher. Metal-support interactions in the presence of certain atmospheres and some localized metal-support interactions in the presence of defects in the support structure can exceed Van der Waals interactions ( $\sim 20$  kcal/g atom), but to require these interactions to be 60 kcal/g atom in order for sintering to occur appears unjustifiable.

Ruckenstein and Dadyburjor(62) noted that Flynn and Wanke(61) assume that all particles of less than 14 atoms are inherently unstable and reduce instantaneously to single atoms. This is true if all the particles are in the form of fcc crystal structures. Certainly small clusters of atoms will not have the same structure as the bulk metal, but this does not mean that they cannot exist in some form other than atomic. A problem with the

practical application of the atomic migration model is that the initial PSD has to be known, but reliable data of this type are difficult to obtain.

#### 4.3-3 Atom-Particle Migration Model

This model entails the emission, migration and coalescence of metal particles of every size, including single atoms. The rate at which one particle is captured by another is determined by the rate of diffusion of particles from the bulk to the interface of the other particles and the kinetics of the capture process at the interface. The rate of emission is proportional to the equilibrium concentration, on the original particle interface, of particles having the size of the particles to be emitted.

The activation energy for emission of dimers was found to be about twice that for single atom emission; since the activation energy is exponentially related to emission rate; the rate of emission of dimers is many orders of magnitude smaller than the corresponding rate for single atoms. Hence, even if particles can lose single atoms to the support by activated breaking of bonds the loss of aggregate of two or more atoms must occur via another mechanism. This alternate mechanism is not entirely clear but is probably due to the existence of cracks on the crystallite and their propagation due to internal stresses caused either thermally or by the formation of chemical compounds. Ruckenstein and Dadyburjor(62) considered the emission of only single atoms for detailed studies.

For identical set of conditions, the value of the sintering index  $p$  [Eq. 4.6] was evaluated for the crystallite migration and the present model. The crystallite migration model predicted a value of 6 whereas

based on the present model, the value was found to vary between 7.6 and 24.5. Thus the large values of  $p$  obtained in sintering experiments by Wynblatt and Gjostein(64) can be explained by the atom-particle migration model.

This model can predict a continuous decrease in surface area with time and a decrease followed by an increase in surface area, as well as a continuous increase in surface area with time and an increase followed by a decrease. The behaviour depends upon the relative magnitude of emission, diffusion and capture and also on metal loading. It should be noted that only the case of single atom emission was considered quantitatively and that crystallite fracture was not modelled.

#### 4.3-4 Comparison of the Different Models

Experimental attempts to determine which of the two mechanisms, i.e., crystallite or atomic migration, is predominantly responsible for the sintering of supported metal catalysts have not been conclusive because of the complexity of the sintering process. If support surfaces were energetically homogeneous, a number of tests could distinguish between crystallite and atomic migration. For example, the crystallite migration model predicts that the rate of sintering is relatively unaffected by initial PSD, while the atomic migration model predicts a marked dependence on the initial PSD. However, real surfaces are energetically heterogeneous; if strong trapping sites and preferred adsorption areas are included, either model can account for a wide variety of phenomenon.

Bett, Kinoshita and Stonehart(68) argued that an increase in sintering rate with an increase in metal loading supports the crystallite migration model. However, the atomic migration model also predicts a sintering rate which is dependent on metal loading(61).

Flynn and Wanke(48) attempted to differentiate between the two mechanisms by examining identical areas of a catalyst surface before and after thermal treatment by transmission electron microscopy. The detection of all small Pt crystallites and carbon contamination of large particles posed detectability problems. It was found that at least some Pt particles remained in a fixed location during continued thermal treatments and that agglomeration of Pt occurred during these steps. On a heterogeneous surface, the crystallite migration model can account for fixed particles and the atomic migration model can account for the appearance of particles at new locations. Hence, these studies do not allow either model to be definitively selected. The authors also tried to sinter a catalyst while observing it in the electron microscope using a heated grid holder, but the attempt was unsuccessful because drift of the specimen prevented resolution and recording of the metal particles of the order of 10nm and less.

Furhman and Parravano(55) observed from their experimental results that the variation in the ratio of the rate constant,  $K$ , [Eq. 4.6] and the platinum content of the catalyst was small and hence concluded that the sintering of platinum on alumina catalyst occurs via an atomic transport mechanism. Since both models show metal load dependence, the experimental observations of Furhman and Parravano(55) cannot be very conclusive.

Fedorow and Wanke(49) attempted to differentiate between the two mechanisms based on their redispersion results. In the crystallite migration model, particle splitting has been proposed to account for redispersion. Hence the redispersion should be relatively independent

of metal loading and initial metal crystallites size, while the atomic migration model predicts a dependence on these properties. Four catalysts were prepared to determine the effect of metal loading on redispersion. Since the Pt was not uniformly distributed throughout the support pellets, the effect of metal loading could not be determined. The maximum dispersion obtained was found to increase with decreasing initial crystallite size. The authors concluded that the dependence of the increase in dispersion on the initial dispersion supports the atomic migration model.

With the exception of redispersion, most of the experimental observations can be explained by either the crystallite or the atomic migration model on a heterogeneous support. Sintering rate data are insufficient for discrimination between the two mechanisms. Other experiments such as in situ microscope sintering studies of Baker et al(57) are needed to have greater understanding of the sintering mechanisms.

The atom-particle migration model which combines the characteristics of both the atomic and the crystallite migration models can obviously be manipulated to explain most experiment results.

#### 4.4 Proposed Redispersion Procedure

Redispersion using oxygen has received more attention and more quantitative information is available than for procedures utilizing chlorine (and other halogen compounds). With this in mind, the redispersion procedure involving oxygen treatment was selected as a first area of investigation.

Most of the redispersion work in oxygen environments has been restricted to 400°-600°C. This has been explained by associating redispersion



with a metal-support complex that is formed in the presence of oxygen. The upper temperature limit is set by the decomposition temperature of the complex and the lower temperature limit is set by the low rate of complex formation.

Ruckenstein and Malhotra(51) observed sintering on heating the catalyst in air at 500°C and 600°C for 24 hours. Heating at 500°C after the initial heating at 600°C caused redispersion. Heating at 400°C followed by rapid cooling to liquid nitrogen temperature caused the crystallites to disappear, i.e., either they evaporated or became smaller than the resolving power of the microscope. Similar results were observed at treatment times of 4, 8 and 24 hours. The reason why heating at 500°C caused sintering and reheating at 500°C after an initial heating at 600°C caused redispersion is not entirely clear. It was suggested by Ruckenstein and Malhotra(51) that the sintered crystallites are in a strained state which helps in their splitting during the complex formation stage. The reason for disappearance of crystallites on heating at 400°C followed by rapid cooling was not discussed.

Flynn and Wanke(48) observed redispersion on a commercial 0.5% Pt catalyst after it was heated for 16 hours in oxygen at 450-550°C. An effort to determine whether redispersion is a transitory phenomenon followed by particle growth failed when 0.3% Pt commercial catalyst on treatment in air at 575°C for time periods from 6 hours to 1 month showed no evidence of redispersion but sintered extensively. No explanation of this behaviour was offered.

Fiedorow and Wanke(49, 50) observed redispersion of Pt catalysts on oxygen treatment at temperatures upto 600°C. They studied the effect of

treatment periods of 1 to 128 hours on dispersion. It was found that exposure to oxygen for 1 hour resulted in maximum redispersion.

Hasan et al(38) reported a treatment time of 2 hours in the temperature range 300-800 °C to be sufficient to attain stationary values of dispersion and activity.

The literature review reveals that treatment times of less than 1 hour in oxygen atmosphere have not been attempted. The work of Fiedorow and Wanke(49) shows a definite need to study the effect of very short treatment times on dispersion. Rather than finding the conditions under which maximum redispersion occurs, finding the minimum conditions under which a reasonable redispersion can be obtained would be of much more significance as this would contribute to the understanding of the redispersion mechanism and would also have important industrial implications. With this in mind, experiments with very short exposure times at low partial pressures of oxygen have been started.

## CHAPTER 5

EXPERIMENTAL STUDIES OF PRETREATMENT AND  
REDISPERSION OF SUPPORTED METAL CATALYSTS

## REVIEW

## 5.1 Introduction

Selective gas adsorption on the metal surface has become a standard technique for the determination of the dispersion of supported metal catalysts. To obtain reproducible chemisorption results, proper outgassing and reduction of the catalyst is essential. Experiments were designed to establish the proper outgassing and reduction procedures and the effect of these treatments on the dispersion of a supported Pt catalyst was examined.

Preliminary experiments on the redispersion of Pt on an alumina support were designed to study the effect of short treatment times and repeated oxidation - reduction treatments on the dispersion. The results are compared with the work of other investigators.

## 5.2 Review of Catalyst Preparation

The most commonly used methods for the preparation of supported metal catalysts are:

- (1) Impregnation
- (2) Precipitation
- (3) Ion-Exchange

## 5.2-1 Impregnation

In this method, the support is wetted by a solution of the desired metal salt or compound, followed by drying and hydrogen reduction. The support is sometimes evacuated prior to contacting it with the impregnating solution, thus resulting in a more uniform distribution of the active

component (69) through the support particle.

Repeated impregnations with intermediate drying may be used for introducing higher metal concentrations and for introducing more than one component. For multicomponent catalysts, the order of impregnation may be important.

#### 5.2-2 Precipitation

In this method, a hydroxide or carbonate of the metal is generally precipitated from a solution of the metal salt on the carrier suspended in the solution. In general metal nitrates are used because other anions (e.g., chloride or sulfate) sometimes act as catalyst poisons if they are present in the final product (69). In the co-precipitation method, both the carrier and the metal compound are precipitated simultaneously from the solution.

One of the primary problems arising in the preparation of a precipitated catalyst is that of purification from occluded or adsorbed impurities (69).

#### 5.2-3 Ion-Exchange

In this method, the metal cations are introduced to the support by exchange with ions on the surface of the support in a solution of high pH; the metal uptake being dependent on the pH of the solution and the acidic nature of the support (70). Precipitation at these pHs can be avoided by the addition of enough ammonia or amine (70).

### 5.3 Catalyst Preparation, Pretreatment and Redispersion Procedures of other Investigators

In their work, Spenadel and Boudart (14) prepared the catalyst by impregnation of the support with aqueous chloroplatinic acid, followed by drying at 550°C for 1 hour. Before hydrogen adsorption isotherm measurements, the catalyst was outgassed in vacuo at 500°C for a few hours, then kept

under 1 atmosphere of hydrogen at 500°C for 1/2 hour to reduce the surface and finally outgassed at 500°C for 16 hours. Increase in the final outgassing time from 16 to 72 hours did not result in any detectable difference in adsorption. The outgassing was considered complete when a pressure of less than  $10^{-3}$  mm Hg could be maintained for more than 15 minutes with the system cut off from the pumps at the temperature of the experiment.

Gruber (13) prepared catalyst samples by impregnation of the support with platinum salt solutions. The standard pretreatment consisted of reduction in flowing hydrogen for 2 hours at 500°C followed by evacuation at 500°C for 16 hours at a pressure of less than  $10^{-5}$  mm Hg. Evacuation at a temperature of 450°C or lower, and for a time of 6 hours or less was found to result in unsatisfactory reproducibility of the adsorption measurements. The reproducibility of hydrogen adsorption measurements was  $\pm 1\%$ .

Benson and Boudart (27) used Pt/Al<sub>2</sub>O<sub>3</sub> catalysts obtained from Esso Research and Engineering Company. The catalysts were prepared by impregnation of  $\eta$ -alumina with aqueous chloroplatinic acid followed by calcination in air at 593°C for 4 hours. The pretreatment procedure used before adsorption measurements was: outgassing under evacuated conditions for 1/2 hour at room temperature and 3 hour at 150°C; reduction in flowing hydrogen at 500°C for 12 hours and finally outgassing at 500°C for 1 hour.

Mears and Hansford (28) studied the effect of different atmospheres on outgassing times, for a commercial Pt/Al<sub>2</sub>O<sub>3</sub> catalyst. They found that several hours of outgassing time was required at 500°C to achieve a vacuum of  $10^{-5}$  torr after the catalyst had been subjected to hydrogen atmosphere. In contrast, only 10 minutes was required at 25°C to achieve the vacuum of  $10^{-5}$  torr for the catalyst subjected to a helium atmosphere. Based on these findings, they suggested that after reduction, the catalyst should be

outgassed for at least 10 hours at 500°C. The pretreatment procedure used in their work consisted of: outgassing for 15-20 minutes at room temperature and 1-2 hours at 150°C; reduction in flowing hydrogen for 2 hours at 500°C, and final outgassing at 500°C for 16 hours.

The catalysts used in the work of Weller and Montagna (23), were prepared by impregnation of  $\eta$ -alumina with aqueous chlorplatinic acid and pretreated according to the following schedule: heated from 25° to 450°C in 2 hours in flowing hydrogen; held at 450°C for 1/2 hour; heated from 450° to 550°C in 1/2 hour; and held at 550°C for 1 hour, all in flowing hydrogen. The reduction was followed by evacuation at 550°C for 2 hours. The standard pretreatment, after the catalyst had been exposed to oxygen atmosphere, consisted of reduction in flowing hydrogen for 1 hour at 550°C followed by evacuation at 550°C for 2 hours.

Kikuchi, Flynn and Wanke (29) prepared the catalysts by wetting alumina in an  $H_2PtCl_6$  solution, followed by evaporation (at 110°C) to dryness and reduction in flowing hydrogen for 1 hour at 250°C. The standard pretreatment before adsorption measurements was reduction in flowing hydrogen for 2 hours at 500°C and then evacuation for another 2 hours at 500°C.

Wanke et al (49,50) prepared the catalysts by wetting the support with distilled water ( $1\text{ cm}^3 H_2O/g$  of  $Al_2O_3$ ), followed by addition of 1 ml of  $H_2PtCl_6$  solution/g of  $Al_2O_3$ . The mixture was allowed to stand for 24 hours with intermittent stirring before being dried at 110°C for 24 hours. Before adsorption experiments, the catalysts were reduced in flowing  $H_2$  for 16 hours at 150°C, 2 hours at 250°C and 1 hour at 500°C. The reduced catalysts were then stored in air at room temperature.

The following redispersion and adsorption procedures were employed: the catalyst was redispersed or sintered in flowing oxygen at a pressure of approximately 0.92 atm. After the catalyst had been redispersed or sintered for the desired period of time at the desired temperature, it was pretreated for hydrogen adsorption measurements. The procedure employed was:

1. The flowing oxygen was replaced by an inert gas while the sample was at the sintering temperature.
2. The sample was removed from the furnace and the furnace was cooled from the sintering temperature to 500°C.
3. The inert gas flow was replaced by hydrogen while the sample was at room temperature and then the sample was placed into the furnace, and the hydrogen flow was continued for 1 hour at 500°C.
4. The hydrogen flow was replaced by nitrogen, and the catalyst was kept in flowing nitrogen at 500°C for 2 hours.
5. The sample tube was removed from the furnace and cooled to room temperature, and hydrogen adsorption uptaken were measured by a pulse technique.

The treatment between adsorption measurements consisted of reduction in flowing hydrogen at 500°C for 1 hour followed by degassing in flowing nitrogen at 500°C for 2 hours. The average coefficient of variation for repeated adsorption determinations and repeated sintering experiments was found to be 2.9 and 6.8% respectively.

Hassan et al. (38) prepared catalysts by impregnation of  $\gamma$ -alumina with chloroplatinic acid solution. After filtration, drying for 24 hours at 110°C and calcination at 300°C, the catalyst were reduced in flowing  $H_2$  for 4 hours at 300°C. Finally the catalyst samples were evacuated for 4 hours at 250°C and at a pressure of less than  $10^{-5}$  mm Hg. It is reported that this standard pretreatment resulted in good reproducibility of the adsorption measurements. The catalysts

were sintered by heating in the sintering atmosphere for 2 hours at the desired temperature.

Dautzenberg and Wolters (39) prepared the catalysts by impregnation of preclacined aluminas with an aqueous solution of  $\text{Pt}(\text{NH}_3)_4(\text{OH})_2$  or  $\text{H}_2\text{PtCl}_6$ . The impregnated aluminas were dried for 15 minutes at 100-120°C and subsequently calcined for 1 hour at 280°C, followed by 3 hours at 500°C. Prior to adsorption, all catalyst samples were reduced in hydrogen at 400°C and atmospheric pressure for 1 hour, followed by heating under vacuum ( $10^{-6}$  torr) at 400°C for 16 hours. After oxygen treatment, the samples were reduced in hydrogen for 2 hours at 400°C.

## EXPERIMENTAL

### 5.4 Catalyst Preparation and Pretreatment

Kaiser 201 Alumina (Kaiser Chemicals, Baton Rouge, Louisiana) was used as the support material. It was ground and screened and the 10-12 mesh range was used for the catalyst preparation. The BET surface area of Kaiser  $\text{Al}_2\text{O}_3$  was found to be 322  $\text{m}^2/\text{g}$ .

1.62% Pt on Kaiser 201 alumina was prepared in the following way: 72.5 ml of an  $\text{H}_2\text{PtCl}_6$  solution containing 0.976764 grams of Pt metal was added to 60.29347 grams of Kaiser 201 alumina. The  $\text{H}_2\text{PtCl}_6$  solution was prepared by dissolving chloroplatinic acid crystals (40% Pt) (Matheson Coleman and Bell, Norwood, Ohio) in distilled water. The mixture was allowed to stand for 1/2 hour, dried at 105°C for 18 hours, followed by reduction in flowing hydrogen at 250°C for 1 hour. Before gas uptake measurements the catalysts were further reduced in flowing hydrogen at 500°C for 1/2 hour, followed by evacuation for 2 hours at 500°C. The evacuation time was measured from the time that the desired vacuum level ( $>10^{-5}$  torr) had been achieved in the system with the sample in position.



The alumina blank for the adsorption measurements was treated identically to the catalyst preparation, except that the platinum salt solution was replaced by distilled water.

### 5.5 Adsorption of Hydrogen on the $\text{Al}_2\text{O}_3$ support

A hydrogen adsorption isotherm on the alumina support was measured at  $250^\circ\text{C}$  for the purpose of obtaining a value for the blank correction. The results, in terms of moles of hydrogen adsorbed vs. pressure are shown in Fig. 5.1 with the moles adsorbed at 240 mm Hg noted (Chapter 3).

The scattering in the experimental data at the lower end of the isotherm can be explained as follows: inaccuracy in the calculated value of the moles of hydrogen adsorbed depends on the inaccuracies in reading pressure, volume and temperature. Assuming an accuracy of 100% in reading volume and temperature, and an error of  $\pm 0.5$  mm in pressure reading, the inaccuracy levels at the upper and lower end of the isotherm would be of the order of  $10^{-7}$  and  $10^{-6}$  moles respectively. Since the moles of hydrogen adsorbed are of the order of  $10^{-6}$ ; an inaccuracy of the order of  $10^{-6}$  results in significant errors and hence scattering of data at the lower end.

The way to minimize error is to use larger sample so that the adsorption values are higher; but practical consideration limited the size of the sample in this work.

A number of curves could be drawn through the experimental points shown in Figure 5.1. In drawing the actual curve, more importance was given to the points on the upper end of the curve because of the higher accuracy involved at that end.

The moles of hydrogen adsorbed at a pressure of 240 mm Hg were found from the plot ( $\approx 3.58067 \times 10^{-7}$  moles/g  $\text{Al}_2\text{O}_3$ ) and this value was used for the blank correction.

wt. of sample = 18.43228 g.

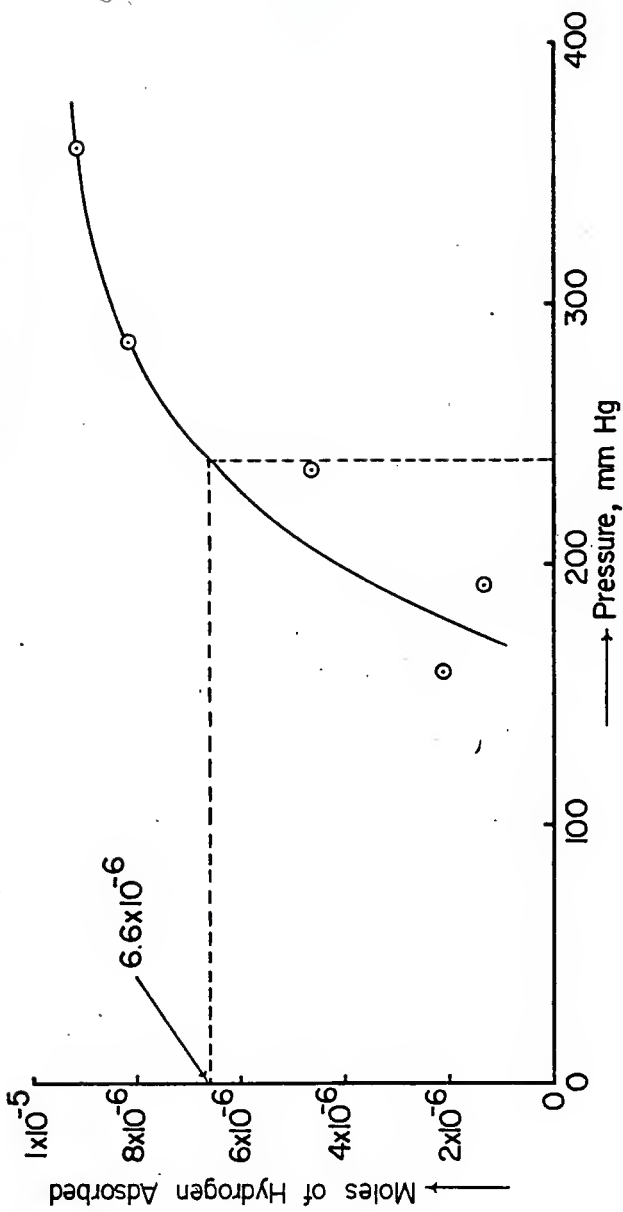


Fig. 5.1 Hydrogen Adsorption Isotherm for the  $\text{Al}_2\text{O}_3$  Support

### 5.6 Adsorption of Hydrogen on Fresh Pt/Al<sub>2</sub>O<sub>3</sub> Catalyst

A 1.62% Pt/Al<sub>2</sub>O<sub>3</sub> catalyst was used in the entire work. The hydrogen adsorption isotherm at 250°C for the fresh catalyst is shown in Fig. 5.2. The Pt dispersion, surface area and average crystallite size were calculated from the hydrogen adsorption uptake and are listed in Table 5.1.

The dispersion of the fresh catalyst was found to be 1.03. This ratio in excess of unity can result from: (1) reaction of hydrogen with oxygen present in the system because of the incomplete reduction of the catalyst, (2) hydrogen spillover from the metal to the support, and (3) changing stoichiometrics of hydrogen chemisorption in different ranges of dispersion. No attempt was made to isolate the specific reason for this ratio being greater than unity.

To check the reproducibility of the adsorption measurements, another determination of hydrogen adsorption uptake was carried out on the same sample. The treatment between adsorption measurements consisted of evacuation at pressures less than 10<sup>-5</sup> torr for 4 hours at 300°C. The adsorption isotherm is shown in Fig. 5.2 and the results obtained are listed in Table 5.1.

The dispersion of the catalyst dropped from 1.03 to 0.82. This decrease in the dispersion can result from (1) lower adsorption due to the presence of residual hydrogen on the catalyst surface because of incomplete desorption and (2) sintering of the catalyst in the vacuum treatment at 300°C.

To distinguish between incomplete desorption and sintering in vacuum as the possible cause of the decrease in the dispersion of the catalyst, the catalyst was evacuated for 4 hours at 500°C and another hydrogen adsorption uptake measurement was made. The adsorption isotherm and the results obtained are shown in Fig. 5.2 and Table 5.1.

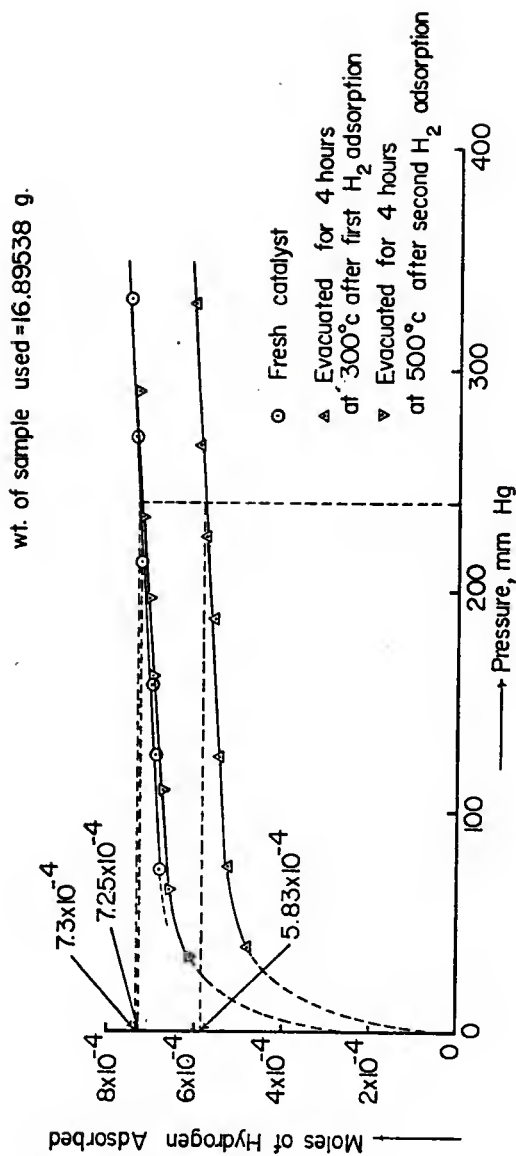


Fig. 5.2 Hydrogen Adsorption Isotherms for the Fresh Catalyst

Table 5.1  
Data on Pt Dispersion for the Pt/Al<sub>2</sub>O<sub>3</sub> Catalyst

Catalyst	Net adsorption, μmoles H <sub>2</sub> /g sample	Dispersion	Pt Surface Area, m <sup>2</sup> /g Pt	Average crystallite size Å
Fresh Catalyst	4.28490 x 10 <sup>-5</sup>	1.03	285	8
Catalyst after being evacuated for 4 hours at 300°C following first H <sub>2</sub> adsorption	3.41484 x 10 <sup>-5</sup>	0.82	227	10
Catalyst after being evacuated for 4 hours at 500°C following second H <sub>2</sub> adsorption	4.25531 x 10 <sup>-5</sup>	1.02	283	8

The dispersion of the catalyst was found to be 1.02 which was in excellent agreement with the value for the fresh catalyst (=1.03). This result ruled out the possibility of sintering in vacuum up to 500°C and was consistent with the hypothesis of incomplete desorption as the probable reason for the observed decrease in the dispersion of the catalyst in the first two runs.

From the above set of experiments, it was concluded that the outgassing of the catalyst under evacuated conditions for 4 hours at 500°C, after the catalyst had been subjected to hydrogen atmosphere at the chemisorption conditions, resulted in reproducibility of the adsorption measurements.

#### 5.7 Effect of Reduction Conditions on the Dispersion

To find the optimal reduction conditions, the Pt/Al<sub>2</sub>O<sub>3</sub> catalyst was exposed to the atmosphere and was checked for hydrogen uptake after various reduction treatments. The hydrogen adsorption isotherms for these experiments are shown in Fig. 5.3 and the calculated dispersion results are listed in Table 5.2.

Run 4: The catalyst from the previous run (dispersion = 1.02) was exposed to the atmosphere overnight at room temperature and was then reduced for 1 hour at 500°C. From hydrogen adsorption measurements, the dispersion of the catalyst was found to be 0.63. The decrease in the dispersion from 1.02 to 0.63 may be due to either sintering of the metal crystallites in hydrogen atmosphere at 500°C or incomplete desorption of hydrogen.

To distinguish between sintering in hydrogen at 500°C and incomplete desorption as the cause for the decrease in the dispersion, two set of experiments were performed. In Run 5, the catalyst from Run 4 was evacuated for 4 hours at 500°C (desorption step) and the hydrogen uptake measurements were made. The experimental data points, as shown in Fig. 5.3, were found to be so close to the adsorption isotherm of Run 4 that no distinction

wt. of sample used = 16.89538 g.

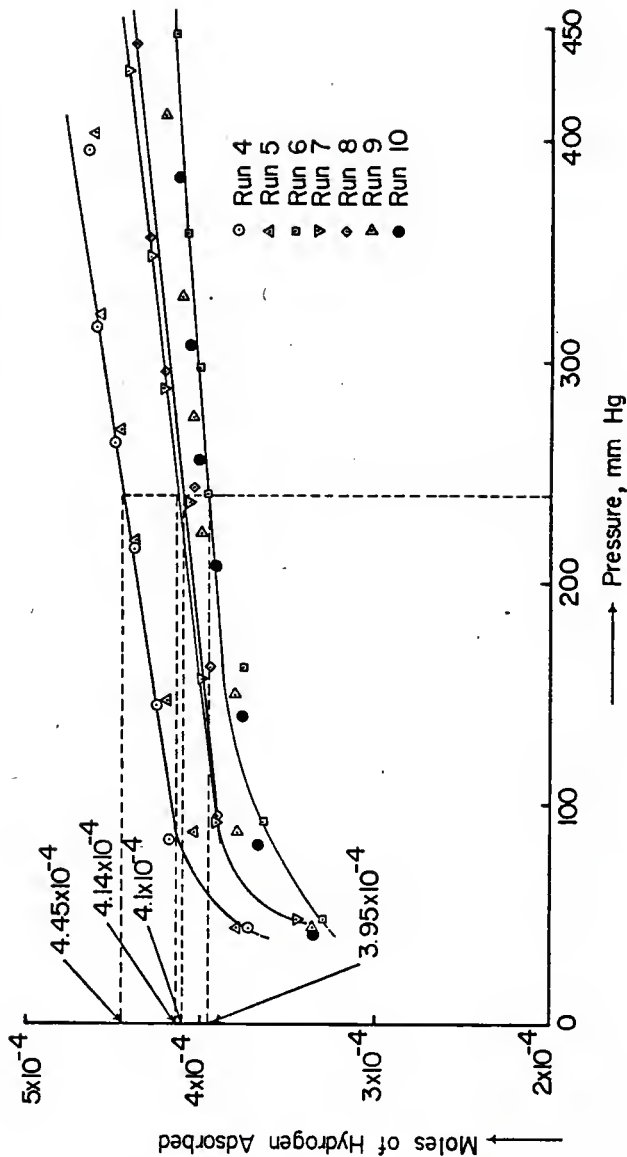


Fig. 5.3 Effect of Reduction Conditions on Hydrogen Uptake

Table 5.2  
Results of Effect of Reduction Conditions on the Pt Dispersion

Run	Treatment	Net adsorption, moles $H_2/g$ Sample	Dispersion	Pt surface area, $m^2/g$ Pt	Average crystallite size, $\text{\AA}$
4	Reduced @ 500°C for 1 hour	$2.959805 \times 10^{-5}$	0.63	173	14
5	Degassed @ 500°C for 4 hours	←	same as in Run 4	Run 4	→
6	Reduced @ 500°C for 1 hour	$2.30211 \times 10^{-5}$	0.55	153	15
7	Reduced @ 250°C for 2 hours	$2.41457 \times 10^{-5}$	0.58	160	15
8	Reduced @ 300°C for 2 hours	$2.39089 \times 10^{-5}$	0.58	159	15
9	Reduced @ 325°C for 4 hours	←	same as in Run 6	Run 6	→
10	Reduced @ 325°C for 4 hours	←	same as in Run 6	Run 6	→



was made in the adsorption isotherm of Run 4 and 5. This result ruled out the possibility of incomplete desorption as the cause for the decrease in the Pt dispersion and again showed reproducibility of the adsorption measurements.

To confirm that sintering in hydrogen at 500°C was the probable cause for the decrease in the metal dispersion, in Run 6, the catalyst from Run 5 was again exposed to atmosphere for overnight at room temperature, reduced in hydrogen for 1 hour at 500°C and evacuated for 4 hours at 500°C. From adsorption measurements, the dispersion of the catalyst was calculated and was found to be 0.55. The decrease in the dispersion between Run 5 and 6 supported the hypothesis of sintering of the catalyst in hydrogen at 500°C.

To avoid sintering of the catalyst, reduction treatments at lower temperatures were employed in the next few runs. In Run 7, the catalyst after being exposed to the atmosphere overnight at room temperature, was reduced in flowing hydrogen for 2 hours at 250°C followed by evacuation for 4 hours at 500 C. The dispersion was found to increase from 0.55 to 0.58 (0.582) in this run. This increase in the dispersion may be due to redispersion of the catalyst or incomplete reduction.

To distinguish between the above two causes, in Run 8, the catalyst was treated the same way as in Run 7 except the reduction was carried out at 300 C. The dispersion of the catalyst was found to be 0.58 (0.576). This value lies in between those found for Run 6 and 7 and hence indicates incomplete reduction as the probable reason for the increase in the dispersion between Run 6 and Runs 7 and 8.

In Run 9, the catalyst was treated the same way as in Run 8 except the reduction was carried out for 4 hours at 325°C. The experimental points, as shown in Figure 5.3, were found to be very close to the adsorption isotherm

of Run 6 and so no separate isotherm was drawn for this run.

To confirm that incomplete reduction caused the increase in the dispersion between Run 6 and Run 7 and 8 and also that complete reduction of the catalyst was achieved by treating in flowing hydrogen for 4 hours at 325°C, in Run 10, the catalyst was again exposed to the atmosphere overnight at room temperature, reduced in flowing hydrogen for 4 hours at 325°C and evacuated for 4 hours at 500°C. The hydrogen adsorption results were found to be very close to those found for Run 6 and so no distinction was made in adsorption isotherm for Run 10 and 6. The excellent agreement between Run 6 and Runs 9 and 10 confirms that the increase in the dispersion between Run 6 and Run 7 and 8 was due to incomplete reduction and also that complete reduction was achieved by treating in flowing hydrogen for 4 hours at 325°C after the catalyst had been exposed to the atmosphere at room temperature.

From the above set of experiments, the following conclusions are drawn:

- (1) Evacuation for 4 hours at 500°C leads to complete desorption of the hydrogen from the catalyst surface and results in excellent reproducibility of the adsorption measurements.
  - (2) Treatment in vacuum at 500°C up to 4 hours does not result in sintering of the crystallites.
  - (3) Treatment in flowing hydrogen at 500°C for 1 hour results in sintering of the crystallites. (but see Dautzenberg and Wolters (39))
  - (4) Treatment in flowing hydrogen for 4 hours at 325°C results in complete reduction of the catalyst and a lower time-temperature combination does not reduce the surface properly.
- 5.8 Effect of Treatment in Oxygen on the Dispersion.

A temperature of 550°C and a partial pressure of oxygen equal to 0.5

atmosphere were selected as the treatment conditions. A 50/50 (volume basis) mixture of oxygen and helium at a total pressure of approximately 1 atmosphere was used in the experiments. The treatment in oxygen and the pretreatment for hydrogen adsorption after treatment in oxygen consisted of the following steps:

1. The catalyst from the previous run was evacuated for 4 hours at 500°C.
2. The sample was heated to 550°C under evacuated conditions.
3. The O<sub>2</sub>/He mixture was passed through the sample tube for the desired length of time at 550°C.
4. The O<sub>2</sub>/He mixture was replaced by helium.
5. The furnace was removed from the sample tube immediately after the gas change and the sample was allowed to cool to room temperature.
6. The catalyst was evacuated at room temperature, the furnace was placed around the sample tube and the temperature brought to 325°C.
7. The catalyst was reduced in flowing hydrogen for 4 hours at 325°C.
8. The hydrogen flow was replaced by helium.
9. The furnace was removed from the sample tube immediately after the gas change and the sample was cooled to room temperature.
10. The catalyst was evacuated at room temperature, the furnace was placed around the sample tube and the temperature was brought up to 500°C. The sample was kept under evacuated conditions at 500°C for 4 hours.

Since the emphasis in this work is on finding the minimum conditions under which reasonable redispersion can be obtained, 5 minutes was selected as the initial treatment time. The hydrogen adsorption isotherms after different treatments in oxygen are shown in Fig. 5.4 and the calculated Pt dispersion results are listed in Table 5.3.

The catalyst from Run 10 (dispersion = 0.55) was treated in the oxygen atmosphere for 5 minutes and the hydrogen adsorption results showed

wt. of sample used = 16.89538 g.

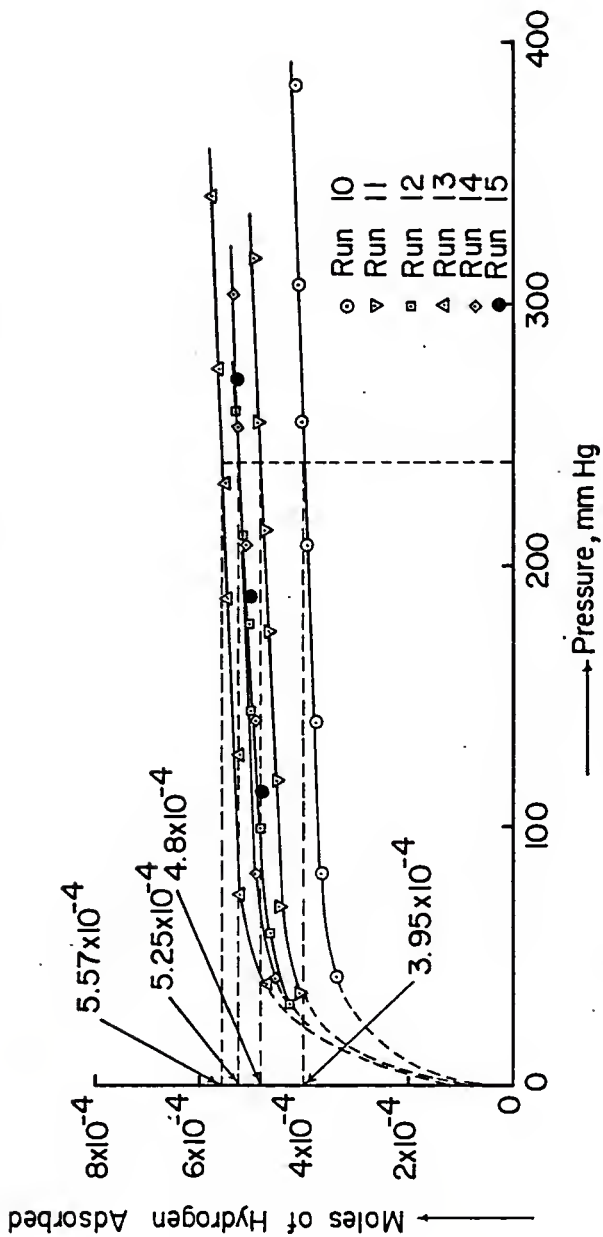


Fig. 5.4 Effect of Treatment in Oxygen on Hydrogen Uptake

Table 5.3  
Results of Effect of Oxygen Treatment on the Pt Dispersion

Run	Treatment	Net adsorption, moles/H <sub>2</sub> /g Sample	Dispersion	Pt surface area, m <sup>2</sup> /g Pt	Average crystallite size, Å
10	Reduced @ 325°C for 4 hours	2.30211 x 10 <sup>-5</sup>	0.55	153	15
11	Redispersed for 5 min.	2.80521 x 10 <sup>-5</sup>	0.68	186	13
12	Redispersed for 5 min.	3.07155 x 10 <sup>-5</sup>	0.74	204	11
13	Redispersed for 5 min.	3.26095 x 10 <sup>-5</sup>	0.79	217	11
14	Redispersed for 10 min.	3.07155 x 10 <sup>-5</sup>	0.74	204	11
15	Degassed @ 500°C for 4 hours	←	same as	Run 14	→

an increase in dispersion to 0.68 (Run 11). Since a significant increase in dispersion (~13%) was observed in 5 minutes, an additional treatment in oxygen for 5 minutes was attempted on the catalyst. The dispersion was found to increase to 0.74 (Run 12). The increase in dispersion (~6%) in this run was lower than that observed in the previous run (~13%). To check whether the trend of decrease in the rate of increase of dispersion with successive 5 minute oxygen treatments was followed, the catalyst was treated in the oxygen for an additional 5 minutes. The dispersion was found to be 0.79 (Run 13), yielding an increase of approximately 5%, and thus indicating that the above stated trend was followed.

To examine the effect of treatment time on the degree of redispersion, the catalyst was treated in the oxygen atmosphere for 10 minutes. Unexpectedly, the dispersion was found to decrease from 0.79 (Run 13) to 0.74 (Run 14). To verify that the observed decrease in the dispersion was due to the oxygen treatment and not because of some error in measuring the hydrogen uptake, the catalyst was evacuated at 500 °C for 4 hours, and another hydrogen uptake measurement was made (Run 15). No measurable difference was found in the hydrogen uptake between Run 14 and 15 and hence it was concluded that the oxygen treatment was responsible for the observed decrease in the dispersion.

To have a greater understanding of the effect of the treatment time on the dispersion, another treatment in the oxygen atmosphere for 5 minutes for the same catalyst was planned. Due to accidental burning of the sample, no results were obtained.

At this stage, insufficient data on the effect of oxygen treatment on the catalyst is available to make it worthwhile to attempt to explain the results and draw conclusions.

## 5.9. Discussion and Conclusions

The purpose of these experiments was to establish proper degassing and reduction procedures that result in reproducible measurements of  $H_2$  uptake and to obtain the preliminary information on the effect of short time oxygen treatments on the dispersion of  $Pt/Al_2O_3$  catalyst.

The results indicate that the  $H_2$  uptake depends on the extent of degassing, and, in the case when the catalyst is exposed to oxygen, the  $H_2$  uptake depends on the extent of reduction. The proper degassing and reduction conditions established from the experiments were evacuation for 4 hours at  $500^\circ C$  and heating in flowing hydrogen for 4 hours at  $325^\circ C$  respectively.

The results of the oxygen treatment experiments confirm the ability of very short-time (5 minutes) treatments at  $550^\circ C$  to redisperse the  $Pt/Al_2O_3$  catalyst.

Wanke et al. (49,50), Hassan et al (38) and Dautzenberg and Wolters (39) have studied the effect of treatments in hydrogen and oxygen on the dispersion of  $Pt/Al_2O_3$  catalysts.

Wanke et al. (50) and Dautzenberg and Wolters (39) did not observe any change in the dispersions of the  $Pt/Al_2O_3$  catalysts on heat treatment in hydrogen at  $500^\circ C$  for 1 hour, although a decrease in the dispersions was observed at temperatures higher than  $550^\circ C$ . This is contrary to the observation made in this work. The catalyst was found to sinter on heat treatment in hydrogen at  $500^\circ C$  for 1 hour. However, it should be noted that the catalyst was exposed to the atmosphere before hydrogen treatment, in the present work. It is possible that the presence of the adsorbed oxygen enhances the sintering as is suggested by the theoretical work showing excessive temperatures on the Pt surface when an exothermic reaction occurs.

Hassan et al (38) report a decrease in Pt surface area due to treatment in hydrogen at temperatures below 400°C and an increase at temperature higher than 400°C. In the present work, treatment in hydrogen at 325°C did not result in any change in the Pt surface area.

Wanke et al (49,50) observed significant increases in dispersions of Pt/Al<sub>2</sub>O<sub>3</sub> catalysts on subjection to oxygen treatment (0.92 atm) at 550°C. These redispersion results are in general agreement with those found in the present work. Wanke et al (39,50) found the increases in dispersion to be relatively independent of treatment time which was varied from 1 to 128 hours. In the present work, successive 5 minute treatments in oxygen at 550°C were found to result in an increase in the dispersion of the catalyst. Attempts to determine whether two 5 minute oxygen treatments were equivalent to one 10 minute treatment were frustrated when sintering instead of redispersion was observed in the 10 minute treatment (Run 14). Dautzenberg and Wolters (39) also found the increase in dispersion at a given oxidation temperature to be independent of the length of the oxidation treatment which was varied from 15 minutes to 6 hours. However, on repeated oxidation-reduction a further increase in the dispersion was observed. Some further experiments at very short treatment times (5 minutes or lower) should be conducted to identify the transient portion of the dispersion vs. treatment time plot. This pursuit will be by no means of academic interest only, since knowledge of the transient portion would suggest the minimum treatment time to achieve the maximum possible level of resispersion.

For fresh as well as presintered (in O<sub>2</sub> atmosphere) catalysts, Dautzenberg and Wolters (39) observed sintering during heat treatment in air at 500°-650°C for 6-70 hours. During heat treatment in hydrogen at temperature higher than



500°C, they observed a decrease in the dispersion and on subsequent treatment in oxygen below 550°C, the dispersion was found to increase. They also found that the dispersion increased with every additional oxygen treatment, although the increase became progressively smaller. The results of oxygen treatment (after pretreatment in hydrogen) are in agreement with those found in the present work.

Dautzenberg and Wolters (39) concluded that during heat treatment in hydrogen agglomeration of Pt does not take place, rather, a certain amount of Pt becomes inaccessible for hydrogen adsorption and causes the observed decrease in H/Pt ratio. Oxidation at temperature around 500°C restores the original contribution to the H/Pt value. They suggested that the decrease in H/Pt ratio and sintering should not be linked. Since no method other than chemisorption (electron microscope or x-ray line-broadening) was used to measure the Pt dispersion in the present work, no distinction between decrease in H/Pt value and sintering can be made.

Hassan et al (38) report a decrease in Pt surface area due to treatment in vacuum at temperatures below 400°C and an increase at temperature higher than 400°C. They also report a monotonic decrease in Pt surface area with increasing treatment temperatures in oxygen atmosphere. The reported results on treatment in vacuum are contrary to the observations made in the present work. No sintering of the catalyst was observed on heat treatment in vacuum up to 500°C.

For fresh as well as presintered (in O<sub>2</sub> atmosphere) catalysts the results obtained after O<sub>2</sub> treatment, by different investigators, are contradictory. Wanke et al (49,50) observed redispersion of Pt on oxygen treatment at 550°C, whereas Dautzenberg and Wolters (39) and Hassan et al (38) observed sintering. Since no attempt was made in the present study to redisperse the

fresh catalyst or the catalyst which had been presintered in an  $O_2$  atmosphere, additional experiments are recommended.

An outline of the recommended experiments is listed in Chapter 6.

CHAPTER 6  
PROPOSED EXPERIMENTS

The burning of the sample prevented the running of the experiments needed to complete the preliminary redispersion studies. A blank, i.e. pure He at 550°C should have been run in addition to the He-O<sub>2</sub> runs. Sintering of the catalyst was reported after subjection to H<sub>2</sub> at 500°C for 1 hour. With proper reduction and degassing procedures having been determined, this point should have been rechecked.

For future experiments chemisorption of hydrogen at room temperature should be studied. The amounts of hydrogen adsorbed on the metal under saturation conditions at room temperature and 250°C should be compared. If the adsorbed amount are found to be the same, future hydrogen adsorption measurements should be made at room temperature rather than at 250°C as done in the present work. This would simplify the adsorption procedure and would also save some time.

It has been reported (39,49) that the increase in dispersion obtained on oxygen treatment at 550°C is independent of the length of the oxidation period which has been varied from 15 minutes to several hours. It appears that a definite minimum amount of oxygen is required to achieve the maximum redispersion possible in a single treatment and any amount in excess of this minimum does not play any role in the redispersion process. To verify this hypothesis, two sets of experiment should be conducted. In the first set, at a fixed partial pressure of oxygen, the effect of treatment time on the dispersion of a catalyst should be studied. In the second set, the effect of oxygen partial pressure on the dispersion of the catalyst for a fixed treatment time (~ 5 minutes) should be studied. If it is observed that beyond certain treatment time and certain partial pressure of oxygen, no

further improvement in the dispersion of the catalyst is possible, the results would be consistent with the above stated hypothesis.

Redispersion of catalysts with similar crystallite size which has been obtained by different thermal treatments, for example, by treatment in oxygen or hydrogen or helium or vacuum should be examined. Dautzenberg and Wolters (39) observed that an oxidative treatment can only recover the fraction of platinum lost by severe heat treatment in a hydrogen atmosphere, and that it is incapable of actually redispersing the big crystallites obtained during heat treatment in oxygen. During heat treatment in helium or vacuum, agglomeration of Pt rather than a certain part of the Pt becoming inaccessible for chemisorption would be expected. The results from subsequent treatments in oxygen should yield considerable insight into the redispersion phenomena.

The extent of redispersion as a function of initial, that is prior to redispersion, crystallite size should be ascertained. This is important from an industrial point of view when considering when to regenerate the catalyst.

The characteristics of the redispersed catalysts, both with regard to sintering and with regard to redispersion should be examined. Weller and Montagna (23) found that redispersed catalysts were more stable to oxygen treatment than the original preparation, whereas, in industrial operations, it is found that the time between successive regenerations must be continually decreased. It is possible that the ease or extent of redispersion changes with multiple redispersions and this possibility should be examined.

Repeated oxidation-reduction cycles under suitable conditions have been found to result in increased metal dispersion. However, the increase in

dispersion becomes progressively smaller with successive treatments. Experiments should be conducted to find the optimal number of these cycles.

Surface area and pore size distribution of the support may have some influence on redispersion of the metal crystallites. Procedures for determination of the pore size distribution of the support should be established and the effect of surface area and pore size distribution of the support on redispersion should be examined.

Thermal treatment of the catalyst normally decreases the support surface area and thereby results in a loss of the accessible metal. Hence a correction in the measured dispersion for the change in the support surface area is necessary. Correlation between the loss in support surface area and the loss in accessible metal should be established.

Redispersion of the Pt/SiO<sub>2</sub> system should be investigated as a start toward the study of the effect of different supports on the redispersion phenomenon.

Although regeneration of catalysts using halogens and traces of water is standard practice, redispersion studies using these compounds have received very little attention and hardly any quantitative information is available. Redispersion procedures using halogens and water should be investigated.

In addition to H<sub>2</sub> chemisorption, electron microscopy and x-ray line broadening should be used to determine the crystallite size and the metal surface area. The work of Dautzenberg and Wolters (39) which indicated that chemisorption will sometimes indicate a change that cannot be seen by either electron microscopy or line broadening makes it imperative that an additional technique be used. Some preliminary work using the transmission

electron microscope with samples prepared by a holey carbon technique have been started in this laboratory though the techniques have not been perfected to the point that the resolution limit of the microscope ( $\sim 9\text{\AA}$ ) has been reached.

Although crystallite sizes  $< 50\text{\AA}$  cannot be determined by line broadening, the technique should not be ignored primarily because of the availability of a controlled environment attachment (Department of Geology). This permits observing changes in situ under most conditions of interest.

It should be noted that chemisorption measurements yield a surface average size, line broadening yields a volume average size and the electron microscope results can be used to calculate either a surface average or volume average size.

In addition to surface area measurements, activity measurements of the Pt in various degrees of dispersion and after the different sintering and redispersion studies seem in order. A good choice of reactions for the activity measurements appears to be the reduction of NO with  $\text{NH}_3$  (71) both in the absence of  $\text{O}_2$  (structure insensitive) and in the presence of  $\text{O}_2$  (structure sensitive). The structure sensitive reaction exhibits an increase in specific rate with increasing crystallite size up to approximately 5 nm. Above 5 nm the rate is independent of crystallite size.

These reactions can thus be used as an independent measure of whether the crystallite size is increasing or decreasing. For example; starting with a well dispersed and constant amount of catalyst if a given "treatment" results in sintering then for the structure sensitive reaction an increase in rate and an increase in conversion should be observed, while for the structure insensitive reaction no change in rate and a decrease in conversion should be observed. Below a crystallite size of  $\sim 5$  nm a procedure

that results in redispersion should yield a decrease in both rate and conversion for the structure sensitive reaction, while the structure insensitive reaction would show an increase in conversion but no change in rate. A schematic of the behavior is shown on Fig. 6.1.

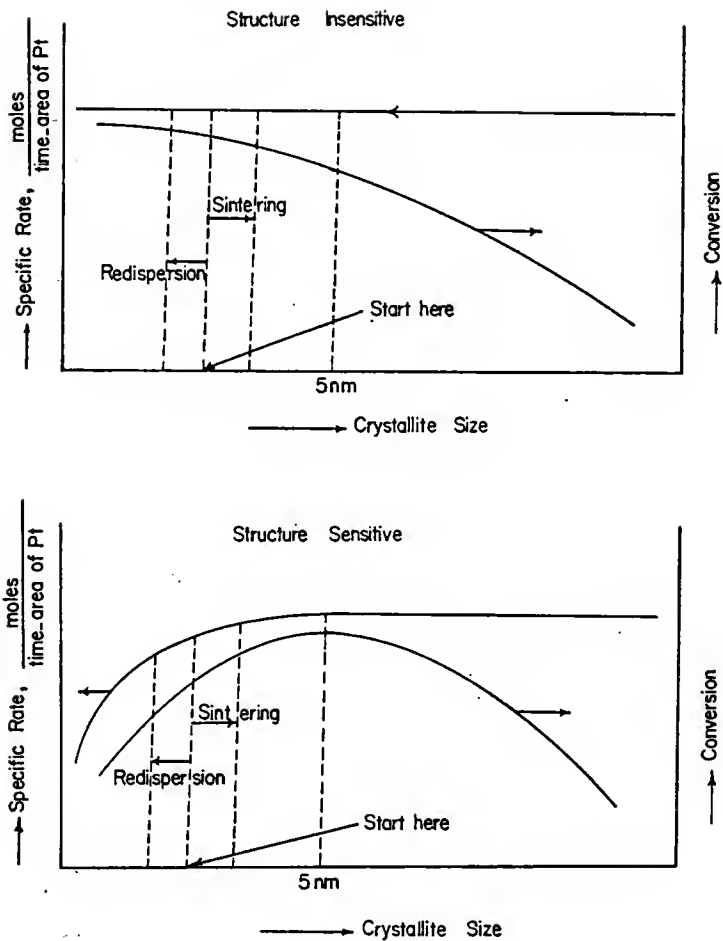


Fig. 6.1 Proposed Activity Measurement Experiments



## ACKNOWLEDGMENTS

The author wishes to express sincere gratitude to Dr. John C. Matthews for his advice and encouragement during this work. The author also extends his gratitude to the Department of Chemical Engineering and Engineering Experiment Station for financial support. Thanks are due to Mr. Mitsugi Ohno, who constructed and assembled the glass apparatus used in this study and also to Mr. Duane Morey, who was quite helpful in equipment modification and construction.

Final consideration must go to my friend, Susan Gross, who helped me in numerous ways during the course of this work.

## REFERENCES

1. Poltorak, O. M., and Boranin, V. S., Russ. J. Phys. Chem. 40, 1436 (1966).
2. Gregg, S. J., "The Surface Chemistry of Solids", Second Ed., Reinhold Publishing Corporation (1961).
3. Brunauer, S., Emmett, P. H., and Teller, E., J. Amer. Chem. Soc. 60, 309 (1938)
4. Gregg, S. J., and Sing, K. S. W., "Adsorption, Surface Area and Porosity", p. 43, Academic Press (1967).
5. Nelsen, F. M., and Eggertsen, F. T., Anal. Chem. 30, 1387 (1958).
6. Instructions - The Perkin-Elmer Shell Model 212D Sorptometer.
7. Perry, J. H., "Chemical Engineers Handbook", p. 3-71, Fourth Ed., McGraw-Hill (1963).
8. Flynn, P. C., Ph.D. Thesis, Univ. of Alberta (1974).
9. Gruber, H. L., Anal. Chem. 34, 1828 (1962).
10. Benesi, H. A., Atkins, L. T., and Mosely, R. B., J. Catal. 23, 211 (1971).
11. Dorling, T. A., Warren Spring Laboratory Report LR 144 (CA), Department of Trade and Industry (London), 1971.
12. Faeth, P. A., "Adsorption and Vacuum Technique", The Univ. of Michigan Report 66100-2-x, 1962.
13. Gruber, H. L., J. Phys. Chem. 66, 48 (1962).
14. Spenadel, L., and Boudart, M., J. Phys. Chem. 64, 204 (1960).
15. Adams, C. R., Benesi, H. A., Curtis, R. M., and Meisenheimer, R. G., J. Catal. 1, 336 (1962).
16. Wilson, G. R., and Hall, W. K., J. Catal. 17, 190 (1970).
17. Dorling, T. A., Burlace, C. J., and Moss, R. L., J. Catal. 12, 207 (1968).
18. Freel, J., J. Catal. 25, 139 (1972).
19. Freel, J., J. Catal. 25, 149 (1972).
20. Adler, S. F., and Keavney, J. J., J. Phys. Chem. 64, 208 (1960).
21. Poltorak, O. M. and Boranin, V. S., Russ. J. Phys. Chem. 39, 781 (1965).
22. Zaidman, N. M. Dzisko, V. A., Karnaukhov, N. P., Krasilenko, N. P., and Koroleva, N. G., Kinetika i kataliz 10, 652 (1969).

23. Weller, S. W., and Montagna, A. A., *J. Catal.* 20, 394 (1971).
24. Wilson, G. R., and Hall, W. K., *J. Catal.* 24, 306 (1972).
25. Bond, G. C., *Proc. Int. Congr. Catal.* 4th, Moscow p. 266 (1968).
26. Karnaukhov, A. P., *Kinetika i kataliz* 12, 1520 (1971).
27. Benson, J. E., and Boudart, M., *J. Catal.* 4, 704 (1965).
28. Mears, D. E., and Hansford, R. C., *J. Catal.* 9, 125 (1967).
29. Kikuchi, E. Flynn, P. C., and Wanke, S. E., *J. Catal.* 34, 132 (1974).
30. Eischens, R. P., and Pliskin, W. A., "Advances in Catalysis", Vol. X, p. 18, Academic Press (1958).
31. Dorling, T. A., and Moss, R. L., *J. Catal.* 7, 378 (1967).
32. Brennan, D., and Hayes, F. H., *Phil. Tran. Roy. Soc. London*, A258 (1089), 347 (1965).
33. Hardeveld, R. V., and Hartog, F., *Proc. Int. Congr. Catal.* 4th, Moscow, p. 295 (1968).
34. Blyholder, G., *J. Phys. Chem.* 68, 2772 (1964).
35. Renouprez, A. Hoang-Van, C., Compagnon, P. A., *J. Catal.* 34, 411 (1974).
36. Wentrcek, P., Kimota, K., and Wise, H., *J. Catal.* 33, 279 (1973).
37. Hausen, A., and Gruber, H. L., *J. Catal.* 20, 97 (1971).
38. Hassan, S. A., Khalil, F. H., and El-Gamal, F. G., *J. Catal.* 44, 5 (1976).
39. Dautzenberg, F. M., and Wolters, H. B. M., *J. Catal.* 51, 26 (1978).
40. Kearby, K. K., Thorn, J. P., and Hinlicky, J. A., U.S. 3,134,732 (1964).
41. Brennan, H. M., Seelig, H. S., and Vander Haar, R. W., U.S. 3,117,076 (1964).
42. Koegler, H., and Queck, S., *Chem. Tech.* 14, 541 (1962).
43. Webb, G. M., U.S. 3,011,968 (1961).
44. Malo, R. V., Munster, I., and Webb, G. M., U. S. 2,879,232 (1959).
45. Coe, R. H., and Randaltt, H. E., U.S. 3,278,419 (1965).
46. Johnson, F. L., and Keith, C. D., *J. Phys. Chem.* 67, 200 (1963).

47. McHenry, K. W., Bertolacini, R. J., Brennan, H. M., Wilson, H. M., and Seelig, H. S., Proc. Int. Congr. Catal. 2nd, Paris, Vol II, p. 2295 (1960).
48. Flynn, P. C., and Wanke, S. E., J. Catal. 37, 432 (1975).
49. Fiedorow, R. M. J., and Wanke, S. E., J. Catal. 43, 34 (1976).
50. Fiedorow, R. M. J., Chahar, B. S., and Wanke, S. E., J. Catal. 51, 193 (1978).
51. Ruckenstein, E., and Malhotra, M. L., J. Catal. 41, 303 (1976).
52. Maat, H. J., and Moscou, L., Proc. Int. Congr. Catal. 3rd, N. Holland, p. 1277 (1965).
53. Jaworska-Galas, Z., and Wrzyszczyk, J., Int. Chem. Eng. 6, 604 (1966).
54. Kraft, M., and Spindler, H., Proc. Int. Congr. Catal. 4th, Moscow, p. 342 (1968).
55. Furhman, Z. A. and Parravano, G., Proc. Int. Congr. Catal. 6th, London, Vol. I, p. 686 (1976).
56. Emelianova, G. I., and Hassan, S. A., Proc. Int. Congr. Catal. 4th, Moscow, p. 342 (1968).
57. Baker, R. T. K., Thomas, C., and Thomas, R. B., J. Catal. 38 510 (1975).
58. Ruckenstein, E., and Pulvermacher, B., AIChE J. 19 (2), 356 (1973).
59. Ruckenstein, E., and Pulvermacher, B., J. Catal. 29, 224 (1973).
60. Flynn, P. C., and Wanke, S. E., J. Catal. 34, 390 (1974).
61. Flynn, P. C., and Wanke, S. E., J. Catal. 34, 400 (1974).
62. Ruckenstein, E., and Dadyburjor, D. B., J. Catal. 48, 73 (1977).
63. Wanke, S. E., and Flynn, P. C., Catal. Rev. 12 (1), 93 (1975).
64. Wynblatt, P., and Gjostein, N. A., Prog. Solid State Chem. 9, 21 (1975).
65. Thomas, M. J., and Walker, P. L., J. Chem. Phys. 41, 587 (1964).
66. Baker, R. T. K., Haris, P. S., and Thomas, R. B., Surf. Sci. 46, 311 (1974).
67. Baker, R. T. K., and France, J. A., J. Catal. 39, 481 (1975).
68. Bett, J. A., Kinoshita, K., and Stonehart, P., J. Catal. 35, 307 (1974).
69. Ciapetta, F. G., and Plank, C. J., Catalysis 1, 315 (1954).

70. Benesi, H. A., Curtis, R. M., and Studer, H. P., J. Catal. 10, 328 (1968).
71. Pusateri, R. J., Katzer, J. R., and Manogue, W. H., AIChE J. 20 (2), 219 (1974).
72. Den Otter, G. J., and Dautzenberg, F. M., J. Catal. 53, 116 (1978).-

## APPENDIX A

## CALIBRATION OF BURETTES

Table A.1  
 Calibration of Linear Burette (B'')

S. No.	Mass of Hg, g	Temperature, °F	Density of Hg, g/cm <sup>3</sup> (7)	Volume, cm <sup>3</sup>	Average volume, cm <sup>3</sup>
1.	90.7	72	13.5404	6.698	
2.	90.0	72	13.5404	6.647	6.682
3.	90.7	75	13.5360	6.700	

Table A.2  
Calibration of Small Burette (B')

Bulb No.	Mass of Hg, g	Temperature, °F	Density of Hg, g/cm <sup>3</sup> (7)	Volume, cm <sup>3</sup>	Average Volume, cm <sup>3</sup>
1.	66.7	72	13.5404	4.926	4.922
	66.6	72	13.5404	4.919	
	66.6	75	13.5360	4.920	
2.	133.1	72	13.5404	9.830	9.833
	133.2	72	13.5404	9.837	
	133.1	75	13.5360	9.833	
3.	193.9	72	13.5404	14.320	14.332
	194.3	72	13.5404	14.350	
	193.9	75	13.5360	14.325	
4.	297.0	72	13.5404	21.934	21.942
	297.1	72	13.5404	21.942	
	297.1	75	13.5360	21.949	
5.	334.0	72	13.5404	24.667	24.670
	334.1	72	13.5404	24.674	
	333.9	75	13.5360	24.668	
6.	429.8	72	13.5404	31.742	31.724
	429.8	72	13.5404	31.742	
	428.9	75	13.5360	31.686	



Table A-3  
Calibration of Large Burette (B)

Bulb No.	Mass of Hg, g	Temperature, °F	Density of Hg, g/cm <sup>3</sup> (7)	Volume, cm <sup>3</sup>	Average Volume, cm <sup>3</sup>
1.	62.6	75	13.5360	4.625	4.628
	62.7	75	13.5360	4.632	
2.	182.1	75	13.5360	13.453	13.453
	182.1	75	13.5360	13.453	
3.	329.9	75	13.5360	24.372	24.372
	329.9	75	13.5360	24.372	
4.	711.2	75	13.5360	52.541	52.545
	711.3	75	13.5360	52.549	
5.	1783.4	75	13.5360	131.752	131.741
	1783.1	75	13.5360	131.730	

THE REDISPERSION OF SUPPORTED METAL CATALYSTS

by

PAWAN KUMAR HANDA

B.S., Indian Institute of Technology (Delhi), 1973

---

AN ABSTRACT OF A MASTER'S THESIS

submitted in partial fulfillment of the

requirements for the degree

MASTER OF SCIENCE

Department of Chemical Engineering

KANSAS STATE UNIVERSITY  
Manhattan, Kansas

1978

## ABSTRACT

The objective of this work was to develop the capability of studying the redispersion of supported metal catalysts. The catalyst chosen was Pt on an alumina support and was prepared in the laboratory by impregnation of chloroplatinic acid. Pt dispersion was measured by hydrogen chemisorption at 250°C using a static, volumetric BET system constructed for this purpose. Support areas were measured with a commercial nitrogen adsorption apparatus.

Procedures for degassing and reducing the catalyst after subjection to oxygen (a part of the redispersion procedure) have been developed which do not, in the process, change the Pt area. Using these procedures reproducible Pt dispersion measurements have been achieved.

Preliminary experiments on redispersion have been conducted. It was found that a significant (55 to 68%) increase in Pt dispersion occurred on treatment in an oxygen atmosphere (0.5 oxygen, 0.5 helium) for 5 minutes at 550°C. Increases in Pt dispersion were observed with successive oxygen treatments although the increases became progressively smaller. A 10 minute treatment resulted in sintering.

Based on these results and those available in the literature a program for the study of redispersion is provided.